

A STUDY OF THE
ALTITUDE DEPENDENCE OF THE
LARGE COSMIC-RAY SHOWERS

Thesis by
Mark Muir Mills

In Partial Fulfillment of the Requirements
For the Degree of
Doctor of Philosophy

California Institute of Technology
Pasadena, California

1948



ACKNOWLEDGMENTS

The writer wishes to thank Mr. E. W. Cowan for the observational data on zenith angle distributions and for discussion of them. Mr. H. L. Kraybill very kindly supplied the results of his counting rate measurements in advance of publication. Messrs. E. R. Cohen and R. Latter also engaged in helpful discussion.

Mrs. Melba Nead assisted very much with a portion of the numerical computations.

Finally, the writer wishes to give his warmest thanks to Professor R. F. Christy for suggesting the problem, for many hours of helpful discussion, and for many important suggestions.

ABSTRACT

Assuming primary electrons, the theoretical variation of shower counting rate with altitude has been computed and a comparison made with the observations of Kraybill. Expressed as the ratio to sea level, the observed counting rate has a maximum of 63 as compared to 24 for the theoretical curve. The observed maximum is near 27,000 feet while the computed maximum is at 22,000 feet. Approximations in the calculation and observational uncertainties may make this difference in the elevations of the maxima spurious. The approximations are such as to give too low a theoretical counting rate, but an estimate of their magnitude seems to leave the theoretical maximum counting rate too small by a factor of 1.5 to 2. A computation based upon a mechanism for the multiple production of secondaries by primary protons, which has been proposed by Lewis, Oppenheimer and Wouthuysen, would probably lead to better agreement with the observations.

The zenith angle distribution of showers detected by Kraybill's counters at 30,000 feet has been computed and compared with one determined by Mr. E.W. Cowan from cloud chamber measurements. The theoretical distribution is twice as broad as the observed one. The angular distribution inferred from the altitude dependence observed by Kraybill is in much better agreement with the theoretical than with the cloud chamber distribution. The discrepancy of the cloud chamber observations may arise from the fact that it was only possible to assign a direction to the tracks in 20 to 30 per cent of the photographs.

TABLE OF CONTENTS

Acknowledgements ii
Abstract iii
I. INTRODUCTION AND CONCLUSIONS 1
1. Primary Particles 2
2. Status of the shower theory 4
3. Success at low altitudes 6
4. The comparison of theory and experiment . . 8
 (a) Variation of counting rate with alti-
 tude 8
 (b) Variation of counting rate with zenith
 angle at 30,000 feet 11
 (c) Conclusions 15
II. THE SHOWER THEORY 17
5. The number of electrons 18
6. The lateral distribution 21
 (a) General discussion 22
 (b) The lateral distribution adopted . . . 24
 (c) Density in the vicinity of the axis . . 26
 (d) Description of the radial function . . 30
7. Fluctuations 32
 (a) Experiments related to the fluctuation
 problem 32
 (b) Procedure adopted 34
III. COMPUTATIONS 35
8. Vertical density spectrum 36
9. Correction due to lateral counter separa-
 tion 39
10. Integration over zenith angles 43
11. The counting rate 46
 (a) Evaluation of $I(\delta)$ 48
 (b) The counting rate 49
12. Comparison with experiment 51
13. Estimate of approximations 54
 (a) Fluctuations 54
 (b) The assumption of uniform electron den-
 sity 56
14. Zenith angle distribution of showers . . . 58
 (a) Theoretical distribution at $t = 7.5$. . 59
 (b) Experimental distributions 61
 (c) Comparison with theory 63
References 66

LIST OF TABLES

TABLE
I Shower theory units 19
1. The atmosphere in radiation units 70
2. E and ϵ 71
3. Position and number of electrons at maximum of an
 electron shower 72
4. Shower theory parameters 73
5. Number of electrons as a function of depth . . 74
6. Factors entering lateral distribution function . 75

TABLES (CONT'D.)

TABLE

7. Values of $f_s(r)$	76
8. Number of electrons as a function of energy and shower radius as a function of energy and density	77
9. The weight function for lateral separation	82
10. The primary spectrum	83
11. Integral vertical density spectrum	84
12. Smoothed constants for interpolation functions	85
13. Effect of atmospheric structure on counting rate	86
14. Integral vertical frequency corrected for counter separation and atmospheric structure	87
15. Integral frequency including all zenith angles	88
16. Counting rate as a function of altitude	89
17. Comparison of theory and experiment	90
18. Estimate of uncertainties in calculation	91
19. Integral frequency spectrum as a function of direction	92
20. The angular distribution of showers	93
21. The mean shower radius as a function of s	94
22. Miscellaneous mathematical functions	95
23. Observed angular distributions	96

LIST OF FIGURES

FIGURE

1. Variation of the number of electrons with depth	97
2. Variation of the number of electrons with the energy of the initiating electron	98
3. Radial distribution functions	99
4. Variation of shower radius with the energy of the initiating electron and with electron density	100
5. Integrand for the integral vertical density spectrum	101
6. Integral vertical density spectrum	102
7. Variation of integral vertical frequency with depth	103
8. Variation of integral vertical frequency with depth when air density and counter separation are included	104
9. Comparison of density spectra for $t = 10$	105
10. Fit of theoretical curve to observational data of Hilberry	106
11. Comparison of theory with the observations of Kraybill	107
12. Comparison with the curve given by Kraybill over the entire altitude range	108
13. Theoretical variation of counting rate per unit solid angle with the zenith angle	109
14. Comparison of angular distributions	110
15. Geometrical arrangement of counters	111

I. INTRODUCTION AND CONCLUSIONS

Since its early investigation, cosmic radiation has yielded a series of such important physical discoveries as the finding of new fundamental particles, the determination of their characteristics, and, in some cases, it has led to a valid theoretical description of their interactions with one another. An important by-product of the discovery of the mesotron by Anderson and Neddermeyer (Ref. 1, 2) was the clarification and experimental verification of the Bethe-Heitler (Ref. 65) theory of the interaction of electrons and radiation in the domain of high energies. This quantum theory of radiation, along with the theory of multiplicative showers developed independently by Carlson and Oppenheimer, and Bhabha and Heitler (Ref. 3, 4), has in turn become a valuable analytical tool for the disentanglement of many complex phenomena observed in cosmic radiation. One of these problems is the question of the nature of the primary cosmic ray particles, and the genetic relationships between these particles and the secondary radiations observed in the atmosphere.

One facet of this fundamental problem is the interpretation of the large air showers which were experimentally studied in considerable detail by Auger and his collaborators (Ref.5). In this thesis we will investigate the altitude dependence of these showers from the point of view of the primary electron hypothesis. In particular, we will extend the previous theoretical investigations, which ranged only from sea level to mountain top heights (about 15,000 feet), up to a distance of only five radi-

ation units from the top of the atmosphere (about 39,000 feet). This extension will include that interesting range of altitudes where the observed counting rate curve exhibits a maximum.

1. Primary Particles

Broadly speaking, there are two different hypothesis as to the nature of the primary cosmic ray particles: the primary electron and the primary proton hypothesis. The large air showers are most easily described by means of primary electrons; but this description, which has been rather successful up to mountain top heights, on the basis of results given here, seems to be somewhat less successful at higher elevations. It is more difficult to explain the penetrating component and the presence of fast nucleons and stars on the basis of primary electrons, than by primary protons which give a natural explanation of these features and which are also suggested by the experiments of Schein and of Vallarta and their collaborators (Ref. 6, 7). There has been some difficulty (arising from the long lifetime of the mesotrons) in obtaining soft radiation rapidly enough from primary protons to explain the very high elevation found for the maximum of the Pfotzer curve, but the recent theories of Lewis, Oppenheimer, and Wouthuysen; Hamilton, Heitler and Peng; Heitler and Power; offer a reasonable mechanism for this process (Ref. 8, 9, 10). In particular (Oppenheimer (Ref. 63) has proposed that the soft radiation may be explained by the multiple production, by primary protons, of neutral mesotrons which rapidly decay into photons. Finkelstein has calculated

the lifetime of such neutral mesotrons and finds that they are indeed sufficiently short (Ref. 11).

With reference to the large showers themselves, there is a growing body of experimental evidence that they possess a complicated structure and penetrating components which, perhaps, are not describable by primary electrons and the cascade theory even assuming rather strong production of fast nucleons and mesotrons by the soft radiation. However, Cocconi and his collaborators do find evidence for the strong production, in lead, of penetrating particles by the soft radiation (Ref. 12a, 12b). Alichanian, Asatiani, and Muskhelishvili find narrow showers which seem to have a different structure from that of the large air showers as well as showers of penetrating particles (Ref. 13). George, Jason, and Trent find penetrating showers and penetrating bursts separately and also associated with the large air showers (Ref. 14, 15). Broadbent and Janossy have found considerable difficulty in explaining the mechanism of production in absorbers of penetrating particles by soft radiation, and have come to the conclusion that the penetrating particles which they have observed to be produced by soft radiation are not mesotrons (Ref. 16). This evidence is all recent, and has involved the utilization of rather complicated counter arrangements.

On the other hand, primary electrons have sufficed to describe with remarkable success the less elaborate studies of the large air showers in the lower portion of the atmosphere, and from this point of view it certainly is possible to assume that there are primary electrons as well as primary protons in

the energy range, 10^{14} to 10^{16} e.v., responsible for these showers. However there is a difficulty, first noted by Follin and studied by Feenberg and Primakoff, that collisions of electrons originating in intergalactic space with the photons of starlight and sunlight would be sufficient to reduce their energy below that of the cosmic ray range (Ref. 17, 18).

2. Status of the Shower Theory

After its initial development, the shower theory was put into convenient analytical form by Snyder and Serber (Ref. 17, 20). The theoretical calculation of the number of electrons in a shower as a function of the energy of the initiating electron and the distance from the point of initiation has been checked in many important features by the experimental studies of Anderson and Neddermeyer; Bowen, Millikan and Neher; and Arley (Ref. 21, 22, 23). Against this background, the theory has been subjected to careful study by Rossi and Klapman and also to critical discussion by Tamm and Belenky (Ref. 24, 25); and the analytical expressions given by Rossi and Greisen (Ref. 26), which will be used here (Sec. 5), have been shown to be generally satisfactory. It should be mentioned here, that this shower theory does not take into account the possibility of additional effects such as photo-nuclear production of fast nucleons or of mesotrons.

The spatial distribution (lateral distribution away from the shower axis) of electrons is given at present by theory with only rather indirect experimental tests. A value of approximately 60 meters (for air at sea level density) for the root mean square radius of the lateral distribution at the shower maximum is now

generally agreed upon by a number of investigators including Bethe, Nordheim, Wolfenstein, Moliere and their collaborators (Ref. 27 to 32). The most elaborate investigation of the detailed shape of the distribution has been given by Moliere on the basis of integro-differential equations derived by Landau which include both the lateral scattering of the electrons and the generation of new shower particles (Ref. 33, 34). Moliere's distribution, derived for the shower maximum, after suitable modification for positions off the maximum*, has been used here (Sec. 6).

The shower theory just described yields results for only the average number of particles and their average spatial distribution. The problem of fluctuations in the number of electrons has been studied theoretically by Furry; Nordsieck, Lamb, and Uhlenbeck; Scott and Uhlenbeck; Bhabha, and Heitler; and an exhaustive comparison of theory and experiment has been made by Arley (Ref. 35 to 39). The fluctuation problem is so complicated that so far it has not been treated in an entirely satisfactory manner. The general conclusion has been that the correct distribution lies somewhere between the one derived by Furry and the Poisson distribution. Fluctuations in the spatial distribution of electrons present an even more complicated problem since correlations in the electron density due to their manner of formation and to scattering will be superposed on their fluctuations in number. For the computations given here, no treatment of the

*The writer wishes to express his thanks to Professor R.F. Christy for suggesting the modification of the lateral distribution which has been used here.

effect of fluctuations has been included. This will make our values generally too low, which is not serious in itself since we have had to adopt a normalization procedure. However, our density distributions, $H(> p)$, (See Sec. 8, Fig. 6), become steeper at higher altitudes and this may be expected to make the correction larger at high altitudes than at low. Christy and Kusaka find a fluctuation correction of a factor of about 1.5 for mesotron induced ionization bursts (Ref. 40). The additional fluctuations of the spatial distribution of electrons would be expected to increase this in our case to a gross correction of 2 or more. The relative correction for high altitude as compared to sea level is obviously smaller, and should amount to something like a factor of 1.2 or less.

3. Success at Low Altitudes

Euler and Wergeland (Ref. 41) first calculated the effects of the large air showers by a method which has since had considerable success in the lower portion of the atmosphere. They assume an isotropic primary integral electron spectrum of the form $(\text{energy})^{-\gamma}$ with γ about 1.6 to 1.8 (See Heisenberg, Ref. 42), and use the shower theory to predict the effects of cascade electrons generated by the primary electrons on the counter systems employed by Auger and his collaborators (Ref. 5). Later work by Euler himself, Hillberry, Pomeranchuk, Migdal, Moliere, and particularly Cocconi and his collaborators has shown such satisfactory agreement between theory and experiment that this method must be considered very successful (Ref. 33, 43 to 48).

Wolfenstein was not able to account for the ionization bursts observed by Lewis (Ref. 49), but Lewis' results are very difficult to understand when compared with Hilberry's (Ref. 44) counter measurements which were carried out at the same place, and it is likely that ionization bursts due to slow heavy particles from nuclear disruptions and elsewhere completely smothered the effects of the large showers in Lewis' measurements. Recently Skobeltzyn, Zatsepin and Miller have made measurements with counter systems of very wide separation (up to 1000 meters) which seemed to be in very marked disagreement with the results of the theory (Ref. 50). However, Cocconi has shown that this disagreement arose from the neglect, in their calculations, of the apparent reduction in the separation of their counters for showers inclined at large angles with the vertical; and that the agreement is actually very good (Ref. 51). This is a severe and successful test of the theoretical lateral distribution. Recently Cocconi (Ref. 52) has calculated the altitude dependence of the large showers up to 15,000 feet and found reasonable agreement between theory and the experiments of Auger, Daudin, and Cosyns (Ref. 52, 53, 54).

The marked success of this method at lower altitudes makes it of considerable interest to extend it to higher elevations where further and perhaps more exacting tests of its validity may be made. The recent experimental determination by Kraybill and Ovrebo (Ref. 55,56) of the counting rate of the large showers as a function of altitude up to 40,000 feet with the demonstration of a maximum at 30,000 feet makes this especially desirable.

4. The Comparison of Theory and Experiment

(a) Variation of counting rate with altitude

In this thesis the shower counting rate as a function of altitude has been calculated, by a method first used by Cocconi (Ref. 46), for Kraybill's counter arrangement (Fig. 15, and Ref. 56), from sea level to 39,000 feet. The method of computation differs from that of Cocconi in two respects: the lateral distribution function adopted here has been modified in shape for positions off the shower maximum (Sec. 6) while Cocconi utilizes everywhere a shape corresponding to the shower maximum; the finite separation of the counters has also been taken into account (Sec. 9) while Cocconi has treated the calculation as if the counters were at the same place. This last correction is an essential feature of any computation extending above 15,000 feet (where, incidentally, Cocconi's calculations stop). In Parts II and III the computation is described in some detail. In order to reduce the labor of computation, the correction for the finite separation of the counters has been done in an approximate way (Sec. 9, 12). This approximation, and our omission of a treatment of fluctuations (Sec. 7) are both such as to make the theoretical counting rate computed in this way too low, each omission contributing a factor of roughly 1.2 so that the net reduction amounts to a factor of 1.5 to 1.4 or less. It may help to keep this in mind when studying the altitude dependence of the showers.

In computations of this kind it is usually necessary to adopt a normalizing procedure. This is not surprising, since the

primary spectrum we have employed (Ref. 42) has been determined partly by considerations of just this type (See, for example, Hillberry, Ref. 44, and also Sec. 12). The normalization we have adopted consists in multiplying our theoretical counting rate, N_a , by a factor of 3 determined by fitting our theoretical curve to Hillberry's data in the region from sea level to 15,000 feet (Fig. 10). From now on we will consider the correct theoretical counting rate to be given by $3N_a$, and will use this notation for this quantity. In Fig. 11 the curves $3N_a$, and also $8.33N_a$ are plotted along with Kraybill's curve and experimental points in the region from 15,000 to 39,000 feet. The $3N_a$ curve is seen to lie considerably below the experimental curve. The factor 8.33 was determined to bring the maximum of the theoretical curve roughly equal to the maximum of the experimental curve. Of course this throws off the normalization at low altitudes. The two curves, $3N_a$ and $8.33N_a$, are compared with Kraybill's experimental curve over the whole altitude range in Fig. 12, and it is clear that there is a marked discrepancy in the height of the maximum. The details in the shapes of the curves are somewhat different, the theoretical curve having a maximum at a lower altitude (10.5 radiation units as compared to 8.5 radiation units for the experimental curve) and falling off somewhat more rapidly at high altitudes. Expressed as the ratio to sea level, the maximum of the theoretical curve is only 24 compared to 64 for the experimental curve. So far as the position of the maximum is concerned, the uncertainties in the experimental points and in the theory are such that a suitable adjustment could bring

the two maxima to nearly the same place. However, there would remain the difficulty that the theoretical curve decreases more rapidly at high altitudes. The discrepancy in the height of the maximum may be expressed by the ratio $(64/24)^2 = (8.33/3) = 2.75$.

There are various effects which tend to reduce, somewhat, the magnitude of this discrepancy. There is a transition effect for the showers as they pass through the 1.3 gm./cm.² of aluminum and wood of the aircraft skin (Ref. 55). Near the maximum of the counting rate curve the showers are considerably inclined so that we may double the amount of material to obtain about 0.1 of a radiation unit with critical energy about half that of air. The most this can contribute to an increase in shower density is about two per cent, and since the counting rate varies about as (counter area)², a maximum increase in counting rate of four or five per cent is all that can be expected from this source.

The effect of the approximation used to correct for the finite counter separation may be estimated to be a reduction by a factor of 1.35 to 1.20. The former factor comes from an estimate of an "effective counter separation" based upon the average separation of the counters which turns out to be a separation of 6 feet rather than of 9 feet which was used in the computation (end of Sec. 10); the latter factor was based upon a detailed, but a posteriori, discussion of the errors introduced by this approximation (Sec. 13). It is believed that this latter estimate is more nearly correct.

The effect of fluctuations is very difficult to estimate.

The normalization procedure washes out many gross effects, leaving only the ratio of effects at higher altitude compared to those at low altitude. It is believed this may amount to a factor of 1.2 or less.

Taking all these effects together we obtain a factor $(1.05) (1.20) (1.20) = 1.50$, or at most a factor of $(1.05) (1.35) (1.20) = 1.85$. These may be compared with a factor of 2.75 needed to bring agreement between theory and experiment, and there still remains a discrepancy of a factor of 1.8 (more reliable) to 1.5 (less reliable). The discrepancy thus seems to be real although not, perhaps, as marked as indicated by Fig. 11. The rapid decrease of the theoretical curve above the maximum also remains rather hard to explain away, although the position of the maximum may well be given too low an altitude by our approximation.

(b) Variation of counting rate with zenith angle at 30,000 feet

The variation of counting rate per unit solid angle $N(x, \varphi)$ as a function of the zenith angle (θ, φ) , (Fig. 15) has been computed for Kraybill's counter arrangement at 30,000 feet and is shown in Fig. 13 (in this plot θ is represented via x where $x = \cos \theta$). From this has been derived the counting rate per unit plane angle by projecting the zenith angle, (θ, φ) , into the angle ψ lying in the plane of a cloud chamber (See Sec. 14 for details); and this last has been compared (Fig. 14) with the cloud chamber studies of Mr. E. W. Cowan (Ref. 57) who has determined this projected angle distribution at 31,000 feet

utilizing photographs taken of a cloud chamber controlled by Kraybill's counter arrangement. The details are given in Sec. 14.

The experimental distributions are listed in Table 23, and we note that from all the photographs taken at a given altitude only 20 or 30 per cent could be used since it was impossible to assign an angle in the remainder in an unambiguous way. Consequently the corresponding experimental angular distribution is in some doubt since the data hidden in the unclassified photographs could smother the tabulated distribution and might very well change its character altogether. A partial explanation of the difficulty found in assigning a direction to the electrons appearing in the photographs may lie in the relative orientation of the counter system and the cloud chamber (Fig. 15). In Fig. 14 the counting rate per unit solid angle has been shown as the dashed curves for $\varphi = 0$ and $\varphi = 90^\circ$ where for these two curves the angle ψ is to be understood as meaning the angle θ . The much larger maximum for the $\varphi = 0$ curve (it goes off scale, but has a maximum 3 times the $\varphi = 90^\circ$ curve) as compared to the $\varphi = 90^\circ$ curve is evident. The showers at $\varphi = 0$, however, lie in a plane perpendicular to the plane of the cloud chamber, and consequently just these more numerous showers with the large inclination to the vertical will be rendered difficult to classify.

The theoretical projected distribution has been calculated for all showers and for those showers (about 20% of the total, which corresponds to the 20% which could be classified) for which

the zenith angle lies in a region adjacent to the plane of the cloud chamber and outside of the directions contained in a right circular cone with vertex in the center of the cloud chamber and axis perpendicular to the face of the cloud chamber with half vertex angle equal to $\arccos 0.25$ (the edges of the cloud chamber are given by $\arccos 0.16$). This latter partial projection was selected to take into account the possibility that showers lying near the perpendicular to the face of the cloud chamber could not be classified. The "partial projection" distribution is shown as a solid curve in Fig. 14 and is seen to be even higher than the "total projection" also shown as a solid curve.

(All curves were arbitrarily normalized to 10 at $\psi = 0$ so that their shapes could be compared). The experimental distribution A (See Table 23) was considered as representative of the experimental results and is shown as the stippled curve in Fig. 14, it falls off twice as rapidly with increasing angle as either of the two theoretical curves.

The result of the comparison is that the half angle for the experimental distributions is in the range of 15 to 20 degrees in every case while the half angle for the theoretical total projection is about 30 degrees, and is even larger for the partial projection. On the basis of angles for half maximum the experimental distributions lie between 30 and 40 degrees, and the theoretical between 60 or 70 degrees. We have a body of experimental data which are consistent within themselves and also consistently in disagreement with the theoretical distribution, being too narrow. Two other factors that may bias this comparison

are the selection of the photographs for measurement, which was done by requiring that there be ten or more parallel tracks; and the fact that the comparison is made for different altitudes. The ten track requirement corresponds to a requirement of high particle density and near the counting rate maximum, where these data were taken, on the general grounds of a longer distance for shower multiplication one would expect this to broaden, not narrow, the observed distribution. The theoretical curves would be made broader, and so increase the disagreement, if a correction for this is introduced. The theoretical computation, made at a slightly lower altitude than the observations, would be expected to be narrower than the "correct" theoretical curves and therefore a correction for this would also increase the disagreement.

This discrepancy is all the more surprising since an approximate angular distribution may be inferred from Kraybill's observed altitude curve by means of a Gross transformation, and this derived angular distribution agrees rather well with the theoretical one and not at all with the distribution obtained from the cloud chamber studies.

The disagreement found here between the cloud chamber and theoretical distribution should not be given too much weight because of the uncertain statistics of the former. Nevertheless it is surprising and interesting, and has been given some study since instances of the investigation of cosmic radiation by the simultaneous application of counter and cloud chamber techniques are rather rare.

(c) Conclusions

There seems to be a discrepancy between the theoretical variation of counting rate with altitude, based on the assumption of primary electrons, and the variation observed by Kraybill (Ref. 56). The experimental curve exhibits a stronger maximum by a factor of 2.75 when compared with the theoretical curve. Various approximations present in the theoretical calculation are such as to reduce this discrepancy, but an estimate of their magnitude seems to leave a discrepancy of a factor of 1.5 to 2.0 still remaining. The maxima of the two curves are not at the same place (The depth at the maxima from the top of the atmosphere, t , measured in radiation units, is 8.5 for the experimental and 10.5 for the theoretical curve.), but this difference may well be accounted for by uncertainties in the observations and calculations. The more rapid decrease of the theoretical counting rate above the maximum as compared to the experimental is more difficult to explain away.

It is possible that a more accurate calculation of the altitude effect taking into account the effect of fluctuations and making no computational approximations would remove the discrepancy found here, but the study presented here makes this unlikely. It may also be possible to remove this discrepancy within the domain of the primary electron hypothesis by selecting a smaller value, say 1.7 or 1.6 rather than the value 1.8 used here, for the exponent in the primary electron spectrum. However, the normalization procedure of fitting theory to experimental data in the lower portion of the atmosphere will have to be followed,

and this might make such a treatment unsuccessful.

Lewis, Oppenheimer, and Wouthuysen (Ref. 8) have proposed a mechanism for the multiple production of secondaries by primary protons. Their mechanism should lead to a stronger maximum at higher elevations for the counting rate curve, and therefore should yield better agreement with the observations than the curve derived here assuming primary electrons.

There has been found a rather marked disagreement between the theoretical angular distribution of showers at the maximum of the counting rate curve and one observed by means of a cloud chamber (Ref. 57). The observed distribution being twice as narrow as the theoretical one. Too much weight should not be given this discrepancy since the statistical basis of the cloud chamber distribution is rather insecure and because the angular distribution inferred from Kraybill's observed altitude dependence by means of a Gross transformation is in rather good agreement with the theoretical distribution. Nevertheless this point deserves further investigation, and something of interest may turn up.

Finally, it may be said, that the results of the present investigation indicate that the primary electron hypothesis which has been remarkably successful in describing the experimental studies of the large showers in the lower portion of the atmosphere has encountered some difficulties upon being extended to higher elevations, and that the satisfactory answers formerly derived from it may be looked upon as the result of a highly successful prescription rather than as proof of the real exist-

ence of primary electrons.

II THE SHOWER THEORY

The shower theory describes the multiplication of a single high energy electron* or photon by virtue of the processes of pair production and bremsstrahlung (Ref. 58) into a shower consisting of many electrons and photons (Ref. 59). The multiplication depends upon the material in which the shower occurs, and is stopped by dissipation of the incident energy through ionization of the surrounding atoms by the shower electrons. As a shower develops, it keeps a generally well defined direction or axis, but the electrons, due chiefly to multiple coulomb scattering by the nuclei of the surrounding material, also spread out laterally in a direction perpendicular to the shower axis. In many cases, depending on the surrounding material, one may separate the development of the shower along the axis from the lateral spreading of the electrons. This is possible when the angle of deflection of the electrons is small enough so that their path of travel is nearly the same as the projection of the path on the shower axis, and is a satisfactory approximation for showers in air, water, and aluminum but not for lead. This approximation is adopted here. A suitable description of both the number and lateral distribution of electrons is needed for interpretation of many experiments with cosmic radiation. In most cases, the distribution of photons may

*The term electron will be used for both positive and negative electrons.

be neglected, since it is the ionization produced by electrons which is detected by counters and ionization chambers.

5. The Number of Electrons

We will now consider the calculation of the number of electrons as a function of the distance along the shower axis, and of the energy of the initiating electron. The expressions giving the total number of electrons as a function of depth have been subject to experimental study and critical discussion (Ref. 21, 23, 24, 25, 39), indicating that their uncertainty is less than that introduced by the rather incomplete treatment of fluctuations (Sec. 7). In fact, this constitutes one of the successful tests of the correctness of the quantum theory of radiation. The more detailed expressions giving the energy distribution of the electrons are somewhat less accurately known. We will consider only electron (not photon) initiated showers.

The development of a shower depends upon the material in which it occurs, but it may be described in a dimensionless form independent of the material by expressing lengths along the shower axis in terms of a "radiation length" (length measured in these units will be denoted by t), lengths perpendicular to the shower axis in terms of a "lateral unit" (lateral distances measured in these units will be denoted by r), and energies by their ratio to a "critical energy" denoted by β . The radiation length is defined as the distance an electron must go to reduce its energy to $1/e$ of its initial value due to bremsstrahlung, and is about $7/9$ of the distance a photon must go in order to produce a pair. The critical energy is the amount of

energy an electron loses by ionization in going one radiation unit. Thus an electron with the critical energy is likely to be stopped by ionization rather than multiply further, and so may be considered as lost to the shower. For any one substance, it turns out that the lateral unit is a constant multiple of the radiation unit, although the ratio of the two units varies from substance to substance.

Fundamentally, the radiation unit depends upon the number of nuclei or the amount of matter which the shower traverses, and it is most appropriately expressed as a number of grams per square centimeter. However, it is useful and sometimes necessary to have a geometrical measure of the radiation unit. This is listed in the table below (from Ref. 33), and the data for air correspond to sea level density. If the air density decreases, then the size of the radiation unit and the lateral unit undergoes a corresponding increase (See Table 1). The values for lead are only approximate because of the large scattering.

TABLE I. SHOWER THEORY UNITS

Substance	Radiation Unit, cm.	Lateral Unit, cm.	Critical Energy, (10^8 e.v.)
Air	33,000	5950	1.13
Water	43	7.8	1.13
Aluminum	9.6	3.1	0.63
Iron	1.8	1.2	0.31
Lead	(0.51)	(1.0)	(0.10)

Rossi and Greisen (Ref. 26, approximation B) give a parametric expression for the number of electrons in a shower which is used here. It may be written as follows:

$$\Pi = K(s) e^{l(s)t + \epsilon s} [1 + n(s)t]^{-\frac{1}{2}} \quad (5.1a)$$

$$t = \frac{s\epsilon - 1}{m(s)} \quad (5.1b)$$

$$\epsilon = \ln(E/\beta) \quad (\text{See Table 2 for air}). \quad (5.1c)$$

The functions K , l , m , n are given in Table 4 and have been recomputed from functions tabulated by Rossi and Greisen in order to have the more convenient form of Eq. 5.1. The symbols are defined as:

Π = the total number of electrons in the shower.

t = distance or depth along the shower axis from the point of initiation measured in radiation units.

E = energy of the initiating electron measured in the same units as .

β = the critical energy. (10^8 e.v. was used for air in the computations given here. This is very near 0.98×10^8 as given by Rossi and Greisen, Ref. 2, and believed more reliable than Moliere's value, Ref. 33, given in Table I).

s = a parameter entering the shower theory.

The parameter s will be used (Sec. 6) as a guide in constructing a lateral distribution function; consequently, its

behavior will be discussed. It increases with depth for fixed initial energy, and decreases with increasing energy for fixed depth. At $s = 1$ the shower has the maximum number of electrons. The maximum number of electrons and the position of the maximum is listed in Table 3.

The general nature of Eq. 5.1 is illustrated as follows: The variation of the number of electrons with depth for various fixed energies is listed in Table 5 and plotted in Fig. 1. The parameter s is also plotted in Fig. 1 as if it were a dependent variable, and may be seen to vary rather slowly. The variation of the number of electrons with initiating energy for various fixed depths is listed in Table 8 and plotted in Fig. 2. The parameter s is again plotted as if it were a dependent variable. The much less rapid increase of the number of electrons with energy for $t = 5$ than for $t = 10$ is noteworthy. It is primarily due to the smaller value of s at the smaller value of t . Physically, it means that five radiation units are not enough for much multiplication to take place, and large increases in the amount of energy produce only a moderate increase in the number of electrons. This tendency will appear later later as a strong cut-off in the counting rate at $t = 5$.

6. The Lateral Distribution

The lateral spreading of the shower electrons away from the shower axis has only recently (1940) been the subject of theoretical investigation (Ref. 27 to 32, 41, 43, 45). So far, the results of these investigations have not been subject to direct quantitative verification, as has been the case for the number of electrons, although indirect comparisons seem to be in rea-

sonable agreement with counter observations on the large air showers carried out at elevations ranging from sea level to mountain top heights (Ref. 33, 44, 51). Furthermore, the fluctuations in the surface density of electrons in a shower around the average distribution will be expected to be much greater than the fluctuations in the number of electrons, since the fluctuation of their distribution in space will be superposed on their fluctuation in number. In particular, Auger's studies (Ref. 5) seemed to indicate that the density fluctuations do not follow a Poisson distribution, although the interpretation of his results is uncertain because of the effect of the walls of his cloud chamber, and because he had two 1.0 millimeter tungsten and one 5 millimeter lead plates in the chamber. When the problem of the mean radial density distribution is solved, there will still remain much to be done.

An incorrect estimate of the lateral spreading of the shower electrons will affect computed effects considerably, since, if one defines a mean shower radius in a suitable way, then the counting rate will vary roughly as $r_m^{-1.6}$ (See the end of this section). For these various reasons, a rather elaborate discussion of the lateral distribution is given.

(a) General discussion

The lateral or radial spreading of the electrons out from the shower axis is due mainly to their multiple coulomb scattering by the nuclei in the surrounding material, the angular divergence arising from the process of their creation being negli-

gible when compared with the scattering deflection. The shape of the radial distribution at the shower maximum is approximately of the form $(1/r) \exp(-r)$, the earlier investigations being mainly concerned with estimating the mean radius (i.e. the size of the unit to be used when writing the expression above) of the shower. This mean radius has undergone wide fluctuations as more refined theoretical investigations were undertaken, ranging from about 20 meters in the pioneer investigations of Euler, Wergeland, and Hilberry (Ref. 41, 43,44) to 120 meters in the studies of Pomeranchuk and Migdal (Ref. 47, 48), and finally settling down to about 60 meters in the more recent work of Bethe, Wolfenstein, Moliere, Nordheim, Richards, and Roberg (Ref. 27 to 33, see also 26). In these investigations (excluding Moliere), the mean radius was calculated on the basis of the mean square angular deflection at a given energy (Ref. 60) averaged in an appropriate way over the energy spectrum of the electrons, and over the scattering for about one radiation unit. This distribution was then "grafted on" to the one dimensional shower theory.

The physical reasons for this procedure are quite reasonable. The mean square angular deflection of an electron in a thickness of matter dt is given by (Ref. 60):

$$\overline{\theta^2} = (E_s/E)^2 dt \quad (6.1)$$

where E is the energy of the electron, and the constant E_s is about 2.1×10^7 e.v. In air, this energy is somewhat less than the critical energy, (10^8 e.v.) so that only electrons, with the critical energy or less, will undergo appreciable deflection.

However, electrons with the critical energy will be stopped and lost from the shower in about one radiation length, so that it seems reasonable to set dt equal to unity in Eq. 6.1. The general picture is this: only rather low energy electrons will be appreciably scattered and contribute to the lateral distribution of the shower, but these electrons will be lost in one radiation length, so that most of the scattering takes place in the last radiation unit. For this reason, the general shape of the distribution will not change very much as the shower develops. The exponential lateral decay follows from the same considerations.

(b) The lateral distribution adopted

However, these arguments of a general nature do not give a very precise notion of the shape of the distribution; in particular the contribution to the distribution of the scattering in the earlier generations is not very carefully treated. Landau (Ref. 34) has set up equations which combine both the development of the shower and the scattering in a suitable way. Recently, Moliere (Ref. 33) has solved these equations by a difficult numerical procedure, and obtained the distribution function at the shower maximum which can be represented with good accuracy by an expression of the form

$$(1/r) [A \exp(-\alpha r) + B \exp(-\beta r)]$$

(See Fig. 3). This is the most reliable distribution function so far available. For our calculations, we will adopt this expression at the shower maximum, but introduce a slight modi-

fication* to take into account the change in shape of the distribution on either side of the maximum. The expression adopted for the surface density, ρ , of the shower electrons is:

$$\rho = \Pi(E, t, s) f_s(r) \quad (6.2a)$$

$$f_s(r) = \frac{1}{r^{2-s}} R(s) R_1(r) \quad (6.2b)$$

$$R(s) = \left[2\pi \Gamma(s) \left(\frac{A}{\alpha^s} + \frac{B}{\beta^s} \right) \right]^{-1} \quad (\text{See Table 6}), \quad (6.2c)$$

$$R_1(r) = Ae^{-\alpha r} + Be^{-\beta r} \quad (\text{See Table 6}), \quad (6.2d)$$

Here: $A = 2.94$, $B = 0.31$,

$\alpha = 2.88$, $\beta = 0.855$ per lateral unit.

t = depth along shower axis in radiation units.

E = energy of the initiating primary electron.

r = the radial distance from the axis of the shower, measured in lateral units. (about 60 meters for air at sea level).

ρ = the surface density of electrons, measured as the number of electrons per square lateral unit (the number in a square 60 meters by 60 meters for air at sea level).

Π = the total number of electrons in the shower.

s = the shower theory parameter, which is defined implicitly when E and t are given.

*The writer wishes to thank Professor R.F. Christy for suggesting this modification.

$R(s)$ = a normalizing factor chosen so that the integral of the density equals Π , ($\int_0^{\infty} \rho 2\pi r dr = \Pi$).

On setting $s = 1$ (the shower maximum), we obtain Moliere's distribution. For s different from unity, the shape of the shower is slightly modified (while retaining the gross features of the distribution represented by the exponential terms) to give a more appropriate radial function. In a general way, it is clear that a modification of this type is required, since for $s < 1$ the average energy of the shower electrons is greater than at the maximum and so they will scatter less. Eq. 6.2 indicates a correspondingly greater density near the shower axis. A converse situation obtains beyond the maximum. One may see that the analytic form of Eq. 6.2 is reasonable by constructing the approximate density distribution in the vicinity of the shower axis.

(c) Density in the vicinity of the axis

The mean square angular deviation given by Eq. 6.1 implies (assuming the angles are small enough so that the angle is equal to its sine) that the radial distribution of those electrons, which have the same energy, may be represented by a Gaussian function of the form:

$$\rho(E, r) = \frac{1}{2\pi} \left(\frac{E}{E_s} \right)^2 \exp \left[-\frac{1}{2} \left(\frac{E}{E_s} r \right)^2 \right] \quad (6.3)$$

Here: E = the energy of the electrons in the shower, (not the initiating electron).

r = radial distance from the shower axis in lateral

units.

E_s = a scattering energy (about 6.6×10^7 e.v. for air). (This is different from the E_s of Eq. 6.1 by the factor (330/60) introduced because the radial distance is measured in lateral units, not radiation units, and also by the factor (1.2/2.1) which was determined by Roberg (Ref. 31) by a self-consistent method of treating the scattering of electrons.)

The probability, p , has been normalized so that

$$\int_0^{\infty} p 2\pi r dr = 1.$$

From the shower theory (Ref. 26, Approximation A) we have for the differential energy spectrum of the shower:

$$\pi(E_0, E, t) dE = -\frac{dy}{2\pi i} \int_{\delta-i\infty}^{\delta+i\infty} ds H_1(s) e^{y^s + \lambda_1(s)t} \quad (6.4a)$$

$$y = \ln(E_0/E) \quad (6.4b)$$

Here: $\pi(E_0, E, t)dE$ = the number of electrons in the shower with energy within dE at E .

E_0 = the energy of the initiating electron.

E = the energy of the shower electrons.

t = the depth below the start of the shower, in radiation units.

$H_1(s)$, $\lambda_1(s)$ are functions tabulated in Ref. 26.

s = a parameter of integration.

Eq. 6.4 does not take into account energy loss of the shower due to ionization of the air. It gives a reliable estimate of

the spectrum of the electrons only for energies five to ten times the critical energy; below this energy it predicts much too large a number of electrons. We may now estimate the radial distribution of the electrons by integrating over the energy:

$$\rho(E_0, r, t) = \int_{5\beta}^{\infty} \pi(E_0, E, t) dE \rho(E, r) \quad (6.5)$$

The integration may be extended to infinity on the upper limit, since the spectrum is zero for E above E₀. We will also take the lower limit to be zero, since the excessively large number of electrons at low energy will be diluted by distribution over a very large area by the scattering function ρ . Since we are only interested in the density near the axis, where there are mostly high energy electrons, this will not introduce a serious error. With these limits, and exchange of the order of integration, an elementary integration yields:

$$\rho(E_0, r, t) = \frac{1}{4\pi^2 i} \int_{\delta-i\infty}^{\delta+i\infty} ds H_1(s) e^{\lambda_1(s)t} \frac{1}{r^2} \left(\frac{E_0 r}{\sqrt{2} E_s} \right)^s \Gamma(1 - \frac{s}{2}) \quad (6.6)$$

This integral may now be evaluated by the saddle point method (See Ref. 26) to give:

$$\rho(E_0, r, t) = \frac{1}{(2\pi)^{3/2}} \frac{1}{r^2} \frac{H_1(s) \Gamma(1 - \frac{s}{2})}{\sqrt{\frac{1}{4} \psi'(1 - \frac{s}{2}) + t \lambda_1'(s)}} \left(\frac{E_0 r}{\sqrt{2} E_s} \right)^s e^{\lambda_1(s)t} \quad (6.7a)$$

$$\ln \left(\frac{E_0 r}{\sqrt{2} E_s} \right) = \frac{1}{2} \psi(1 - \frac{s}{2}) - t \lambda_1'(s) \quad (6.7b)$$

Here Γ is the usual Γ -function, ψ is its logarithmic derivative, and $\frac{d}{dx} \psi(x) = \psi'$. The functions H_1, λ_1 , etc. are tabulated (Ref. 26). As a matter of fact, Eq. 6.7 gives an estimate of the density for small r which agrees very well with the numerical values obtained by Wolfenstein, (Ref. 32) using a more correct energy spectrum and numerical integration. It is obvious that Eq. 6.7 cannot be correct for large r , since, in general, $\int_0^{\infty} \rho^2 \pi r dr$ will not converge. (This is not surprising since the energy integral of the electron spectrum, if extended to zero, will diverge; and we find this infinite number of electrons again when we go to large distances where they have been placed by the scattering function.)

However, the fact that Eq. 6.7 gives numerical values in good agreement with a more accurate procedure indicates that it may be used as a guide to modify Moliere's distribution function, when away from the maximum. We notice that the radial dependence is of the form $1/r^{2-s}$ and for $s = 1$ it gives $1/r$ as in the case of Moliere. Furthermore, this same radial dependence, at short distances, has been derived by Pomeranchuk and Migdal (Ref. 47, 48) by a different method, so that one may feel somewhat more confidence in it. This, then, gives the analytic form indicated in Eq. 6.2.

For very short distances, the electron density increases without limit. This cannot be correct, because, even if all the electrons in the shower had the energy of the initiating electron, they would be scattered over a circle of finite though perhaps small radius given by inserting the initial energy into

Eq. 6.1, with $dt = 1$. Actually, this density increase must stop at some larger radius, since even the most energetic shower electrons must have an energy less than that of the primary. The extremely short radii, where this failure of the expression occurs, contribute nothing to our computations except for the vertical integral density spectrum above $t = 10$, when there is no correction for the counter separation (Sec. 8, 9). When a correction is made for counter separation, and this was done in computing the counting rate to compare with the observations, the effect of this divergence at small radii is completely removed.

(d) Description of the radial function

The radial function, Eq. 6.2, is listed in Tables 6 and 7, and in Fig. 3 $\ln(rf_1(r))$ is compared with the corresponding function of Moliere. In Table 21, values of the mean radius are given as a function of s , expressed as meters for air at sea level density, and as the ratio to the radius at $s = 1$. The root mean square radius at $s = 1$ is 57 meters, agreeing with other investigators. It will be noted that the mean radius, which is somewhat more sensitive to changes in the shape of the lateral function than the root mean square radius, varies considerably with s so that an adjustment in the shape of the lateral function should certainly be made for showers off the maximum.

One may also obtain some idea of the significance of the modification of Moliere's function in the following way. If the integral primary electron spectrum is given in the form

$D(\beta/E)^\gamma$, and we assume that the shower electrons are spread uniformly over a circle of the mean radius, r , then the frequency of occurrence of a density of ρ or greater will be given by:

$$H(>\rho) = \pi r^2 D(\beta/E)^\gamma \quad (6.8)$$

where E on the right side is that E which is just sufficient to produce the density ρ . Now, the density ρ is approximately related to E by an expression:

$$\rho = \frac{\pi}{\pi r^2} = (\text{approx.}) \frac{G_1(E/\beta)^s}{\pi r^2} \quad (6.9)$$

where G_1 depends on t , but only weakly on E . Substituting Eq. 6.9 into Eq. 6.8 we obtain:

$$H(>\rho) = (\text{approx.}) \left[D \pi^{(1-\frac{\gamma}{s})} G_1^{\frac{\gamma}{s}} \right] \frac{1}{\rho^{\frac{\gamma}{s}}} \frac{1}{(r^2)^{\frac{\gamma}{s}-1}} \quad (6.10)$$

Thus the integral frequency (and the counting rate which is roughly proportional to $H(>\rho)$) varies as $r^{-2(\gamma/s-1)}$. This function of $r(s)$ is given in Table 21 in terms of its value at $s = 1$, assuming $\gamma = 1.8$. This gives a rough notion of the effect that the change in shape of the radial distribution has on the counting rate. For very small values of s (below 0.6), the very large increase indicated in Table 21 is misleading since it is due to those extremely small radii for which the radial distribution is not valid. As mentioned above, these small radii contribute nothing to the computation of those counting rates which are compared

with experiment.

7. Fluctuations

The shower theory just outlined gives only the average number of electrons and their average distribution in space. For any individual shower, it must be expected that there will be considerable fluctuations away from this average. These fluctuations would be expected to alter the results of computations based only on the average values. Arley (Ref. 39) has given a rather exhaustive discussion of the fluctuations in the number of particles (Ref. 26 also gives a list of references regarding this problem; see also Ref. 38). So far, no attempt has been made to investigate fluctuations in the spatial distribution of electrons except for a discussion of local correlation of electron pairs (Ref. 47, 61).

(a) Experiments related to the fluctuation problem

It has been mentioned that the spatial distribution observed by Auger and co-workers (Ref. 5) utilizing a combined counter-cloud chamber technique does not seem to follow a Poisson distribution very closely, although the presence of metal plates in his cloud chamber makes the interpretation of his results uncertain. In the comparison between theory and experiment given by Moliere (Ref. 33), in which he computes the coincidence counting rate for two counters as a function of their separation and compares it with Auger's experiments, the experimental counting rate considerably exceeds the calculated counting rate for sepa-

rations in the range from 10 cm. to 1.0 meter. Moliere suggests that this discrepancy may be due to the fact that, in his calculations, he used throughout the lateral distribution function corresponding to the shower maximum, and that, if he had modified the shape of the function for showers not at their maximum, he would have obtained better agreement. The results of the calculations in this thesis indicate that only showers very near their maximum, or beyond (but not before), contribute very much to the counting rate at these separations at sea level. On quite general grounds, (Sec. 6) it is difficult to see how the spatial distribution could be narrower beyond the maximum than at the maximum. Consequently, the explanation offered by Moliere does not seem to be satisfactory.

Pomeranchuk and Berestetzky (Ref. 47, 61) have offered an explanation of this discrepancy by computing the local spatial correlations of pairs of electrons due to the fact that the shower electrons are produced in pairs in which both electrons originate at (macroscopically) the same point. Their results seem to explain this particular discrepancy satisfactorily. However, the same rapid increase in counting rate for small separations has been observed by Geiger and Stubbe (Ref. 62) utilizing five and six-fold coincidences. This observation would seem to make the explanation based on pairs untenable, although the general notion of local spatial correlation of the shower electrons, because of their manner of formation, seems reasonable. Thus, one would expect both this sort of correlation and chance correlations due to scattering to play a part

in the density fluctuations.

It may be that the excessive counting rate at narrow counter tube separations may be due to a different mechanism than fluctuations, such as local showers initiated by meson decay or knock on electrons from mesons.

(b) Procedure adopted

Since there is no adequate theory of the spatial fluctuations, no attempt has been made to include either spatial fluctuations or fluctuations in the number of particles in these computations. It may be remarked that the fluctuations would be expected to increase the frequency of the integral density curve, and hence the counting rate as compared to a computation with no fluctuations. This follows (assuming a moderately symmetrical distribution) from the rapid decrease of this curve with increasing density (See Fig. 6). Fluctuations upward from the very numerous low density portions of the curve should overcompensate for the loss of portions of the high density events, due to the same type of fluctuations. In taking into account fluctuations in the number of electrons produced by mesotrons in lead, Christy and Kusaka (Ref. 40) found an increase of a factor of about 1.5 as compared to a calculation not including fluctuations. In our case, the fluctuations may be expected to introduce possibly a factor of two or more since fluctuations in the spatial distribution also enter.

III COMPUTATIONS

This Part will outline the computational procedure followed in order to calculate various effects to be compared with experiment. Our general approach will be one first followed by Cocconi (Ref. 46), which has the advantage that a large portion of the calculation may be completed before inserting the specific details of any particular measuring apparatus.

The basic calculations will all be carried out using shower units and lateral units which change their geometrical values as the air density varies with altitude (Table I and Table 1). This is done to avoid a great deal of tedious conversion of units in the great bulk of the computation. This should be borne in mind when inspecting the results of calculations which do not yet include this correction.

The differential primary electron spectrum adopted is essentially the same as that of Euler, Heisenberg, and Cocconi (Ref. 41, 42, 43, 46), but has been expressed in units especially appropriate for the computations:

$$P(E)dE d\Omega = D\left(\frac{\beta}{E}\right)^{\gamma} \frac{dE}{E} d\Omega \quad (\text{III.1})$$

$$E > 10^{10} \text{ e.v.}$$

Here: $P(E)dE d\Omega$ = the number of primary electrons per hour which strike on one square lateral unit (at sea level density 60 x 60 meters) within the solid angle $d\Omega$ and the energy range dE at E .

β = the critical energy in air, 10^8 e.v.

$$D = 7.52 \times 10^{12} / (\text{hr.})(\text{lateral unit})^2(\text{steradian}).$$

$\gamma = 1.8$ for the computations in this thesis.

The corresponding integral spectrum is:

$$P(>E) = \frac{2\pi}{\gamma} D \left(\frac{\beta}{E}\right)^\gamma; E > 10^{10} \text{ e.v.} \quad (\text{III.2})$$

Here $P(>E)$ is the number of electrons of energy greater than E , which strike one square lateral unit per hour from any direction in the upper hemisphere.

8. Vertical Density Spectrum

In this section, we will calculate the integral density spectrum at any (various) point in the atmosphere due to primaries that enter the atmosphere within the small solid angle $d\Omega$ near the vertical. This is the frequency per hour $H^Y(>\rho, t)d\Omega$ with which a surface density of electrons, equal to ρ or greater, will pass any point in the atmosphere at depth t .

In Sec. 5, 6 there was derived an expression for the density of electrons due to a shower initiated by a primary of energy E , at a depth t , and at a distance r from the axis of the shower:

$$\rho(E, t, r) = \prod(E, t, s) f_s(r) \quad (8.1)$$

Conceptually (and numerically) we may invert this equation to obtain:

$$r = r(t, \rho, E) \quad (8.2)$$

Note that for given E and t , if the density is ρ at r , then it is greater than ρ for any radius smaller than r . Hence, if we consider only showers due to primaries of energy E , then those

primaries striking on or within a circle of radius r , given by Eq. 8.2 about some fixed but arbitrary point at depth t , will give rise to a density of ρ or greater. The total vertical frequency will be obtained by integrating over the primary energy to obtain:

$$H^V(>\rho, t) = \int_0^{\infty} \pi [r(t, \rho, E)]^2 P(E) dE \quad (8.3)$$

The lower limit may be taken to be zero, since r goes to zero very rapidly for energies below 10^{10} e.v. For ease of computation, it is best to make the transformation

$$\varepsilon = \ln(E/\beta) \quad (8.4)$$

which gives, on inserting the primary spectrum:

$$H^V(>\rho, t) = \pi D \int_{-\infty}^{\infty} d\varepsilon e^{-\gamma\varepsilon} [r(t, \rho, \varepsilon)]^2 \quad (8.5)$$

Some general features of the integral vertical density spectrum are revealed by an approximate treatment of Eq. 8.3. If one neglects the dependence on s of $f_s(r)$ in Eq. 8.1 by substituting $f_1(r)$, and makes use of the fact that $\Pi(E)$ varies roughly as E^s (See Fig. 2), then the inversion implied by Eq. 8.2 may be written as:

$$r = f_1^{-1}\left(\frac{\Pi}{\rho}\right) = f_1^{-1}\left(\frac{G_1\left(\frac{E}{\beta}\right)^s}{\rho}\right) \quad (8.6)$$

where G_1 and s depend on t but vary slowly with E , and are assumed constant in our approximation. Inserting Eq. 8.6 and III.1 into 8.3 we obtain:

$$H^V(>\rho, t) = \pi D \int_0^{\infty} \left[f_1^{-1} \left(\frac{G_1 (E/\rho)^s}{\rho} \right) \right]^2 \left(\frac{\beta}{E} \right)^{\gamma} \frac{dE}{E}$$

The change of variable:

$$u = (G_1 / \rho) (E/\rho)^s \quad (8.7)$$

gives:

$$H^V(>\rho, t) = \pi D \rho^{-\frac{\gamma}{s}} \int_0^{\infty} \frac{G_1^{\frac{\gamma}{s}}}{s} \left[f_1^{-1}(u) \right]^2 \frac{1}{u^{\frac{\gamma}{s}}} \frac{du}{u} \quad (8.8)$$

This shows that the integral vertical frequency will vary approximately as a power law in ρ with the power approximately $(-\gamma/s)$. In particular, the ratio γ/s should get smaller at greater depths in the atmosphere, since s increases with t .

These general considerations are borne out by the corresponding numerical values. In Table 8 and Fig. 4, the shower radius (Eq. 8.2) is shown as a function of t, ρ and ϵ . The integrals (Eq. 8.5) are listed in Table 11 and plotted in Fig. 6 and 7. In particular, Fig. 7 shows that below about $t = 10$ the integral vertical frequency for constant ρ varies roughly as $\exp(-\rho t)$.

The simple change of variable indicated in Eq. 8.4 has been of very great help in reducing the amount of labor necessary to carry out the numerical integrations. It was done primarily to eliminate the importance of the "tail" on the high energy side of the integrand, since for large energies r rises slowly with ϵ (Fig. 4), while the primary spectrum decreases as $\exp(-\gamma\epsilon)$, (Table 10) so that the integrand falls off exponentially. Consequently, in the ϵ -scale the "tail" will contribute no more to

the integral than the last value neglected, while, in the E-scale, one must integrate over about three orders of magnitude before the "tail" is negligible. In addition, this change of variable also made the primary spectrum (Table 10) much easier to handle, and indicated a useful integration technique. In the ϵ -scale, the integrand resembles a Gauss function (See Fig. 5), and, by measuring the breadth at $1/e$ of the maximum, the integral could be taken to be $(\sqrt{\pi}/2)(\text{breadth})(\text{height of maximum})$. The integrand and its "equivalent" Gauss function are plotted in Fig. 5. In this particular case, the value of the integral, obtained by the "numerical saddle point" procedure, was 2.264×10^{-13} while a careful application of Simpson's method gave 2.270×10^{-13} . Spot checks for other integrals consistently gave as satisfactory results. This method was adopted for this set of integrations.

In Table 12, are listed a number of constants entering into some convenient interpolation formulae for the density spectrum, for t greater than fifteen radiation units. These constants have been obtained by graphically smoothing the results of the calculation.

9. Correction due to Lateral Counter Separation

The calculations, indicated in Sec. 8, give the density spectrum at a single point, but counter systems are usually separated by lateral (horizontal) distances of a few meters in order to register only showers which are energetic enough to produce a rather high electron density over large areas. In this section,

we will calculate the frequency, $H^Y(>\rho, t, a) d\Omega$, with which a surface density of ρ or greater occurs at a given point in the atmosphere, when, at the same time, a density of ρ or greater occurs at a second point, separated from the first by a distance $2a$. This will be done only for showers which are initiated by electrons entering the atmosphere within the small solid angle $d\Omega$ near the vertical. As will be evident later, this is not precisely the function that should be used in the calculation of the counting rate; but it is believed to furnish a reasonably good approximation to the correct function, and avoids the necessity for introduction of the details of the counter arrangement into the computation at an early stage.

Consider again a circle of radius r given by Eq. 8.2 around each of two arbitrary (fixed) points separated by a distance $2a$. When r is taken greater than a , those showers, which strike within the common area of the two circles, give rise to a density of ρ or greater at each point (See the sketch in Table 9). When r is less than a , no shower of sufficient density at one point will have sufficient density at the other, and so the lower limit of integration over energy will correspond to the case where $r = a$. When r is greater than a , it is convenient to express the common area of the two circles as a fraction, $C(a/r)$, of the area of one of them. The integral vertical frequency for two points then becomes (See Eq. 8.5):

$$H^Y(>\rho, t, a) = \pi D \int_{\epsilon(r=a)}^{\infty} e^{-\gamma\epsilon} [r(\rho, t, \epsilon)]^2 C(a/r) d\epsilon \quad (9.1)$$

The function $C(a/r)$ is given explicitly in Table 9, along with some numerical values.

The integral (Eq. 9.1) has been carried out by numerical methods similar to those used for Eq. 8.5. In some cases, a simple polynomial approximation (given in Table 9) to the function C has been helpful in reducing the amount of labor. The results of the integration are listed in Table 11. For depths below $t = 15$ to 20 the dependence of H^V on a is small.

So far, all the computations have been carried out in terms of the lateral unit. The geometric size of this unit increases at higher altitudes (or smaller t , See Table 1) by the ratio, σ , of the sea level air density to the density of air at that altitude. Thus, in terms of this unit, the surface area of a counter decreases by a factor $1/\sigma^2$, and counter separation decreases by a factor $1/\sigma$. In addition, those showers, which are r lateral units away from a counter system in the calculation above, will correspond to primaries striking with a circle of radius σx (the sea level size of the lateral unit), and the sea level size of the lateral unit has been used in setting up the expression used for the primary spectrum (Eq. III.1). Consequently, the integral vertical frequency spectrum, which corresponds to a density relative to a counter of fixed geometric size, ρ_0 , and a fixed geometric counter separation a_0 , is given in terms of the function just calculated by:

$$H^V(>\rho_0, t, a_0) = \sigma^2 H^V(>\sigma^2 \rho_0, t, a_0/\sigma) \quad (9.2)$$

This correction has been carried out for $\log a_0 = 1.644$, (which corresponds to a 9 foot counter separation) and the corresponding function is listed in Table 14, and plotted in Fig. 8. The resulting curves are much less altitude sensitive than the uncorrected curves. Actually the σ -correction should be made utilizing a σ roughly one radiation unit above the point of observation; this has been done in the final calculation of the counting rates, but, for the purpose of illustration, the value of σ at the corresponding t has been used.

In Fig. 7 and Table 11, there is shown a rather abrupt increase in the vertical integral spectrum for the higher densities on going from $t = 10$ to $t = 5$ for the case $a = 0$ ($\log a = -\infty$). This effect is due to those small radii for which the radial function adopted here is not correct. These small radii play an important part here, because small values of s become increasingly important at the small values of t near the top of the atmosphere.

Table 11 also shows the very large modification introduced into the vertical integral frequency spectrum by finite separation of the points of observation. This correction is very large at $t = 5$, and becomes essentially negligible below $t = 20$.

The height and position of the counting rate maximum depends essentially on the finite separation of the counters; and, for this reason, it is unfortunate that the present approximate treatment of this effect had to be followed.

However, this could not be avoided, since the computation had to be started before Kraybill had selected the counter geom-

etry with which the major portion of his observations were made.

The calculation given here would furnish a rigorous treatment for the case of coincident bursts between two unshielded ionization chambers separated by the distance $2a$. Observations of this sort have been made by Lewis (Ref. 49) and analyzed by Wolfenstein (Ref. 45). Unfortunately, it is probable that ionization from stars and slow heavy particles completely masked the effects of showers in Lewis' experiments.

10. Integration over Zenith Angles

The next step is to integrate over the Zenith angles, from which the isotropically distributed primary electrons may come. However, the counter arrangement, which Kraybill used, (Ref. 55, 56) is not equally sensitive to showers coming from all directions, and this must be taken into account in the zenith angle integration. For calculations of this sort, the directional sensitivity of a counter arrangement has usually been neglected in the zenith angle integration. For counter arrangements of limited extent (say less than ten meters horizontal extension) below 15,000 feet elevation, this neglect is essentially justified. Even at these altitudes, Cocconi (Ref. 51) has shown how very large errors may be introduced into the calculation by neglecting this effect for counter extensions greater than 300 meters. In the calculations given here, it is essential to consider the directional sensitivity of the counters, since, near the maximum in the counting rate versus altitude curve, the majority of showers tripping the counter system will come from

angles inclined to the vertical by 45 degrees or more.

The geometrical arrangement of Kraybill's counters is indicated in Fig. 15, as well as a sketch indicating the angular coordinates used in the following computations. (The co-latitude angle θ measured from the zenith and the azimuth φ measured from a line joining the centers of the counters). The directional sensitivity is clear, since, as θ increases for $\varphi = 0^\circ$, incoming showers will see a constant counter area (cylindrical counters), and a counter separation decreasing as $\cos \theta$. As θ increases for $\varphi = 90^\circ$; the incoming showers will see a counter area decreasing as $\cos \theta$, and a constant separation between counters. A simple geometric construction shows that, for intermediate values of φ , the effective counter area and effective counter separation vary as:

$$S(\text{effective}) = S g(x, \varphi) = S \sqrt{1 - (1-x^2) \sin^2 \varphi} \quad (10.1a)$$

$$a(\text{effective}) = a f(x, \varphi) = a \sqrt{1 - (1-x^2) \cos^2 \varphi} \quad (10.1b)$$

$$x = \cos \theta \quad (10.1c)$$

and the effective depth below the top of the atmosphere is:

$$t(\text{effective}) = t/x. \quad (10.1d)$$

Since counter surface and shower density are inversely related, we may calculate an effective density spectrum at a given point in the atmosphere, due to showers coming from all directions as follows:

$$H(>\rho, t, a) = \int_0^0 d\chi \int_0^{2\pi} d\varphi H^V(>\rho/g(x, \varphi), \frac{t}{x}, a f(x, \varphi)) \quad (10.2)$$

Here, the directional sensitivity has been included in the integral, in such a way, that in calculating counting rates, one may insert the horizontal counter separation and normal counter area into the formulae, which will involve the function on the left of Eq. 10.2. From Eq. 10.1c we see that $dx d\varphi = -d\Omega$.

The integral (Eq. 10.2) has been calculated by first integrating over x utilizing Simpson's rule (x interval 0.1) for $\varphi = 0, 40^\circ, 90^\circ$, and then integrating over φ by means of graphical interpolation and Simpson's rule (interval 10°). This was done for $\log a = -1.644$ at sea level with appropriate corrections at other altitudes (See Table 13 where the corrected separation, a/σ , is given as a function of altitude). This corresponds to a fixed geometrical counter separation of 9 feet ($a = 4.5$ feet in ordinary units; See Fig. 15). The correction to ρ due to variation in atmospheric density was not carried out at this stage, since it could be postponed. The numerical integration was carried out for $\log \rho = 4, 5, 6, 7$ for t in intervals of 2.5 from $t = 5$ to $t = 15$. Below $t = 15$, a suitable approximation procedure was adopted, based upon the interpolation functions (Table 12), and involving the logarithmic integral (Table 22), but not taking into account any counter separation. Values were calculated from $t = 15$ (to check) by steps of 2.5 to $t = 24$, and 25. The results are listed in Table 15.

The general shape of the integrand in Eq. 10.2, as a function of (x, φ) is illustrated by Fig. 13, which is really the directional counting rate, but is illustrative of the integrand for $t = 7.5$ and $\log \rho$ about 6.5. The complete integral (Eq. 10.2)

for $t = 10$ is plotted in Fig. 9, as a function of ρ , along with the vertical integral spectrum for $a = 0$, and $\log a = -1.5$ for comparison. It is seen that the integration over zenith angles has not greatly affected the slope of the curve relative to the $a = 0$ curve, but the $\log a = -1.5$ curve is much steeper. Above $t = 10$ the integration over zenith angles reduced the slope of the final spectrum. The resulting curves were very nearly a straight line for all depths considered, and the slopes δ (represented by $H = \text{Const. } \rho^{-\delta}$) decrease regularly, with increasing depth (Table 13), as would be expected from Eq. 8.8.

It may be mentioned here, that, since the method of computation being followed is approximate, a more appropriate value for a might be half the average or root mean square counter separation (about 6 feet so a would be 3 feet rather than 4.5 feet), rather than half the extreme counter separation. The dependence of the vertical frequency curves on a , for the most effective direction ($\theta = 60^\circ$, $t(\text{eff}) = 12.5$) at the maximum in the counting rate versus altitude curve, is roughly as $a^{-3/4}$. The indicated change in the value of a would then increase the counting rate, roughly, by a factor of $(4.5/3)^{3/4} = 1.35$. This result has been utilized in the introduction.

11. The Counting Rate

In Sec. 10, the computation of $H(>\rho, t, a)$, Eq. 10.2, the integral density spectrum for two points separated by a distance $2a$ at the depth t , has been indicated. This function gives the frequency of occurrence of a surface density of electrons greater

than or equal to ρ at each of two points separated by a distance $2a$. Now, if this density is uniform over an area of this extent, then $-\frac{\partial H}{\partial \rho} d\rho$ will be the frequency of occurrence of a density between ρ and $\rho + d\rho$ at these two points. However, near the top of the atmosphere, this condition of uniform density is only approximately fulfilled, and, even if it is true for two points, the counter arrangement employed by Kraybill has three counters uniformly spaced 4.5 feet apart (Fig. 15). The expression $-\frac{\partial H}{\partial \rho} d\rho$ actually corresponds to a density between ρ and $\rho + d\rho$ at one counter, and some other density between ρ' and $\rho' + d\rho$ at the other two counters, where ρ' is not determined by our function, except that we know $\rho' \geq \rho$. An a posteriori study of the results of the computation (See Sec. 12) indicate that, for about 75 to 80% of the showers detected near 30,000 feet, the density is nearly uniform. For the remaining 20 to 25% of the showers, the procedure followed in this section will replace the accurate counting rate by an approximate one which replaces one kind of integral over the density by another which, nevertheless, includes all the showers. This approximation is seen to be one of replacing one average by another, and, since it involves an integration, may be expected to modify the results for these showers by at most 50%. The over all counting rate would then be uncertain by about 10%. Since, for the showers of non-uniform density, this method gives somewhat too low an estimate of the density, the counting rate we will compute will be too low rather than too high.

If the sensitive area of a counter is S and the surface

density of electrons is ρ , then the probability that the counter will fire is $[1 - \exp(-S\rho)]$ (Ref. 46). For three counters, all subject to the same density, the probability of coincident discharge of all three counters is $[1 - \exp(-S\rho)]^3$. Within the approximation followed here, the frequency of occurrence of a density between ρ and $\rho + d\rho$ is $-\frac{\partial H}{\partial \rho} d\rho$. After the integration over zenith angles, $H(>\rho)$ may be closely represented by an expression of the form $P\rho^{-\delta}$, where P and δ are constant for any given value of t (Table 15). Consequently, the counting rate, N , is given by:

$$N = \int_0^{\infty} d\rho [1 - \exp(-S\rho)]^3 \delta \frac{P}{\rho^{\delta+1}} \quad (11.1)$$

This expression may be evaluated analytically. First, it is convenient to make a change of variable given by:

$$S\rho = u \quad (11.2)$$

and the expression for N becomes:

$$N = P S^{\delta} I(\delta) \quad (11.3a)$$

$$I(\delta) = \delta \int_0^{\infty} (1 - e^{-u})^3 \frac{du}{u^{\delta+1}} \quad (11.3b)$$

(a) Evaluation of $I(\delta)$.

Clearly, (11.3b) is uniformly and absolutely convergent for $0 + \epsilon \leq \text{Re } \delta \leq 3 - \epsilon$ where ϵ is any positive number, so that $I(\delta)$ is an analytic function. With δ in this closed domain, we may integrate by parts:

$$I(\delta) = -\frac{1}{u^\delta} (1-e^{-u})^3 \Big|_0^\infty + 3 \int_0^\infty \frac{du}{u^\delta} (1-e^{-u})^2 e^{-u}$$

and the integrated part vanishes. The integral becomes:

$$I(\delta) = 3 \int_0^\infty \frac{du}{u^\delta} [e^{-u} - 2e^{-2u} + e^{-3u}] \quad (11.4)$$

Now, the individual integrals in (11.4) each converge, if $\text{Re } \delta < 1$, and in this case the result is:

$$I(\delta) = 3\Gamma(1-\delta) \left[1 - \frac{2}{2^{-\delta+1}} + \frac{1}{3^{-\delta+1}} \right] \quad (11.5)$$

The expression on the right side of (11.5), is an analytic expression defined for $0 < \text{Re } \delta < 3$, since the expression in the square bracket vanishes at the poles $\delta = 1, 2$ of the Γ -function (the limiting values of $I(\delta)$ being $I(1) = 0.8628$ and $I(2) = 1.15702$). Hence (11.5) is equal to $I(\delta)$ for $0 < \text{Re } \delta < 1$, but (11.5) and (11.3b) are both analytic expressions equal over this range, and so are equal everywhere that they are both defined. As a matter of fact, (11.5) furnishes the analytic continuation of the function defined by (11.3b) into the whole complex plane, with exception of the poles of the Γ -function at $3, 4, 5, \dots$. The function $I(\delta)$ has been calculated from (11.5), and is given in Table 22.

(b) The counting rate

The counting rate is now easily computed from Eq. 11.3a utilizing Tables 13, 15 and 22, recalling that the sensitive

area of the counters decreases as $1/\sigma^2$, and the constant P increases by σ^2 (See Eq. 9.2 and Table 13) due to variation in atmospheric density. This introduces a factor $(\sigma^2)^{-(\delta-1)}$ into results obtained utilizing sea level values for the geometrical extension of the lateral unit. The uncorrected results are listed in Table 16, the density correction in Table 13, and the corrected counting rate is listed as N_b again in Table 16. From Table 13, we see that the lower density of the atmosphere at $t = 5$ (38,000 ft.) reduces the counting rate by something more than a factor of ten.

A slight additional correction of this last counting rate, N_b , was made to obtain the counting rate, N_a , which is also listed in Table 16, and which has been taken as "standard" in this thesis. For N_b the value of σ used corresponds to the density of air at the point of observation, rather than the density about one radiation unit above the counter system. It was possible to estimate the direction of the showers which contributed most to the counting rate, and the σ corresponding to a point one radiation unit from the counter system in this direction was then used in the computation of N_a . For points near the top of the atmosphere, where this correction was most marked, the change in σ (and therefore in N) is less than would be introduced by simply utilizing the value of σ one radiation unit vertically above the counters, since the predominant showers make an angle of 45 degrees, or more, with the vertical. This is outlined in the lower part of Table 13, and the x-max. listed there is the cosine of the zenith angle of the important showers.

The value at $t = 17.5$ was also corrected, because the approximations followed in calculating the integral density spectrum (Sec. 10) below $t = 15$ neglected any correction due to the counter separation; these corrections are still appreciable until $t = 20$. This was taken into account by noting the correction for $t = 15$, where the counting rate was calculated both with and without this correction (See Table 15 and 16), and a correction of nearly this amount was applied to the point at 17.5.

12. Comparison With Experiment

The counting rates just computed have been compared with Hilberry's data (Ref. 44, See also Fig. 15) in the lower part of the atmosphere (from $t = 24$ at sea level to $t = 14.6$, 14,200 ft.) to determine an appropriate normalization. Hilberry used four counters grouped 1 - 2 - 1, equally spaced 4.1 feet apart, with the center two forming a wide angle (60 degree included angle) telescope (Fig. 15). This separation is nearly the same as that used by Kraybill (4.5 feet), and the telescopic action of the center (double) counter is unimportant for these altitudes, since most of the showers come vertically. The only correction that needs to be made to the counting rate N_a , which is computed for the arrangement used by Kraybill, is to multiply the values by $(2.336)^{\delta}$ since $2.336 = 196/83.9 =$ the ratio of the counter areas "Hilberry/Kraybill" (See Eq. 11.3a). This is indicated in Table 17. If the theoretical values computed in this way are multiplied by 3, they give reasonable agreement with the data given by Hilberry, as may be seen in Table 17. The theoretical curve

(Theory x3) is plotted in Fig. 10, along with the experimental points given by Hilberry. A somewhat closer fit might be obtained by multiplying by a factor slightly less than 3, but this is an unimportant modification.

This normalizing procedure is to be expected (determination of the factor of 3), since considerations of this same type were followed by Euler, Heisenberg and others (Ref. 41, 42, 43, 44, 33) in setting up the expression used here for the primary spectrum (Eq. III.1). Cocconi (Ref. 52) has considered a primary spectrum of this form with $\gamma = 1.6, 1.7$ and 1.8 , and for $\gamma = 1.8$ (the value selected here) he also finds theoretical values too small by a factor of 3.9 at sea level and 2.0 at 7,500 feet elevation. Our discrepancy in this respect is thus consistent with other computations, and of a reasonable order of magnitude. With this normalization now established, we may compare the theory with the results of Kraybill's observations.

In Table 17, the values $3N_a$ and $8.33N_a$ are compared with values read from the curve given by Kraybill (Ref. 56). Below fifteen radiation units, $3N_a$ agrees moderately well with these values. This is to be expected, since Kraybill determined these values by multiplying Hilberry's data by a constant factor. That this agreement is not quite as good as our fit to these data (Fig. 10) follows from the fact that the correct modification is not to multiply by a constant but by various factors, $(2.336)^\delta$, which vary with altitude (See Table 17 column 3). Above fifteen radiation units, the values of $3N_a$ are considerably below those given by Kraybill. On the other hand, multipli-

cation of N_a by 8.33 gives a somewhat closer fit to Kraybill's curve at higher altitudes, but a large discrepancy at low altitudes (Table 17). In Fig. 11 are shown the curve and experimental points given by Kraybill, along with the theoretical curves $3N_a$ and $8.33N_a$. The dashed curve given by $7.4N_b$ is also shown, and it has essentially the same shape and values as $8.33N_a$, so the refinement by which N_a was derived from N_b may be considered as relatively unimportant (Sec. 11). The theoretical curves reach a maximum at 10.5 radiation units, as compared to a maximum at 8.5 radiation units for the experimental curve, and have a somewhat different shape (Fig. 11). The ratio of the maximum to sea level for the theoretical curves is 24, as compared to 63 for the experimental curve. The theoretical curves, dashed, $3N_a$ and $8.33N_a$ are again compared with the experimental curve over the whole range of altitude on a logarithmic scale in Fig. 12. The necessity for a different normalization at low and at high altitudes is clearly evident. A discussion of these discrepancies between theory and experiment has been given in the introduction; we mention here that a lower value of γ , say $\gamma = 1.6$ or 1.7 might possibly improve the agreement within the domain of the primary electron hypothesis although the necessity of a normalization makes this uncertain, and also, the primary proton hypothesis with the multiple production of secondaries, as proposed by Lewis, Oppenheimer, and Wouthuysen (Ref. 8), should improve the agreement.

13. Estimate of Approximations

The discussion of approximations will be based on an a posteriori examination of some of the features of the approximate calculation that has been carried out. This will give some estimate of the errors introduced by this method, but a true check of the accuracy of the method could only be made by comparison with a rigorous computation. This has not been done.

The various approximations include: (a) the omission of a treatment of fluctuations (Sec. 7), (b) the assumption of a uniform surface density of electrons (Sec. 12), (c) the approximate treatment of the effect of atmospheric structure (Sec. 12), and (d) the uncertainties due to the various numerical and graphical methods which were used. The errors due to this last source, estimated from the scale of plotting, more exact methods of computation applied to various check points, and from results for the same points calculated independently by two separate people, may be placed in the range of zero to ten per cent error. In the writer's opinion, errors exceeding five per cent are rather rare. The "smoothing" effect of many integrations should help to reduce errors of this nature; the errors may be of either sign.

A comparison of N_a , N_b (Table 16) indicates that a more careful treatment of the effect due to variation in atmospheric density would probably not alter the calculation by more than 10 per cent. We discuss only (a) and (b) at length.

(a) Fluctuations

The general effect of fluctuations should be to increase

the counting rate as compared to the computed values for reasons given in Sec. 7. Because the steepness of the integral density spectrum increases with altitude (See the values of δ in Table 15), this effect should increase with altitude. Christy and Kusaka (Ref. 40) have found a factor about 1.5 due to fluctuations in the number of electrons, and, because of additional fluctuations in spatial density, this factor may be of the order of two or more for the calculations given here. The gross effect of the fluctuations, to raise the general counting rate, is not a problem here since a normalization has to be made, but a variation in this effect with altitude will affect the disagreement between theory and experiment exhibited by Fig. 12, and the tendency should be to reduce the amount of disagreement, since larger fluctuations are to be expected at higher altitudes. Another reason for larger fluctuations at higher altitudes is the following.

Near the start of a shower, the parametric expressions for the number of particles may be in error (Eq. 5.1). For very large energies they predict more particles than given by $\exp t$. This is surprising, since a certain number of steps are necessary to subdivide the energy, no matter how large. The explanation has been that the infra-red catastrophe in the bremsstrahlung cross-section (See also the paper by Bethe and Oppenheimer, Ref. 64) makes possible a multiple production of photons in a single collision, so that a very energetic primary can generate a large number of particles within a short distance.* For this process, *The writer wishes to thank Professor Christy for discussion of this point.

fluctuations might be very large, and may have marked effects for showers coming near the vertical at the maximum of the counting rate curve. This would be an additional effect tending to reduce the disagreement.

The gross effect of fluctuations, a general shift of the counting rate upwards, need not concern us here, since a normalization procedure has been adopted. This normalization, of course, washes out this general shift, and leaves only the possibility of a different effect at high altitudes than at low. It is likely that the spatial distribution of electrons is nearer the mean distribution at high altitudes than at low, but that fluctuations in the number of electrons are greater. The energy range, and therefore the number of electrons, important in the considerations of Christy and Kusaka, is smaller than that of our problem by a factor of 10^3 to 10^5 . Since fluctuations in the number of electrons follows a law lying between the Poisson and Furry distributions, this is a factor tending to reduce the effect of these fluctuations in our problem, as compared to theirs. Furthermore, we only need a comparison of this effect between a ρ^{-2} and a $\rho^{-1.5}$ distribution. For these reasons, it is probable that the relative effect of fluctuations is smaller than a factor of 1.2, even including the fluctuations in the spatial distribution.

(b) The assumption of uniform electron density

Clearly this assumption is poor for showers with an extension (extent of the region where the electron density is about

one particle per counter) less than the counter separation. This problem has been studied by examining some of the details of the computation. The electron density ($\rho_{\max.}$), corresponding to the maximum of the integrand for the integral over density (Eq. 11.1) when plotted on a logarithmic density scale, has been determined and is given in Table 18. The direction with the vertical ($\theta_{\max.}$) of the most important showers contributing to the density spectrum was then determined and is also listed. The effective counter separation (a_{eff}) and effective depth ($t_{\text{eff.}}$) for this direction could then be computed. The shower radius corresponding to the maximum of the integral over energy, including the correction for counter separation, for the vertical integral density spectrum (Eq. 9.1) was then determined for the effective counter separation and effective depth mentioned above. At the effective depth and at the density maximum for Eq. 11.1, it was also possible to obtain the ratio of the intensity with no correction for counter separation to the intensity with the correction for counter separation corresponding to the effective counter separation (a_{eff}). The results of all these determinations are listed in Table 18.

For $t = 5, 7.5, 10, 12.5$, the most important showers come from such an angle as to have an effective depth of 12 to 14 radiation units. For these effective depths, the intensity ratio just mentioned (no separation correction/ corrected value) varies from 1.70 at $t = 7.5$ to 1.48 at $t = 5$ and $t = 12.5$. This may be taken as an estimate of the maximum possible error, and since our method of correction for counter separation gives essentially

the minimum value, the true value may be expected to be limited by our value below and 1.7 times our value above. Near the maximum of the theoretical counting rate curve this ratio is less: 1.6. However, on general arguments (Sec. 12), it seems likely that the true value is nearer to our value than to the upper limit. A rough estimate of this may be obtained by considering the proportion of the showers at the maximum of the integrand of the corrected integral over energy (Eq. 9.5), which strike inside a circle of radius a . This is given by the ratio a^2_{eff} to $r^2(\text{max. of integrand})$. The likely error computed on this basis has a maximum value of 20 per cent for $t = 7.5$, and a value of 15 per cent at the maximum of the counting rate curve. In the writer's opinion, the maximum error introduced into the calculation by the assumption of uniform electron density is not over 20 per cent (reduction), and is probably less than this. The error is most marked at high altitudes and therefore is in such a direction as to lead to better agreement between the (corrected) theoretical curve and experiment.

14. Zenith Angle Distribution of Showers

Mr. E.W. Cowan (Ref. 57) and Mr. H.L. Kraybill (Ref. 56) collaborated in their studies of cosmic radiation by utilizing the counter arrangement to operate the cloud chamber, which was built by Cowan. The relative orientation of this apparatus is indicated in Fig. 15. From the cloud chamber pictures obtained in this way, Mr. Cowan could determine, among other things, something about the zenith angle distribution of the showers, which

trip the counter arrangement, and he has very kindly made this information available, so that it can be compared with theory. These observations were made at 31,000 feet and 37,000 feet. The information determined from them is the distribution of the number of showers within various angular ranges, where the angle measured is the projection of the zenith angle onto the plane of the cloud chamber. The theoretical distribution has been calculated for $t = 7.5$ radiation units (30,000 ft.), since the base calculations were already "set up" for this altitude, and the slight difference in elevation would make no substantial difference in the conclusions to be drawn from the subsequent comparison of theory and experiment. Furthermore, if anything, this treatment should reduce the amount of disagreement, which has been found between the two.

(a) Theoretical distribution at $t = 7.5$

First the counting rate per unit solid angle, N , of Kraybill's counters as a function of the zenith angle, (θ, φ) , was computed by inserting the integrand of Eq. 10.2 (See Table 19) into the integral over density of Eq. 11.1. However, an examination of the integral density spectrum for a given zenith angle indicated that it could not be well represented by a power law, so an integration by parts was first performed to obtain:

$$N(\theta, \varphi) = \int_0^{\infty} d\rho (1 - e^{-s\rho})^3 \left(-\frac{\partial H}{\partial \rho} \right) = 3S \int_0^{\infty} H (1 - e^{-s\rho})^2 e^{-s\rho} d\rho \quad (14.1a)$$

$$H = H^v \left(> \rho / g(x, \varphi), 7.5/x, a f(x, \varphi) \right) \quad (\text{Table 19}), \quad (14.1b)$$

To eliminate the "tails" of the numerical integration the following change of variable was made

$$\ln(S\rho) = u, \quad (14.2)$$

which gives:

$$N(\theta, \varphi) = 3 \int_{-\infty}^{\infty} H\left(> \frac{e^u}{S}\right) F_2(u) du, \quad (14.3a)$$

$$F_2(u) = (1 - e^{-e^u})^2 e^{-e^u} e^u, \quad (\text{TABLE 22}). \quad (14.3b)$$

In the u-scale the integrand of Eq. 14.3 has a very sharp maximum, and was easily integrated by numerical methods. The integrals, N, were carried out for $x = \cos \theta$ in steps of 0.2 for $\varphi = 0, 40, 90$ degrees, and other values filled in by graphical interpolation to obtain the counting rate per unit solid angle $N(\theta, \varphi)$ as a function of the zenith angle, (θ, φ) . The results are plotted on a logarithmic scale in Fig. 13 (here θ is represented via x where $x = \cos \theta$).

This is only part of the calculation; we must now project this angular distribution onto the plane of the cloud chamber. The relation connecting the angle ψ between the vertical and the projected zenith angle, and the zenith angle itself, is sketched at the bottom of Fig. 15, and the application of some simple spherical trigonometry gives:

$$\tan \psi = \sin \varphi \tan \theta \quad (14.4)$$

The counting rate per unit angle ψ is now given by:

$$N(\psi) d\psi = d\psi \int_{\cos \psi}^0 dx N[x, \varphi(x, \psi)] \left(\frac{\partial \varphi}{\partial \psi} \right)_{x=\text{const.}} \quad (14.5a)$$

$$\sin \varphi = \frac{\chi \tan \psi}{\gamma \sqrt{1-\chi^2}} \quad (14.5b)$$

The Jacobian in Eq. 14.5 introduces a singularity into the integrand which, although integrable, makes numerical integration very difficult. The change of variable:

$$w^2 + \chi^2 / \cos^2 \psi = 1 \quad (14.6)$$

gives:

$$N(\psi) = \int_0^1 d w N(\chi = \cos \psi \sqrt{1-w^2}, \varphi[w, \psi]) \quad (14.7a)$$

$$\sin \varphi = \left[1 + w^2 / (1-w^2)(\sin^2 \psi) \right]^{-\frac{1}{2}} \quad (14.7b)$$

It turns out that arc cos w is the half angle of a right circular cone, with vertex in the center of the cloud chamber, and axis perpendicular to the face of the cloud chamber. The edges of the cloud chamber correspond to $w = 0.163$. As explained later, Cowan was able to measure projected angles, ψ , for only about one-fifth of the showers. Taking the upper limit of integration in Eq. 14.7 equal to 0.25 gives a ratio of this integral to the total integral of about one-fifth. The angular distribution, $N(\psi)$, was therefore calculated both for the upper limit equal to 1.0 and to 0.25 by numerical means utilizing Fig. 13. The results are listed in Table 20 and plotted in Fig. 14.

(b) Experimental distributions

The observed distributions furnished by Mr. E.W. Cowan are given in Table 23. We found, that, in many cases, it was impos-

sible to determine the direction of the shower from his photographs. The cloud chamber contained two 1.5 cm. lead plates which led him to the following methods of selecting photographs:

At 31,000 feet, with a grand total of 228 photographs:

A. Those photographs were recorded which showed ten or more parallel tracks anywhere in the chamber, 48 out of 228 pictures.

B. Those photographs were recorded which showed ten or more parallel tracks above the lead plates, 38 out of 228 pictures.

C. Those pictures were recorded which showed one hundred or more parallel tracks anywhere in the chamber, 21 out of 228 pictures.

At 37,000 feet, with a grand total of 44 photographs.

D. Those pictures were recorded which showed three or more parallel tracks anywhere in the chamber, 15 out of 44 pictures.

The average of the projected angles, ψ , made by these tracks was then observed and computed, and the number of events falling in each angular range tabulated (Table 23).

The gross features of all the four distributions are not very different. They all show a maximum at or near the vertical with a decrease to half maximum or less at 40 degrees. The distribution, B, shows a somewhat less pronounced maximum than A, and this difference may be attributable to the enhancement of partially developed, nearly vertical, showers by the lead. The 100-track distribution, C, seems to be flatter than A or B, but

it also drops to half maximum at 40 degrees. The tendency for greater flatness of C is reasonable, since the higher density showers should come from angles further from the vertical where there is the possibility of more multiplication in the greater distance.

The distribution, D, taken at 37,000 feet, is somewhat more uncertain statistically than either A or B. Rather surprisingly, it falls to half value at 30 degrees, while A falls only to 0.6 maximum, and B to only 0.7 maximum at this angle. On general grounds, one would expect the distribution at the higher altitude to be as broad or broader than the lower altitude distributions. This may be partially explained by the selection of only three tracks, so that partially developed, near vertical, showers are given greater weight.

(c) Comparison with theory

All the observed distributions disagree with the theoretical distributions by being too narrow. The theoretical distributions and distribution A are shown in Fig. 14, where all the curves are arbitrarily normalized to 10 at $\psi = 0$. The dotted lines represent the counting rate per unit solid angle for $\varphi = 90$ degrees (low curve) and $\varphi = 0$ degrees (the high curve that runs off scale) plotted as if θ were the projected angle ψ . It is unfortunate that the cloud chamber and counter system were not rotated 90 degrees in azimuth relative to each other, so that the $\varphi = 0$ plane (the high curve) was also the plane of the cloud chamber. This would have increased the "sensitivity"

of the cloud chamber by a factor of three. The two solid lines are the theoretical projected distributions, upper limit for $w = 1$ (the low curve) and upper limit for $w = 0.25$ (the high curve). The stippled curve is distribution A.

The half angle of the observed curve, A, is about 17 degrees, and this is not much different for the other distributions. The half angle of the theoretical curve ($w = 1$) is about 30 degrees, and is even larger for the $w = 0.25$ curve. The angle for half maximum is 40 degrees or less for the observed curves, and 60 degrees or more for the theoretical curves. The $w = 0.25$ curve was computed to see if the geometry of the cloud chamber was tending to select showers nearer the vertical (see remarks under Eq. 14.7), but this curve is even broader than the complete projection curve $w = 1$. The value 0.25 was selected to give the intensity ratio of one-fifth which is roughly $48/228$. The method of selecting photographs for measurement (ten or more parallel tracks) would be expected to bias the observations in the direction of greater density. Theoretically, determined by examining the integrand of Eq. 14.3, this should bias the distribution towards larger angles, as would be expected on the quite general grounds of greater distance for the shower to multiply. The narrow observed distribution is also surprising, since it was obtained near the maximum in the counting rate curve, where one would expect showers to come from large angles. This has also been checked by determining the angular distribution implied by Kraybill's observed altitude dependence by means of a Gross transformation. The agreement between this curve and the theo-

retical curve is rather good, while it is very poor for this curve and the cloud chamber distributions.

The statistical features of the cloud chamber observations are, of course, rather poor, especially, since there is a non-analyzable mass of material four times as large as the photographs analyzed, which could smother the tabulated distributions. It is hard to explain the difficulty in assigning angles to these pictures, since the distribution in angle of the electrons in a local portion of a high density shower is only a few degrees.

The general conclusion is that there is a set of cloud chamber data, of rather uncertain statistics, which are consistent among themselves, but in definite disagreement with theory and with the angular distribution derived from the observed altitude curve. This latter is in rather good agreement with theory. The disagreement with the cloud chamber distributions is difficult to understand.

REFERENCES

1. C.D. Anderson and S.H. Neddermeyer; International Conference on Physics, London, 1934 (p. 171, vol. I of the Report, Physical Society, 1935).
2. C.D. Anderson and S.H. Neddermeyer; Phys. Rev. 51, 884 (1937).
3. J.F. Carlson and J.R. Oppenheimer; Phys. Rev. 51, 220 (1937).
4. H.J. Bhabha and W. Heitler; Proc. Roy. Soc. 159, 432 (1937).
5. P. Auger, R. Maze, P. Ehrenfest, and A. Freon; J. Physique et Radium 1, 39 (1939).
6. M. Schein, W.P. Jesse, and E.O. Wollan; Phys. Rev. 59, 615 (1941).
7. M.S. Vallarta, M.L. Perusquia, and J. deOyarzabel; Phys. Rev. 71, 393 (1947).
8. H.W. Lewis, J.R. Oppenheimer, S.A. Wouthuysen; Phys. Rev. 73, 127 (1948).
9. J. Hamilton, W. Heitler, and H.W. Peng; Phys. Rev. 64, 78 (1948).
10. W. Heitler and S. Power; Phys. Rev. 72, 266 (1947).
11. R.J. Finkelstein; Phys. Rev. 72, 215 (1947).
- 12a. G. Cocconi, A. Loverdo, and V. Tongiorgi; Phys. Rev. 70, 852 (1946).
- 12b. G. Cocconi and C. Festa; Nuovo Cimento 3, 293 (1946).
13. A. Alichanian, T. Asatiani, and G. Muskhelishvilli; J. Phys. USSR 11, 16 (1947).
14. E.P. George and A.C. Jason; Nature, 161, 248 (1948).
15. E.P. George and P.T. Trent; Nature 161, 248 (1948).

REFERENCES (CONTINUED)

16. D. Broadbent and L. Janossy; Proc. Roy. Soc. 192, 364 (1948).
17. J.W. Follin; Thesis, California Institute of Technology (1947).
18. E. Feenberg and H. Primakoff; Phys. Rev. 73, 449 (1948).
19. H. Snyder, Phys. Rev. 53, 960 (1938).
20. R. Serber; Phys. Rev. 54, 317 (1938).
21. C.D. Anderson and S.H. Neddermeyer; Phys. Rev. 50, 256 (1936).
22. I.S. Bowen, R.A. Millikan, H.V. Neher; Phys. Rev. 52, 80 (1937); 53, 217, 855 (1938).
23. N. Arley; Proc. Roy. Soc. 168, 519 (1938).
24. B. Rossi and S. Klapman; Phys. Rev. 61, 414 (1942).
25. I. Tamm and S. Belenky; Phys. Rev. 70, 660 (1946).
26. B. Rossi and K. Greisen; Rev. Mod. Phys. 13, 240 (1941).
27. H.A. Bethe; Phys. Rev. 59, 648 (1941).
28. Bethe, Rose, Smith; Proc. Amer. Phil. Soc. 78, 573 (1938).
29. L.W. Nordheim; Phys. Rev. 59, 929 (1941).
30. J.A. Richards and L.W. Nordheim; Phys. Rev. 61, 735 (1942).
31. J. Roberg; Phys. Rev. 62, 304 (1942).
32. L. Wolfenstein; Phys. Rev. 67, 238 (1945).
33. G. Moliere, Cosmic Radiation, Chapter III, Dover, New York (1946).
34. L. Landau; J. Phys. USSR, 3, 237 (1940).
35. W.H. Furry; Phys. Rev. 52, 569 (1937).
36. A. Nordsieck, W.E. Lamb, and G.E. Uhlenbeck; Physics 7, 344 (1940).

REFERENCES (CONTINUED)

37. W.T. Scott and G.E. Uhlenbeck; Phys. Rev. 62, 497 (1942).
38. H.J. Bhabha and W. Heitler; Proc. Roy. Soc. 159, 432 (1937).
39. N. Arley; Thesis, Copenhagen (1943); G.E.C. Gads Forlag.
40. R.F. Christy and S. Kusaka; Phys. Rev. 59, 405, 414 (1941).
41. H. Euler and H. Wergeland; Astrophysica Norwegica 3, 165 (1940).
42. W. Heisenberg; Cosmic Radiation, page 2, Dover, New York (1946).
43. H. Euler; Z. fur Physik 116, 73 (1940).
44. N. Hilberry; Phys. Rev. 60, 1 (1941).
45. L. Wolfenstein; Phys. Rev. 67, 238 (1945).
46. G. Cocconi, A. Loverdo, and V. Tongiorgi; Phys. Rev. 70, 841, 846 (1946).
47. I. Pomeranchuk; J. Phys. USSR, 8, 17 (1944).
48. A. Migdal; J. Phys. USSR, 9, 183 (1945).
49. L.G. Lewis; Phys. Rev. 67, 228 (1945).
50. D.V. Skobel'tzyn, G.T. Zatsepin, and V.V. Miller; Phys. Rev. 71, 315 (1947).
51. G. Cocconi; Phys. Rev. 72, 350 (1947).
52. G. Cocconi; Phys. Rev. 72, 764 (1947).
53. P. Auger and J. Daudin; Phys. Rev. 61, 91 (1942).
54. M.G.E. Cosyns; Nature 145, 668 (1940).
55. H.L. Kraybill and P.J. Ovrebo; Phys. Rev. 72, 351 (1947).
56. H.L. Kraybill; Phys. Rev. 73, 632 (1948).
57. E.W. Cowan; Thesis, California Institute of Technology (1948).

REFERENCES (CONTINUED)

58. W. Heitler; The Quantum Theory of Radiation, second edition, Chapters III and IV, Oxford (1944).
59. W. Heisenberg; Cosmic Radiation, Chapter II, Dover, New York (1946).
60. E.J. Williams; Proc. Roy. Soc. 169, 531 (1939); 172, 194 (1939).
61. V. Berestetzky; J. Phys. USSR 9, 197 (1945).
62. H. Geiger and W. Stubbe; Abh. preuss. Akad. Wiss. 1941, 3, Nr. 10. (This reference is not available at C.I.T., but was mentioned in Ref. 33, p. 39).
63. J.R. Oppenheimer; Phys. Rev. 71, 462 (T) (1947).
64. H.A. Bethe and J.R. Oppenheimer; Phys. Rev. 70, 451, 796 (1946).
65. H.A. Bethe and W. Heitler; Proc. Roy. Soc. 146, 83 (1934)..

TABLE 1

THE ATMOSPHERE IN RADIATION UNITS*

Rad. Units	gm./cm. ²	cm.Hg	alt.Km.	alt.ft.	σ^{**}	σ^2	size rad. units, m.	size lat. unit, m.
0.1	4.3	0.316	37.26	122,250	184.40	34,003.6		
0.5	21.5	1.581	26.74	87,734	36.85	1,357.7		
1	43	3.163	22.22	72,904	18.43	339.6	6129	1114
2	86	6.326	17.71	58,107	9.215	84.91	3065	557
3	129	9.489	15.06	49,412	6.142	37.73	2043	371
4	172	12.65	13.20	43,309	4.608	21.24	1533	279
5	215	15.81	11.75	38,552	3.694	13.65	1229	223
6	258	18.98	10.55	34,615	3.129	9.79	1041	189
7	301	22.14	9.52	31,235	2.756	7.60	917	167
8	344	25.30	8.60	28,217	2.479	6.14	824	150
9	387	28.47	7.76	25,461	2.260	5.11	752	137
10	430	31.63	6.990	22,934	2.082	4.34	693	126
11	473	34.79	6.298	20,664	1.932	3.733	643	117
12	516	37.96	5.640	18,505	1.801	3.245	599	109
13	559	41.12	5.015	16,454	1.688	2.849	561	102
14	602	44.28	4.452	14,607	1.588	2.520	528	96.0
15	645	47.44	3.901	12,799	1.499	2.247	499	90.6
16	688	50.61	3.396	11,142	1.420	2.017	472	85.9
17	731	53.77	2.899	9,512	1.349	1.821	449	81.6
18	774	56.93	2.435	7,989	1.286	1.654	428	77.8
19	817	60.10	1.991	6,532	1.205	1.452	401	72.9
20	860	63.26	1.570	5,151	1.178	1.388	392	71.2
21	903	66.42	1.165	3,822	1.132	1.280	376	68.4
22	946	69.58	0.776	2,545	1.087	1.182	362	65.7
23	989	72.75	0.400	1,314	1.045	1.091	347	63.2
24	1032	75.91	0.0394	129	1.004	1.003	335	60.7
24.03		76.00	0.0000	0	1.000	1.000	332.6	60.5

* Atmosphere pressure and density data from Humphreys, "Physics of the Air", McGraw Hill, New York, 1940. Page 80 (Summer)

** σ = Ratio of density at sea level to density at altitude

TABLE 2

E AND ϵ^*

ϵ	log E	log E	ϵ
0	8.000	0	-18.421
0.5	8.217	1	-16.118
1	8.434	2	-13.816
1.5	8.651	3	-11.513
2	8.869	4	-9.210
2.5	9.086	5	-6.908
3	9.303	6	-4.605
3.5	9.520	7	-2.303
4	9.737	8	0
5	10.171	9	2.303
6	10.606	10	4.605
7	10.040	11	6.908
8	11.474	12	9.210
9	11.909	13	11.513
10	12.343	14	13.816
12	13.212	15	16.118
14	14.080	16	18.421
16	14.949	17	20.723
18	15.817	18	23.026
20	16.686	19	25.328
22	17.554	20	27.631
24	18.423	21	29.934
26	19.292		
28	20.160		
30	21.029		

*E = Energy of primary, electron volts

$$\epsilon = \ln(E/\beta)$$

$$\beta = 10^8 \text{ e.v.}$$

TABLE 3

POSITION AND NUMBER OF ELECTRONS AT MAXIMUM
OF AN ELECTRON SHOWER

log E	log (E/ β)	ϵ	t max.	Π max.*	log Π max.	
12	4	9.20	8.25	1.068	3	3.028
13	5	11.50	10.58	9.50	3	3.978
14	6	13.80	12.89	8.64	4	4.936
15	7	16.10	15.21	8.00	5	5.903
16	8	18.40	17.53	7.47	6	6.873
17	9	20.70	19.84	7.03	7	7.847
18	10	23.00	22.14	6.66	8	8.823
19	11	25.30	24.45	6.35	9	9.803

* The separate number is the power of ten by which the left number should be multiplied. See logarithm.

E = Primary energy, e.v.

$\beta = 10^8$ e.v. = critical energy in air

$\epsilon = \ln(E/\beta)$

Π = Number of electrons at shower maximum

t = Position of shower maximum

TABLE 4

SHOWER THEORY PARAMETERS *

s	K(s)	l(s)	m(s)	n(s)	s	K(s)	l(s)	m(s)	n(s)
0.0	0.1995	*	--	--	1.6	0.3273	-0.395	0.67424	1.446
0.1	0.2528	3.789	2.5005	--	1.7	0.3117	-0.435	0.62747	1.407
0.2	0.2924	2.270	1.8976	3.00	1.8	0.2972	-0.470	0.58284	1.370
0.3	0.3243	1.569	1.6245	2.34	1.9	0.2804	-0.500	0.53979	1.336
0.4	0.3486	1.127	1.4616	2.00	2.0	0.2670	-0.526	0.49960	1.280
0.5	0.3693	0.813	1.3465	1.90	2.1	0.2528	-0.550	0.46242	1.222
0.6	0.3922	0.576	1.2558	1.78	2.2	0.2406	-0.570	0.42746	1.166
0.7	0.3938	0.389	1.1795	1.72	2.3	0.2296	-0.589	0.39537	1.111
0.8	0.3977	0.235	1.1112	1.63	2.4	0.2201	-0.605	0.36552	1.048
0.9	0.3984	0.108	1.0494	1.60	2.5	0.2116	-0.619	0.33850	0.994
1.0	0.39539	0.000	0.9908	1.5634	2.6	0.2161	-0.632	0.31330	0.933
1.1	0.3890	-0.092	0.93511	1.543	2.7	0.1963	-0.643	0.29079	0.875
1.2	0.3789	-0.171	0.87996	1.526	2.8	0.1896	-0.654	0.26992	0.839
1.3	0.3675	-0.239	0.82706	1.509	2.9	0.1832	-0.663	0.25027	0.782
1.4	0.3526	-0.298	0.77434	1.497	3.0	0.1789	-0.671	0.23310	0.720
1.5	0.3430	-0.350	0.72375	1.474	4.0	0.1439	-0.720	0.12280	0.496

* Computed from tables in Rossi and Greism (Rev. Mod. Phys. 13, 240 (1941)), in general one more significant figure has been retained than is justified to avoid rounding up errors.

KEY TO SYMBOLS:

The parameters are to be used in the formulae:

$$\Pi = \frac{K(s)}{\sqrt{1+n(s)t}} e^{l(s)t + s\varepsilon}$$

$$t = \frac{\varepsilon s - 1}{m(s)}$$

$$\varepsilon = \ln(E/\beta)$$

Where:

Π = Total number of electrons. s = Independent parameter.

t = Depth in shower units.

E = Primary energy (usually e.v.)

β = Critical energy (10^8 e.v. for air)

TABLE 5

NUMBER OF ELECTRONS AS A FUNCTION OF DEPTH*

(See Table 4 for definition of symbols)

s	$\epsilon = 6$		$\epsilon = 7$		$\epsilon = 8$		$\epsilon = 9$	
	t	$\ln \pi$						
0.4	--	--	--	--	1.504	3.19	1.777	3.83
0.6	2.068	3.07	2.547	3.87	3.025	4.68	3.500	5.48
0.8	3.42	3.74	4.14	4.63	4.86	5.53	5.58	6.43
1.0	5.05	3.99	6.06	4.91	7.07	5.84	8.07	6.78
1.2	7.05	3.81	8.41	4.70	9.77	5.59	11.13	6.50
1.4	9.56	3.17	11.36	3.95	13.17	4.75	14.98	5.54
1.6	12.75	1.98	15.13	2.56	17.50	3.14	19.87	3.75
1.8	16.81	0.11	19.90	0.38	23.00	0.66	26.09	0.95

s	$\epsilon = 10$		$\epsilon = 11$		$\epsilon = 12$		$\epsilon = 13$	
	t	$\ln \pi$						
0.2	--	--	--	--	0.737	2.31	0.843	2.70
0.4	2.050	4.49	2.326	5.14	2.600	5.80	2.872	6.47
0.6	3.980	6.31	4.455	7.13	4.93	7.96	5.41	8.80
0.8	6.30	7.35	7.02	8.27	7.74	9.19	8.46	10.12
1.0	9.08	7.72	10.09	8.67	11.11	9.63	12.12	10.58
1.2	12.50	7.41	13.86	8.32	15.23	9.25	16.59	10.18
1.4	16.79	6.35	18.60	7.16	20.40	7.98	22.20	8.79
1.6	22.27	4.36	24.61	4.98	27.00	5.59	--	--

s	$\epsilon = 14$		$\epsilon = 15$		$\epsilon = 16$		$\epsilon = 17$	
	t	$\ln \pi$						
0.2	0.948	3.10	1.054	3.50	1.159	3.90	1.265	4.32
0.4	3.147	7.14	3.420	7.81	3.691	8.49	3.966	9.16
0.6	5.88	9.63	6.36	10.47	6.84	11.31	7.32	12.15
0.8	9.18	11.05	9.90	11.99	10.62	12.92	11.34	13.85
1.0	13.13	11.55	14.14	12.51	15.15	13.48	16.16	14.45
1.2	17.96	11.11	19.32	12.04	20.68	12.97	22.06	13.91
1.4	24.01	9.62	25.82	10.44	27.64	11.27	29.45	12.11

s	$\epsilon = 18$		$\epsilon = 19$		$\epsilon = 20$	
	t	$\ln \pi$	t	$\ln \pi$	t	$\ln \pi$
0.2	1.370	4.73	1.475	5.14	1.580	5.55
0.4	4.235	9.84	4.515	10.52	4.78	11.20
0.6	7.80	13.00	8.28	13.84	8.75	14.70
0.8	12.06	14.79	12.78	15.74	13.50	16.68
1.0	17.17	15.42	18.18	16.39	19.19	17.36
1.2	23.41	14.84	24.76	15.77	26.13	16.73
1.4	31.26	12.94	--	--	--	--

* Courtesy of Professor R. F. Christy.

TABLE 6

FACTORS ENTERING LATERAL DISTRIBUTION FUNCTION

r	$\ln R_1(r)$	r	$\ln R_1(r)^*$	r	$\ln R_1(r)$	r	$\ln R_1(r)$
0	1.179	--	--	1.0	2.786	4.5	6.982
0.01	1.154	0.1	0.908	1.2	<u>2.412</u>	5.0	<u>6.555</u>
0.02	1.128	0.2	0.655	1.4	<u>2.075</u>	6	<u>7.700</u>
0.03	1.095	0.3	0.391	1.6	<u>3.777</u>	7	<u>8.845</u>
0.04	1.072	0.4	0.139	1.8	<u>3.511</u>	8	<u>9.990</u>
0.05	1.044	0.5	1.894	2.0	<u>3.359</u>	9	<u>9.135</u>
0.06	1.015	0.6	<u>1.655</u>	2.5	<u>4.747</u>	10	<u>10.280</u>
0.07	0.990	0.7	<u>1.424</u>	3.0	<u>4.286</u>		
0.08	0.963	0.8	<u>1.201</u>	3.5	<u>5.845</u>		
0.09	0.940	0.9	<u>2.990</u>	4.0	<u>5.410</u>		
0.10	0.908	1.0	<u>2.786</u>	4.5	<u>6.982</u>		

s	$\ln [3.25 R(s)]$
0.2	4.824
0.4	<u>3.724</u>
0.6	<u>2.303</u>
0.8	<u>2.709</u>
1.0	<u>1.016</u>
1.2	<u>1.232</u>
1.4	<u>1.407</u>
1.6	<u>1.513</u>
1.8	<u>1.554</u>
2.0	<u>1.594</u>

KEY :

$$R_1(r) = Ae^{-\alpha r} + Be^{-\beta r}$$

$$A = 2.94$$

$$B = 0.31$$

$$\alpha = 2.88$$

$$\beta = 0.855$$

$$R(s) = \left[2\pi \Gamma(s) \left(\frac{A}{\alpha^s} + \frac{B}{\beta^s} \right) \right]^{-1}$$

r = radius from center of shower
in lateral units (60 meters
at sea level)

s = shower theory parameter

$\Gamma(s)$ = Gamma Function

* The underlined characteristics are
negative.

TABLE 7

VALUES OF $\ln f_s(r)^*$

r \ s	0.2	0.4	0.6	0.8	1.0	1.2	1.4	1.6	1.8
0.01	5.089	5.067	4.726	4.211	3.556	2.892	2.145	1.330	0.450
0.02	3.816	3.932	3.730	3.353	2.837	2.312	1.707	1.027	0.285
0.03	2.871	3.249	3.128	2.833	2.398	1.953	1.426	0.831	0.171
0.04	2.512	2.767	2.703	2.466	2.088	1.701	1.231	0.694	0.091
0.05	2.082	2.382	2.363	2.170	1.837	1.494	1.069	0.576	0.018
0.06	1.725	2.062	2.079	1.922	1.626	1.320	0.931	0.474	1.953
0.07	1.424	1.791	1.839	1.713	1.447	1.172	0.714	0.388	1.879
0.08	1.155	1.522	1.624	1.525	1.286	1.037	0.706	0.307	1.843
0.09	0.920	1.338	1.436	1.360	1.145	0.920	0.613	0.237	1.797
0.1	0.701	1.139	1.259	1.204	1.010	0.806	0.520	0.165	1.746
0.2	1.198	1.775	0.033	0.117	0.061	1.997	1.849	1.633	1.352
0.3	<u>2.202</u>	<u>2.861</u>	1.200	1.366	<u>1.391</u>	<u>1.407</u>	<u>1.341</u>	<u>1.206</u>	<u>1.007</u>
0.4	<u>3.434</u>	<u>2.150</u>	<u>2.547</u>	<u>2.770</u>	<u>2.852</u>	<u>2.926</u>	<u>2.917</u>	<u>2.839</u>	<u>2.697</u>
0.5	<u>4.788</u>	<u>3.548</u>	<u>3.989</u>	<u>2.257</u>	<u>2.384</u>	<u>2.502</u>	<u>2.538</u>	<u>2.505</u>	<u>2.408</u>
0.6	<u>4.233</u>	<u>3.028</u>	<u>3.505</u>	<u>3.807</u>	<u>3.970</u>	<u>2.123</u>	<u>2.193</u>	<u>2.196</u>	<u>2.134</u>
0.7	<u>5.711</u>	<u>4.539</u>	<u>3.049</u>	<u>3.383</u>	<u>3.577</u>	<u>3.763</u>	<u>3.866</u>	<u>3.896</u>	<u>3.870</u>
0.8	<u>5.249</u>	<u>4.103</u>	<u>4.638</u>	<u>3.000</u>	<u>3.221</u>	<u>3.433</u>	<u>3.563</u>	<u>3.624</u>	<u>3.621</u>
0.9	<u>6.826</u>	<u>5.703</u>	<u>4.262</u>	<u>4.647</u>	<u>4.892</u>	<u>3.128</u>	<u>3.281</u>	<u>3.362</u>	<u>3.386</u>
1.0	<u>6.432</u>	<u>5.331</u>	<u>5.911</u>	<u>4.317</u>	<u>4.583</u>	<u>4.840</u>	<u>3.014</u>	<u>3.120</u>	<u>3.161</u>
1.2	<u>7.730</u>	<u>6.665</u>	<u>5.282</u>	<u>5.724</u>	<u>4.027</u>	<u>4.320</u>	<u>4.531</u>	<u>4.673</u>	<u>4.757</u>
1.4	<u>7.115</u>	<u>6.082</u>	<u>6.729</u>	<u>5.202</u>	<u>5.536</u>	<u>5.860</u>	<u>4.101</u>	<u>4.274</u>	<u>4.383</u>
1.6	<u>8.577</u>	<u>7.570</u>	<u>6.244</u>	<u>6.744</u>	<u>5.104</u>	<u>5.455</u>	<u>5.723</u>	<u>5.923</u>	<u>4.058</u>
1.8	<u>8.099</u>	<u>7.116</u>	<u>7.813</u>	<u>6.336</u>	<u>6.720</u>	<u>5.095</u>	<u>5.386</u>	<u>5.610</u>	<u>5.878</u>
2.0	<u>9.757</u>	<u>8.795</u>	<u>7.514</u>	<u>6.059</u>	<u>6.463</u>	<u>6.858</u>	<u>5.171</u>	<u>5.416</u>	<u>5.595</u>
2.5	<u>10.744</u>	<u>9.826</u>	<u>8.589</u>	<u>7.178</u>	<u>7.628</u>	<u>6.068</u>	<u>6.425</u>	<u>6.715</u>	<u>6.939</u>
3.0	<u>11.955</u>	<u>9.073</u>	<u>9.873</u>	<u>8.499</u>	<u>8.984</u>	<u>7.461</u>	<u>7.855</u>	<u>6.181</u>	<u>6.441</u>
3.5	<u>11.236</u>	<u>10.386</u>	<u>9.216</u>	<u>9.873</u>	<u>8.389</u>	<u>8.897</u>	<u>7.321</u>	<u>7.678</u>	<u>7.970</u>
4.0	<u>12.561</u>	<u>11.737</u>	<u>10.594</u>	<u>9.277</u>	<u>9.821</u>	<u>8.355</u>	<u>8.806</u>	<u>7.188</u>	<u>7.508</u>
4.5	<u>13.921</u>	<u>11.121</u>	<u>10.001</u>	<u>10.708</u>	<u>9.275</u>	<u>9.833</u>	<u>8.308</u>	<u>8.715</u>	<u>7.056</u>
5.0	<u>13.304</u>	<u>12.525</u>	<u>11.427</u>	<u>10.155</u>	<u>10.743</u>	<u>9.322</u>	<u>9.817</u>	<u>8.245</u>	<u>8.608</u>
6	<u>14.121</u>	<u>13.378</u>	<u>12.317</u>	<u>11.081</u>	<u>11.705</u>	<u>10.321</u>	<u>10.853</u>	<u>9.317</u>	<u>9.717</u>
7	<u>16.988</u>	<u>14.277</u>	<u>13.246</u>	<u>12.041</u>	<u>12.696</u>	<u>11.342</u>	<u>11.905</u>	<u>10.401</u>	<u>10.841</u>
8	<u>17.893</u>	<u>15.208</u>	<u>14.204</u>	<u>13.026</u>	<u>13.708</u>	<u>12.380</u>	<u>12.970</u>	<u>11.492</u>	<u>11.949</u>
9	<u>18.826</u>	<u>16.164</u>	<u>15.183</u>	<u>14.029</u>	<u>14.735</u>	<u>13.431</u>	<u>12.045</u>	<u>12.590</u>	<u>11.071</u>
10	<u>19.781</u>	<u>17.141</u>	<u>16.181</u>	<u>15.048</u>	<u>15.774</u>	<u>14.492</u>	<u>13.126</u>	<u>13.693</u>	<u>12.195</u>

* Underlined characteristics are negative.

$$f(r,s) = \frac{R(s)}{r^2 - s} [Ae^{-\alpha r} + Be^{-\beta r}]$$

$\ln(f(r,s)) = \log_e [f(r,s)]$ in body of table.

TABLE 8

NUMBERS OF ELECTRONS AS A FUNCTION OF ENERGY AND
SHOWER RADIUS AS A FUNCTION OF ENERGY AND DENSITY

(See Table 4 for definition of symbols)

t	ξ	s	$\ln \Pi$	log r* in table for $\log \rho^{**} =$				
				4	5	6	7	8
5	4	1.289	1.88	5.127	7.724	8.322	10.920	11.517
	5	1.123	3.06	4.534	5.393	6.253	7.113	9.972
	6	1.000	3.99	3.306	4.305	5.306	6.306	7.305
	7	0.898	4.82	3.825	4.917	4.010	5.102	6.195
	8	0.819	5.58	2.190	3.351	4.504	5.656	6.809
	9	0.752	6.24	2.455	3.70	4.887	4.086	5.284
	10	0.699	6.87	2.672	3.954	3.186	4.417	5.649
	11	0.651	7.45	2.854	2.150	3.441	4.700	5.958
	12	0.609	8.00	1.000	2.362	3.663	4.944	4.225
	13	0.571	8.54	1.146	2.532	3.84	3.14	4.462
	14	0.541	9.04	1.255	2.672	2.01	3.34	4.659
	15	0.519	9.49	1.355	2.792	2.16	3.500	4.824
	16	0.496	9.92	1.431	2.895	2.272	3.638	4.99
	17	0.474	10.32	1.498	1.01	2.389	3.772	3.116
	18	0.456	10.69	1.568	1.097	2.498	3.888	3.25
	19	0.438	11.07	1.618	1.18	2.62	2.000	3.360
	20	0.421	11.44	1.672	1.255	2.699	2.11	3.49
	21	0.402	11.86		1.328	2.804	2.210	3.60
	22	0.390	12.26		1.406	2.892	2.322	3.715
	23	0.377	12.66		1.462	2.97	2.412	3.82
	24	0.365	13.04		1.525	1.053	2.505	3.92
	25	0.353	13.42		1.586	1.146	2.602	2.013
	26	0.348	13.78			1.21	2.686	2.104
	27	0.332	14.13			1.284	2.76	2.20
	28	0.323	14.47			1.352	2.845	2.283
	29	0.314	14.80			1.398	2.909	2.358
	30	0.306	15.12			1.455	2.98	2.440
	31	0.298	15.43				1.04	2.50
	32	0.291	15.72				1.11	2.580
	33	0.285	16.01				1.170	2.653
	34	0.278	16.28				1.238	2.714
	35	0.273	16.55				1.28	2.76
	36	0.267	16.80					2.82
	37	0.261	17.05					2.88
	38	0.256	17.28					2.94
	39	0.251	17.50					1.00
	40	0.247	17.71					1.05

*Characteristics negative, mantissas positive.

**Characteristics positive, ρ is surface density of shower.

TABLE 8 (CONT'D.)

NUMBERS OF ELECTRONS AS A FUNCTION OF ENERGY AND
SHOWER RADIUS AS A FUNCTION OF ENERGY AND DENSITY

(See Table 4 for definition of symbols)

t	ϵ	s	$\ln \Pi$	log r* in table for log** $\rho =$					
				4	5	6	7	8	
10	6	1.424	3.01	6.89					
	7	1.315	4.34	4.495	5.04	7.57			
	8	1.218	5.56	3.544	4.24	5.00			
	9	1.130	6.66	2.276	3.12	5.98	6.87		
	10	1.060	7.70	2.778	3.78	4.753	5.66		
	11	1.000	8.67	1.161	2.29	3.340	4.33	6.63	
	12	0.945	9.59	1.422	2.69	3.825	4.89	5.34	
	13	0.891	10.44	1.608	1.02	2.212	3.37	5.94	
	14	0.845	11.25	1.760	1.26	2.538	3.73	4.43	
	15	0.808	12.02	1.881	1.45	2.183	2.04	4.85	
	16	0.778	12.73	1.973	1.60	1.042	2.30	3.21	
	17	0.750	13.44	0.060	1.72	1.222	2.54	3.51	
	18	0.722	14.10	0.140	1.82	1.384	2.77	3.795	
	19	0.696	14.75		1.91	1.528	2.97	2.025	
	20	0.669	15.39		1.99	1.642	1.13	2.260	
	21	0.631	16.03			1.740	1.27	2.484	
	22	0.615	16.632				1.40	2.676	
	23	0.597	17.232					2.854	
	24	0.582	17.810					1.020	
	25	0.567	18.375						
30	0.505	20.940							
15	6	1.723	0.97						
	7	1.592	2.62						
	8	1.485	4.13	5.23					
	9	1.395	5.53	4.875	5.277				
	10	1.316	6.87	2.104	4.632	5.170	7.704		
	11	1.250	8.11	2.842	3.612	4.29	6.942		
	12	1.193	9.28	1.312	2.352	3.16	5.902	6.68	
	13	1.140	10.40	1.618	2.906	3.87	4.695	5.50	
	14	1.092	11.47	1.839	1.290	2.472	3.356	4.28	
	15	1.045	12.50	1.982	1.570	2.875	3.929	4.95	
	16	1.000	13.48	0.117	1.767	1.200	2.380	3.52	
17	0.964	14.40	0.233	1.714	1.470	2.763	3.97		
18	0.927	15.31		0.040	1.668	1.097	2.278		
19	0.895	16.17		0.149	1.811	1.336	2.620		
20	0.865	16.98	0.526		1.936	1.528	2.903		

*Characteristics negative, mantissas positive.

**Characteristics positive, ρ is surface density of shower.

TABLE 8 (CON'D.)

NUMBERS OF ELECTRONS AS A FUNCTION OF ENERGY AND
SHOWER RADIUS AS A FUNCTION OF ENERGY AND DENSITY

(See Table 4 for definition of symbols)

t	ϵ	s	$\ln \Pi$	log r* in table for log p**				
				4	5	6	7	8
15	21	0.835	17.74		0.398		1.683	1.114
	22	0.807	18.54				1.816	1.320
	23	0.780	19.33	0.792	0.628	0.238		1.500
	24	0.751	20.11					1.683
	25	0.724	20.88					
	26	0.696	21.63			0.410		1.906
20	10	1.512	5.13		7.850			
	11	1.437	6.63		5.784	6.25		
	12	1.371	8.03	2.667	3.170	5.57	7.99	
	13	1.317	9.32	1.301	2.130	4.69	5.26	
	14	1.268	10.58	1.653	2.895	3.62	4.30	6.92
	15	1.222	11.80	1.902	1.375	2.39	3.175	5.88
	16	1.178	12.95	0.077	1.658	2.98	3.903	4.72
	17	1.138	14.04	0.210	1.881	1.40	2.484	3.44
	18	1.099	15.14	0.371	0.047	1.68	2.996	2.03
	19	1.063	16.23	0.498	0.196	1.87	1.338	2.52
	20	1.032	17.28	0.602	0.330	0.03	1.602	2.97
	21	1.000	18.35	0.693		0.154	1.813	1.301
	22	0.971	19.37	0.765		0.29	1.971	1.54
	23	0.944	20.38				0.107	1.73
	24	0.920	21.33				0.225	1.89
25	0.895	22.25		0.739		0.340	0.041	
25	12	1.537	6.23	4.72	6.56			
	13	1.474	7.85	2.389	4.445	6.63		
	14	1.419	9.20	1.250	3.835	4.12	6.39	
	15	1.369	10.57	1.668	2.806	3.34	5.755	
	16	1.323	11.85	1.929	1.386	2.255	4.840	5.37
	17	1.282	13.12	0.124	1.719	2.998	3.767	4.38
	18	1.242	14.37	0.297	1.957	1.452	2.518	3.27
	19	1.203	15.59	0.453	0.134	1.747	1.107	2.05
	20	1.168	16.83	0.586	0.299	1.962	1.501	2.64
	21	1.133	17.93	0.686	0.441	0.129	1.748	1.097
	22	1.103	19.00	0.763	0.559	0.265	1.934	1.43
	23	1.074	20.00			0.393	0.079	1.703

*Characteristics negative, mantissas positive.

**Characteristics positive, ρ is surface density of shower.

TABLE 8 (CONT'D.)

NUMBERS OF ELECTRONS AS A FUNCTION OF ENERGY AND
SHOWER RADIUS AS A FUNCTION OF ENERGY AND DENSITY

(See Table 4 for definition of symbols)

t	ϵ	s	$\ln \Pi$	log r* in table for $\log \rho^{**} =$				
				4	5	6	7	8
25	24	1.047	21.09			0.525	0.225	1.90
	25	1.024	22.18	0.944	0.808		0.366	0.07
	26	1.000	23.22					0.194
	27	0.978	24.20					0.32
30	12	1.670	4.32	8.95				
	13	1.613	5.95	5.80	7.22			
	14	1.555	7.50	3.820	5.60	6.03		
	15	1.502	9.01	1.09	3.36	5.76		
	16	1.452	10.48	1.634	2.628	3.13	5.09	
	17	1.407	11.94	1.957	1.342	2.279	4.505	
	18	1.362	13.30	0.164	1.771	1.079	3.655	4.09
	19	1.322	14.61	0.346	0.000	1.525	2.550	3.13
	20	1.288	15.91	0.525	0.201	1.81	1.190	2.00
	21	1.253	17.15	0.642	0.38	0.034	1.583	2.756
	22	1.223	18.28	0.740	0.498	0.190	1.826	1.238
	23	1.195	19.48		0.628	0.352	0.025	1.570
	24	1.170	20.65			0.491	0.193	1.810
	25	1.142	21.82	0.942			0.326	0.011
	26	1.117	22.97		0.874		0.484	0.180
	27	1.092	24.10				0.608	0.332
28	1.070	25.18			0.865		0.460	
29	1.048	26.25					0.586	
30	1.022	27.24						
35	13	1.757	3.77	11.47				
	14	1.686	5.38	6.05				
	15	1.622	7.04	4.96	6.32	9.66		
	16	1.563	8.64	2.771	4.655	6.35	11.79	8.08
	17	1.515	10.22	1.568	2.322	4.30	8.18	6.25
	18	1.471	11.67	1.914	1.272	3.78	6.02	5.90
	19	1.432	13.13	0.158	1.734	2.886	5.52	3.275
	20	1.396	14.58	0.370	0.015	1.516	4.73	2.406
	21	1.362	15.62	0.525	0.220	1.813	3.82	1.146
	22	1.330	17.12	0.648	0.389	0.038	2.648	1.576
	23	1.298	18.39	0.764	0.540	0.226	1.857	1.260
	24	1.268	19.62	0.842	0.668	0.394	0.045	1.634
25	1.240	20.85		0.765	0.520	0.236	1.875	

*Characteristics negative, mantissas positive.

**Characteristics positive, ρ is surface density of shower.

TABLE 8 (CONT'D.)

NUMBERS OF ELECTRONS AS A FUNCTION OF ENERGY AND
SHOWER RADIUS AS A FUNCTION OF ENERGY AND DENSITY

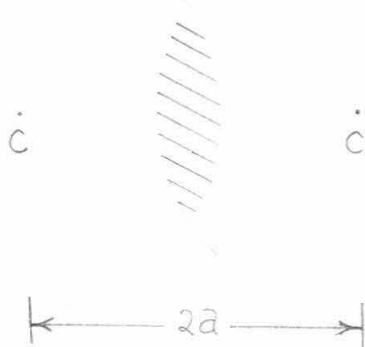
(See Table 4 for definition of symbols)

t	ξ	s	$\ln \Pi$	log r* in table for $\log \rho^{**} =$				
				4	5	6	7	8
35	26	1.214	22.05		0.839	0.640	0.398	0.074
	27	1.187	23.21	(1.017) ^a	0.903	0.752	0.534	0.250
	28	1.166	24.35					0.380
	29	1.144	25.50					0.525
	30	1.123	26.62			0.952		0.634
(a) This number is entirely positive.								

*Characteristics negative, mantissas positive.

**Characteristics positive, ρ is surface density of shower.

TABLE 9

THE WEIGHT FUNCTION FOR LATERAL SEPARATION, C(y)

$C(a/r)$ = Ratio of shaded area to area of circle.

a = Half the separation between counters.

r = Shower radius.

$y = a/r$

$$C(y) = 1 - \frac{2}{\pi} (y \sqrt{1-y^2} + y^2 \sin^{-1} y)$$

$$C(y) = 1.0000 - 0.6366y + 0.02207y^2 - 0.3730y^3$$

y	$\log^* y$	$\log^* C(y)$	$C(y)$	Approx.
0.00	-	0.0000	1.0000	1.0000
0.05	2.6990	1.9859	0.9681	
0.10	<u>1.0000</u>	<u>1.9718</u>	0.9360	0.9362
0.15	<u>1.1761</u>	<u>1.9559</u>	0.9034	
0.20	<u>1.3010</u>	<u>1.9396</u>	0.8701	0.8706
0.25	<u>1.3979</u>	<u>1.9221</u>	0.8358	
0.30	<u>1.4771</u>	<u>1.9033</u>	0.8004	0.8009
0.35	<u>1.5441</u>	<u>1.8828</u>	0.7634	
0.40	<u>1.6021</u>	<u>1.8602</u>	0.7247	0.7250
0.45	<u>1.6532</u>	<u>1.8351</u>	0.6840	
0.50	<u>1.6990</u>	<u>1.8069</u>	0.6410	0.6406
0.55	<u>1.7404</u>	<u>1.7748</u>	0.5954	
0.60	<u>1.7782</u>	<u>1.7379</u>	0.5469	0.5409
0.65	<u>1.8129</u>	<u>1.6948</u>	0.4952	
0.70	<u>1.8451</u>	<u>1.6434</u>	0.4399	0.4373
0.75	<u>1.8751</u>	<u>1.5804</u>	0.3805	
0.80	<u>1.9031</u>	<u>1.5005</u>	0.3166	0.3139
0.85	<u>1.9294</u>	<u>1.3804</u>	0.2410	
0.90	<u>1.9542</u>	<u>1.2380</u>	0.1730	0.1730
0.95	<u>1.9777</u>	<u>2.9594</u>	0.0911	
1.00	0.0000	-	0.0000	0.0125

*Underlined characteristics are negative

TABLE 10
THE PRIMARY SPECTRUM*

ϵ	$\log^{**}e^{-\gamma\epsilon}$	ϵ	$\log^{**}e^{-\gamma\epsilon}$	ϵ	$\log^{**}e^{-\gamma\epsilon}$
1	<u>1.2183</u>	16	<u>13.4922</u>	31	<u>25.7661</u>
2	<u>2.4365</u>	17	<u>14.7103</u>	32	<u>26.7843</u>
3	<u>3.6548</u>	18	<u>15.9287</u>	33	<u>26.2026</u>
4	<u>4.8730</u>	19	<u>15.1469</u>	34	<u>27.4208</u>
5	<u>4.0913</u>	20	<u>16.3652</u>	35	<u>28.6391</u>
6	<u>5.3096</u>	21	<u>17.5835</u>	36	<u>29.8574</u>
7	<u>6.5278</u>	22	<u>18.8017</u>	37	<u>29.0756</u>
8	<u>7.7461</u>	23	<u>18.0200</u>	38	<u>30.2939</u>
9	<u>8.9642</u>	24	<u>19.2382</u>	39	<u>31.5121</u>
10	<u>8.1825</u>	25	<u>20.4565</u>	40	<u>32.7304</u>
11	<u>9.4009</u>	26	<u>21.6748</u>	41	<u>33.9487</u>
12	<u>10.6191</u>	27	<u>22.8930</u>	42	<u>33.1669</u>
13	<u>11.8373</u>	28	<u>22.1113</u>	43	<u>34.3852</u>
14	<u>11.0556</u>	29	<u>23.3295</u>	44	<u>35.6034</u>
15	<u>12.2739</u>	30	<u>24.5478</u>	45	<u>36.8217</u>
4.5	<u>4.4822</u>	15.5	<u>13.8830</u>	26.5	<u>21.2839</u>
5.5	<u>5.7004</u>	16.5	<u>13.1013</u>	27.5	<u>22.5022</u>
6.5	<u>6.9187</u>	17.5	<u>14.3196</u>	28.5	<u>23.7204</u>
7.5	<u>6.1370</u>	18.5	<u>15.5378</u>		
8.5	<u>7.3552</u>	19.5	<u>16.7561</u>		
9.5	<u>8.5735</u>	20.5	<u>17.9743</u>		
10.5	<u>9.7917</u>	21.5	<u>17.1926</u>		
11.5	<u>9.0100</u>	22.5	<u>18.4108</u>		
12.5	<u>10.2283</u>	23.5	<u>19.6291</u>		
13.5	<u>11.4465</u>	24.5	<u>20.8473</u>		
14.5	<u>12.6648</u>	25.5	<u>20.0656</u>		

* $\gamma = 1.8$

**The underlined characteristics are negative, mantissas positive.

TABLE 11
INTEGRAL VERTICAL FREQUENCY ($\log (H^V(>\rho) / \pi D)$)
IN BODY OF TABLE*

		<u>t = 5</u>						
log a =		-∞	-2.5	-2.0	-1.5			
log ρ =	4	<u>10.710</u>	<u>10.534</u>	<u>10.204</u>	<u>11.427</u>			
	5	<u>11.018</u>	<u>12.454</u>	<u>13.779</u>	<u>14.274</u>			
	6	<u>13.345</u>	<u>15.588</u>	<u>16.575</u>	<u>18.502</u>			
	7	<u>15.740</u>	<u>18.645</u>	<u>20.417</u>	<u>23.457</u>			
	8	<u>16.140</u>	<u>22.560</u>	<u>25.720</u>	<u>29.746</u>			
		<u>t = 10</u>						
log ρ =	4	<u>10.294</u>	<u>10.270</u>	<u>10.200</u>	<u>10.092</u>			
	5	<u>12.653</u>	<u>12.620</u>	<u>12.550</u>	<u>12.263</u>			
	6	<u>14.922</u>	<u>14.746</u>	<u>14.517</u>	<u>14.099</u>			
	7	<u>15.184</u>	<u>16.750</u>	<u>16.332</u>	<u>17.659</u>			
	8	<u>17.433</u>	<u>18.443</u>	<u>19.829</u>	<u>20.918</u>			
		<u>t = 15</u>						
log ρ =	4	<u>11.716</u>	<u>11.716</u>	<u>11.688</u>	<u>11.630</u>			
	5	<u>12.184</u>	<u>12.169</u>	<u>12.122</u>	<u>13.970</u>			
	6	<u>14.598</u>	<u>14.578</u>	<u>14.487</u>	<u>14.361</u>			
	7	<u>16.890</u>	<u>16.806</u>	<u>16.700</u>	<u>16.482</u>			
	8	<u>17.263</u>	<u>17.094</u>	<u>18.812</u>	<u>18.415</u>			
		<u>All For a = 0</u>						
t =	5	10	15	20	25	30	35	
log ρ =	4	<u>10.710</u>	<u>10.294</u>	<u>11.716</u>	<u>12.879</u>	<u>13.985</u>	<u>13.196</u>	<u>14.248</u>
	5	<u>11.018</u>	<u>12.653</u>	<u>12.184</u>	<u>13.564</u>	<u>14.711</u>	<u>15.912</u>	<u>15.048</u>
	6	<u>13.345</u>	<u>14.922</u>	<u>14.598</u>	<u>14.020</u>	<u>15.293</u>	<u>16.658</u>	<u>17.777</u>
	7	<u>15.740</u>	<u>15.184</u>	<u>16.890</u>	<u>16.435</u>	<u>17.854</u>	<u>17.246</u>	<u>18.409</u>
	8	<u>16.140</u>	<u>17.433</u>	<u>17.263</u>	<u>18.894</u>	<u>18.328</u>	<u>19.765</u>	<u>19.016</u>

*The underlined characteristics are negative, mantissas positive.
 *a is half the counter separation in lateral units.

TABLE 12

SMOOTHED CONSTANTS FOR INTERPOLATION FUNCTIONS
FOR INTEGRAL VERTICAL FREQUENCY

A. Values of p in $H^V/\pi D = L(\rho, t_0) \exp(-p(t-t_0))$
 p in body of table ($a=0$).

$\log \rho =$	4	5	6	7	8
$t_0 = 15$	0.3339	0.2825	0.2360	0.1946	0.1504
20	0.3960	0.3495	0.3085	0.2710	0.2303
25	0.4260	0.3841	0.3488	0.3152	0.2779
30	0.4363	0.4013	0.3726	0.3456	0.3120

Note: $D = 7.52 \times 10^{12} \times \sigma^2$

B. Values of M, δ, q in $H^V/\pi D = M(\rho, t_0) \exp(-q(t-t_0))/\rho^\delta$
 $\log M^*$ in body of table ($a=0$). q in body of table ($a=0$).

$\log \rho =$	5	6	7	$\log \rho =$	5	6	7
$t_0 = 15$	<u>5.994</u>	<u>4.324</u>	<u>4.524</u>	$t_0 = 15$	0.5250	0.4812	0.4397
20	<u>6.804</u>	<u>5.164</u>	<u>5.488</u>	20	0.5687	0.5273	0.4904
25	<u>7.436</u>	<u>7.891</u>	<u>6.361</u>	25	0.5895	0.5480	0.5135
30	<u>8.252</u>	<u>8.800</u>	<u>7.277</u>	30	0.5964	0.5572	0.5204

*Underlined characteristics negative.

δ in body of table ($a=0$).

$1.8/\delta$ in body of table ($a=0$).

$\log \rho =$	5	6	7
$t_0 = 15$	<u>1.562</u>	<u>1.621</u>	<u>1.662</u>
20	<u>1.448</u>	<u>1.524</u>	<u>1.579</u>
25	<u>1.345</u>	<u>1.433</u>	<u>1.501</u>
30	<u>1.268</u>	<u>1.357</u>	<u>1.433</u>

$\log \rho =$	5	6	7
$t_0 = 15$	<u>1.152</u>	<u>1.110</u>	<u>1.083</u>
20	<u>1.243</u>	<u>1.181</u>	<u>1.140</u>
25	<u>1.338</u>	<u>1.256</u>	<u>1.199</u>
30	<u>1.420</u>	<u>1.326</u>	<u>1.256</u>

TABLE 13

EFFECT OF ATMOSPHERIC STRUCTURE ON COUNTING RATERadiation Unit Adopted at Point of Observation

t	σ	σ^2	S	*	log S	log a	δ	$(\delta-1)\log\sigma^2$
5	3.694	13.647	1.68	<u>7</u>	-6.775	-2.211	2.037	1.178
7.5	2.618	6.854	3.34	<u>7</u>	-6.476	-2.061	1.969	0.810
10	2.082	4.336	5.28	<u>7</u>	-6.277	-1.962	1.855	0.545
12.5	1.745	3.045	7.52	<u>7</u>	-6.124	-1.886	1.737	0.356
15	1.499	2.247	1.02	<u>6</u>	-5.992	-1.820	1.636	0.224
17.5	1.318	1.720	1.32	<u>6</u>	-5.880	-1.763	1.582	0.137
20	1.178	1.388	1.65	<u>6</u>	-5.782	-1.714	1.536	0.076
22.5	1.066	1.132	2.02	<u>6</u>	-5.694	-1.672	1.455	0.020
24	1.000	1.000	2.29	<u>6</u>	-5.640	-1.644	1.426	0.000

Adjustment for Evaluating Radiation UnitAbove Point of Observation

t	x max	t-x	$\sigma^2at(t-x)$	$(\delta-1)\log\sigma^2$	Reduction
5	0.40	4.6	17.441	1.2875	0.7772
7.5	0.65	6.85	7.928	0.8713	0.8684
10	0.80	9.2	4.954	0.5942	0.8913
12.5	1.0	11.5	3.489	0.4000	0.9037
15	1.0	14.0	2.520	0.2553	0.9305

* The separate numbers are the power of 10 by which the left hand number should be multiplied.

TABLE 14
INTEGRAL VERTICAL FREQUENCY CORRECTED FOR
COUNTER SEPARATION AND ATMOSPHERIC STRUCTURE

$\log \rho =$	4	5	6	7
t = 5	<u>12.851</u>	<u>15.673</u>	<u>18.005</u>	<u>23.295</u>
7.5	<u>11.630</u>	<u>13.726</u>	<u>15.519</u>	<u>19.656</u>
10	<u>11.768</u>	<u>13.891</u>	<u>15.725</u>	<u>17.356</u>
12.5	<u>11.672</u>	<u>13.970</u>	<u>14.038</u>	<u>17.991</u>
15	<u>11.470</u>	<u>13.848</u>	<u>14.120</u>	<u>16.356</u>
17.5	<u>11.206</u>	<u>13.716</u>	<u>14.116</u>	<u>16.386</u>
20	<u>12.863</u>	<u>13.513</u>	<u>15.943</u>	<u>16.353</u>
22.5	<u>12.493</u>	<u>13.208</u>	<u>15.743</u>	<u>16.213</u>
25	<u>12.128</u>	<u>14.854</u>	<u>15.436</u>	<u>17.997</u>

Note: The numbers in the body of the table are:

$$\log \left[\frac{1}{\pi D} \sigma^2 H^v(\sqrt{\rho \sigma^2}, t, \frac{a}{\sigma}) \right],$$

for $\log a = -1.644$.

TABLE 15

INTEGRAL FREQUENCY INCLUDING ALL ZENITH ANGLES

<u>log (H(>ρ)/πD) in table for log a = -1.644</u>						<u>Constants**</u>	
log ρ =	4	5	6	7	8	δ	log P
t = 5	<u>10.830</u>	<u>12.933</u>	<u>14.863</u>	<u>16.858</u>		2.037	12.456
7.5	<u>10.605</u>	<u>12.896</u>	<u>14.942</u>	<u>16.958</u>		1.969	12.129
10	<u>10.355</u>	<u>12.720</u>	<u>14.895</u>	<u>15.010</u>		1.855	11.398
12.5	<u>11.973</u>	<u>12.405</u>	<u>14.730</u>	<u>16.931</u>		1.737	10.523
15	<u>11.567</u>	<u>12.082</u>	<u>14.505</u>	<u>16.811</u>		1.636	9.694
17.5*	<u>11.156</u>	<u>13.799</u>	<u>14.263</u>	<u>16.636</u>	<u>17.144</u>	1.582	9.129
20	<u>12.641</u>	<u>13.392</u>	<u>15.880</u>	<u>16.319</u>	<u>18.849</u>	1.536	8.470
22.5	<u>12.160</u>	<u>14.906</u>	<u>15.469</u>	<u>17.996</u>	<u>18.509</u>	1.455	7.582
24	<u>13.868</u>	<u>14.635</u>	<u>15.217</u>	<u>17.782</u>	<u>18.295</u>	1.426	7.147
25	<u>13.680</u>	<u>14.445</u>	<u>15.048</u>	<u>17.630</u>	<u>18.151</u>	1.408	6.869
27.5	<u>13.202</u>	<u>15.984</u>	<u>16.622</u>	<u>17.212</u>	<u>19.776</u>	1.386	6.312
30	<u>14.728</u>	<u>15.537</u>	<u>16.213</u>	<u>18.808</u>	<u>19.410</u>	1.365	5.776
15*	<u>11.636</u>	<u>12.184</u>	<u>14.617</u>	<u>16.949</u>	<u>17.383</u>	1.618	9.699

* These values include no correction for the finite separation of the counters, and this correction is still appreciable until t = 20 or more.

** These are all constants for the expression:

$$H(>\rho) = P/\rho^\delta$$

Where P does not include a correction for the variable density of the atmosphere, the complete correction is made by multiplying by $(\sigma^2)^{\delta+1}$, see table 15.

Note: The underlined characteristics are negative.

TABLE 16
COUNTING RATE AS A FUNCTION OF ALTITUDE

t	I(δ)	$\log [IPS^\delta]$	Na**	Nb***	$\log Na$	$\log Nb$
5	1.643	1.183	0.7874	1.0131	<u>1.89620</u>	0.00561
7.5	1.521	1.206	2.1592	2.4864	<u>0.33429</u>	0.39550
10	1.360	1.069	3.0117	3.3790	0.47881	0.52879
12.5	1.210	0.808	2.5714	2.8454	0.45399	0.45408
15	1.116	0.514	1.8153	1.9509	0.29024	0.29026
17.5*	1.075	0.239	1.2400	1.2420	0.09412	0.09412
20	1.045	<u>1.826</u>	0.5620	0.5620	<u>1.74974</u>	<u>1.74974</u>
22.5	1.000	<u>1.376</u>	0.2191	0.2191	<u>1.34064</u>	<u>1.34064</u>
24	0.987	<u>1.098</u>	0.12523	0.12523	<u>1.09760</u>	<u>1.09760</u>
25	0.980	<u>2.919</u>	0.08316	0.08316	<u>2.9199</u>	<u>2.9199</u>
27.5	0.970	<u>2.482</u>	0.03030	0.03030	<u>2.4814</u>	<u>2.4814</u>
30	0.960	<u>2.059</u>	0.01150	0.01150	<u>2.0605</u>	<u>2.0605</u>
15*	1.100	0.615	2.3262	2.4999	0.36661	0.3980
17.5(i)			1.000	1.002	0.0000	0.0050

* These values include no correction for the finite separation of the counters, and this correction is still appreciable until $t = 20$ or more.

** This is the counting rate per hour with the size of the radiation unit adjusted to a suitable point above the counter (See Table 15).

*** This is the counting rate per hour with the size of the radiation unit evaluated at the point of observation.

(i) Estimated corrected value.

Note: The underlined characteristics are negative.

TABLE 17
COMPARISON OF THEORY AND EXPERIMENT

t rad.units	Na/hr. counts per hr. Theoret.	(2.336) ^δ	Theoret. for Hilberry x3	Hilberry Expt. Counts per hr.	3 Na	Kraybill* Expt. Counts Per hr.	8.33Na
5	0.787				2.362	16.50	6.56
7.5	2.159				6.478	24.65	17.99
10	3.012				9.035	24.20	25.09
12.5	2.571				7.714	17.10	21.42
15	1.815	4.007	21.82	22.2	5.446	7.60	15.12
17.5	1.000	3.827	11.48	9.95	3.000	(3.60)	8.33
20	0.562	3.681	6.21	4.65	1.686	(1.60)	4.68
22.5	0.219	3.437	2.26	2.25	0.657	(0.60)	1.82
24	0.125	3.353	1.26	1.40	0.376	(0.40)	1.04

The ratio of Hilberry's counter area to that of Kraybill's is $196/83.9 = 2.336$.

$$8.33/3 = 2.78.$$

$$7.40/3 = 2.45.$$

* The () numbers are obtained using Hilberry's data to extropolate.

TABLE 18
ESTIMATE OF UNCERTAINTIES IN CALCULATION

t	$\log \rho$ (max)	θ (max) deg.	t(eff)	$\log a$ eff.	Max.error Possible (factor)	%* Likely	ϵ (max)	$\log E$ at max
5	6.638	65	11.9	-2.588	1.48	15	14	14.080
7.5	6.374	52	12.2	-2.273	1.70	20	16	14.948
10	6.180	38	12.8	-2.069	1.59	15	15	14.514
12.5	6.129	27	14.0	-1.936	1.48	10	15	14.514
15	6.038	0	15.0	-1.820	1.26	7	15.5	14.731
17.5	5.948	0	17.5	-1.763	1.20	2	16.0	14.948
20	5.867	0	20.0	-1.714	1.00	0	16.5	15.165
22.5	5.809	0	22.5	-1.672	1.00	0	17.0	15.382
24	5.767	0	24.0	-1.644	1.00	0	17.3	15.512

* This is the proportion per cent of the total integral density spectrum which comes from integration over radii which are equal to the separation radius of the counters or less, and in this range the approximation used may not be very good.

TABLE 19
INTEGRAL FREQUENCY SPECTRUM AS A FUNCTION OF
DIRECTION ($\log (H/\pi D)$ IN BODY OF TABLE).

all at $t = 7.5$

$\log \rho =$	$\varphi = 90^\circ$				$\varphi = 0^\circ$			
	4	5	6	7	4	5	6	7
$x = 1.0$	10.27	12.41	14.08	17.35	10.27	12.41	14.08	17.35
0.9	<u>10.19</u>	<u>12.39</u>	<u>14.20</u>	<u>17.71</u>	<u>10.31</u>	<u>12.53</u>	<u>14.28</u>	<u>16.96</u>
0.8	<u>10.06</u>	<u>12.32</u>	<u>14.28</u>	<u>16.00</u>	<u>10.27</u>	<u>12.59</u>	<u>14.52</u>	<u>16.30</u>
0.7	<u>11.93</u>	<u>12.24</u>	<u>14.26</u>	<u>16.14</u>	<u>10.16</u>	<u>12.53</u>	<u>14.64</u>	<u>16.60</u>
0.6	<u>11.62</u>	<u>13.98</u>	<u>14.14</u>	<u>16.19</u>	<u>11.99</u>	<u>12.40</u>	<u>14.65</u>	<u>16.77</u>
0.5	<u>12.23</u>	<u>13.64</u>	<u>15.97</u>	<u>16.18</u>	<u>11.70</u>	<u>12.15</u>	<u>14.53</u>	<u>16.78</u>
0.4	<u>12.53</u>	<u>13.08</u>	<u>15.49</u>	<u>17.87</u>	<u>11.10</u>	<u>13.72</u>	<u>14.14</u>	<u>16.55</u>
0.3	<u>13.36</u>	<u>14.05</u>	<u>16.59</u>	<u>17.10</u>	<u>13.98</u>	<u>14.71</u>	<u>15.30</u>	<u>17.85</u>
0.2					<u>15.80</u>	<u>16.65</u>	<u>17.37</u>	<u>18.02</u>
0.1								

$\varphi = 40^\circ$

$\log \rho =$	4	5	6	7
$x = 1.0$	10.27	12.41	14.08	17.35
0.9	<u>10.22</u>	<u>12.51</u>	<u>14.28</u>	<u>17.89</u>
0.8	<u>10.20</u>	<u>12.45</u>	<u>14.43</u>	<u>16.18</u>
0.7	<u>10.10</u>	<u>12.43</u>	<u>14.50</u>	<u>16.39</u>
0.6	<u>11.87</u>	<u>12.27</u>	<u>14.47</u>	<u>16.52</u>
0.5	<u>11.57</u>	<u>12.00</u>	<u>14.37</u>	<u>16.58</u>
0.4	<u>12.92</u>	<u>13.54</u>	<u>15.98</u>	<u>16.37</u>
0.3	<u>13.86</u>	<u>14.57</u>	<u>15.15</u>	<u>17.93</u>
0.2	<u>15.70</u>	<u>16.50</u>	<u>17.25</u>	<u>19.85</u>
0.1				

Note: Underlined characteristics are negative.

$$x = \cos \theta$$

TABLE 20

THE ANGULAR DISTRIBUTION OF THE SHOWERSTheoretical* (Arbitrary but consistent scale).

Projected Angle ψ	Intensity per unit solid angle at $\varphi = 90^\circ$ Here $\psi = \theta$	Intensity per unit solid angle at $\varphi = 0^\circ$ Here $\psi = \theta$	Intensity per unit projected angle (complete projection)	Intensity per unit projected angle (project up to $w = 0.25$)
0	6.49	6.49	13.36	1.76
5	6.53	6.69	13.08	1.76
10	6.76	7.42	12.80	1.82
20	7.45	10.20	12.70	2.05
30	8.26	15.00	12.76	2.45
40	9.15	20.90	11.71	2.64
50	8.55	24.95	9.36	2.45
60	5.07	19.30		

Observed**

Range of projected angle ψ deg.	Number Observed
0 to 5	7
5 to 15	15
15 to 25	12
25 to 35	9
35 to 45	3
45 to 55	2

* Theory at 7.5 radiation units.

** A total of 48 out of 228 shower pictures obtained at 31,000 (7 rad. units) by the counter controlled cloud chamber selected on the basis of 10 tracks or more having the same direction. Privately communicated to the author by Mr. E.W. Cowan on 10 March 1948.

Note: $228/48 = 4.75$

TABLE 21

THE MEAN SHOWER RADIUS AS A FUNCTION OF s
AND ITS EFFECT ON THE DENSITY SPECTRUM

s	r mean, lateral units	r mean, meters, sea level	r mean: r at s = 1 set = 1	$F_3(s)^*$
0.0	0	0	0	∞
0.2	0.0889	5.33	0.158	6.41×10^{12}
0.4	0.1945	11.67	0.346	1.69×10^3
0.6	0.2981	17.89	0.530	12.67
0.8	0.4218	25.31	0.750	2.05
1.0	0.5625	33.75	1.000	1.00
1.2	0.7250	43.50	1.289	0.776
1.4	0.8718	52.31	1.550	0.784
1.6	1.1144	66.86	1.981	0.843
1.8	1.3421	80.53	2.386	1.00

$$* F_3(s) = r^{-2\left(\frac{\gamma}{s}-1\right)}, \quad \gamma = 1.8$$

and r is taken from col. 4.

TABLE 22

MISCELLANEOUS MATHEMATICAL FUNCTIONS

δ	$I(\delta)$	x	$\log F_1(x)$	u	$0.4343 u$	$\log F_2(u)$
1.0	0.8628	2	<u>1.442</u>	-6	-2.6058	<u>8.1819</u>
1.1	0.9105	3	<u>1.330</u>	-5	-2.1715	<u>7.4830</u>
1.2	0.9046	4	<u>1.242</u>	-4	-1.7372	<u>6.7806</u>
1.3	0.9320	5	<u>1.171</u>	-3	-1.3209	<u>4.0469</u>
1.4	0.9728	6	<u>1.108</u>	-2	-0.8686	<u>3.2774</u>
1.5	1.0252	7	<u>1.055</u>	-1.5	-0.6514	<u>3.8537</u>
1.6	1.0891	8	<u>1.007</u>	-1	-0.4343	<u>2.3825</u>
1.7	1.1718	9	<u>2.964</u>	-0.5	-0.2171	<u>2.8352</u>
1.8	1.2739	10	<u>2.926</u>	0	0.0000	<u>1.1673</u>
1.9	1.4272	11	<u>2.892</u>	0.5	0.2171	<u>1.3155</u>
2.0	1.5702	12	<u>2.858</u>	1	0.4343	<u>1.1943</u>
2.1	1.9446	13	<u>2.826</u>	1.5	0.6514	<u>2.6951</u>
2.2	2.073	14	<u>2.798</u>	2	0.8686	<u>3.6580</u>
2.3	2.460			3	1.3029	<u>8.5797</u>
2.4	3.012			4	1.7372	<u>22.0257</u>
2.5	3.821			5	2.1715	<u>63.7179</u>
2.6	5.106			6	2.6058	<u>173.3988</u>
2.7	7.350					
2.8	11.42					
2.9	26.70					

Where:
$$I(\delta) = \delta \int_0^{\infty} (1 - e^{-u})^3 \frac{du}{u^{\delta+1}}$$

$$F_1(x) = (1 - xe^x \int_x^{\infty} e^{-u} \frac{du}{u})$$

$$F_2(u) = \left[(1 - e^{-e^u})^2 e^{-e^u} e^u \right]$$

and

$$\log \rho(\text{effective}) = 0.4343u - \log S$$

Note: Underlined characteristics are negative.

TABLE 23
OBSERVED ANGULAR DISTRIBUTION

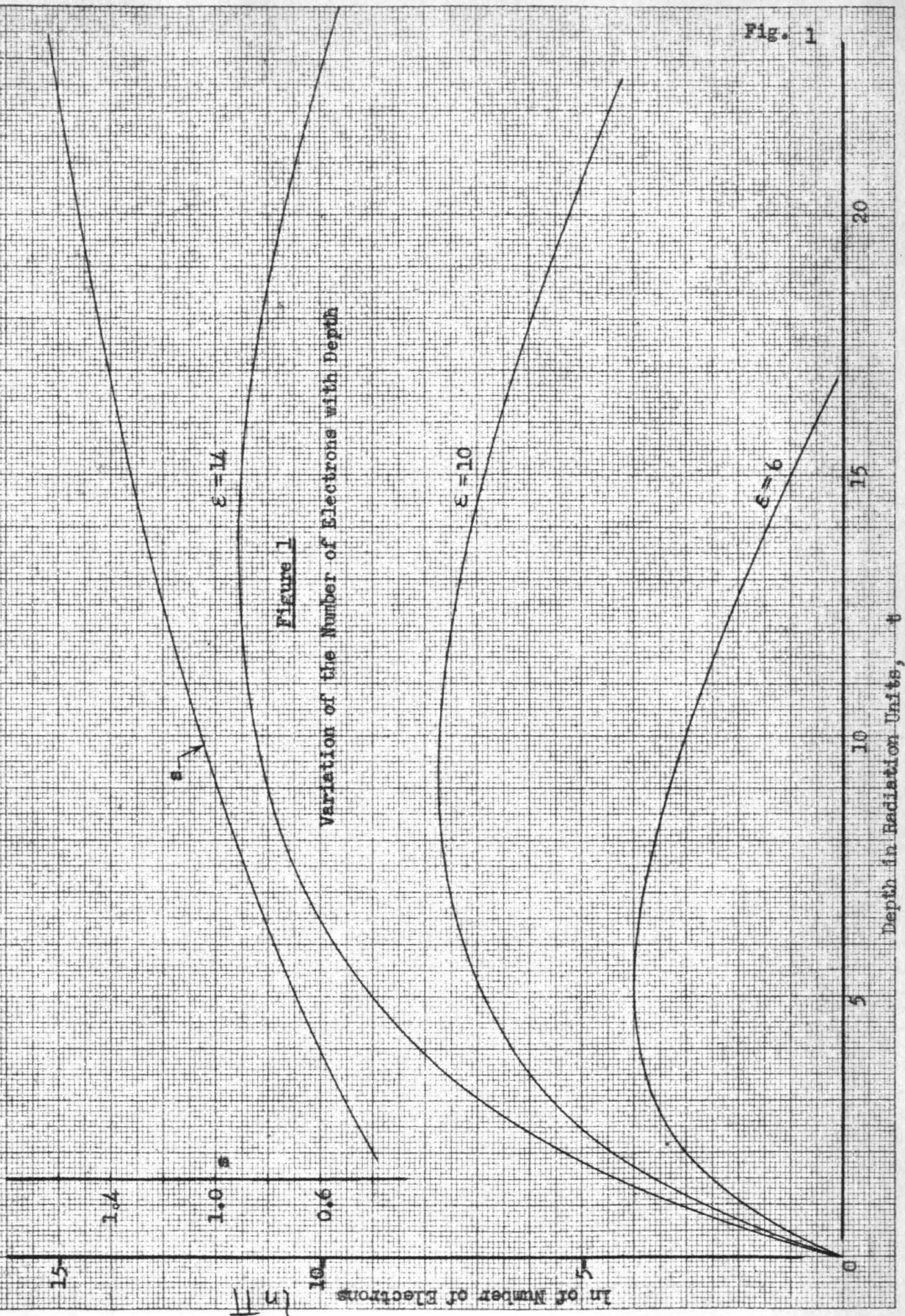
Range of projected angle (degrees)	Number of Measurable Photographs at :			
	31000 feet			37000 feet
	A	B	C	D
0 to 5	7	5	4	2
5 to 15	15	11	4	4
15 to 25	12	10	5	3
25 to 35	9	8	4	2
35 to 45	3	2	2	2
45 to 55	2	2	2	1
55 to 65				1
Total photos. used	48	38	21	15
Total photos. taken	228	228	228	44

SELECTION PROCEDURE

- A* Ten or more parallel tracks anywhere in chamber.
- B Ten or more parallel tracks above the lead.
- C One hundred or more parallel tracks anywhere in chamber.
- D Three or more parallel tracks anywhere in chamber.

*The distribution A is also given in Table 20.

Fig. 1



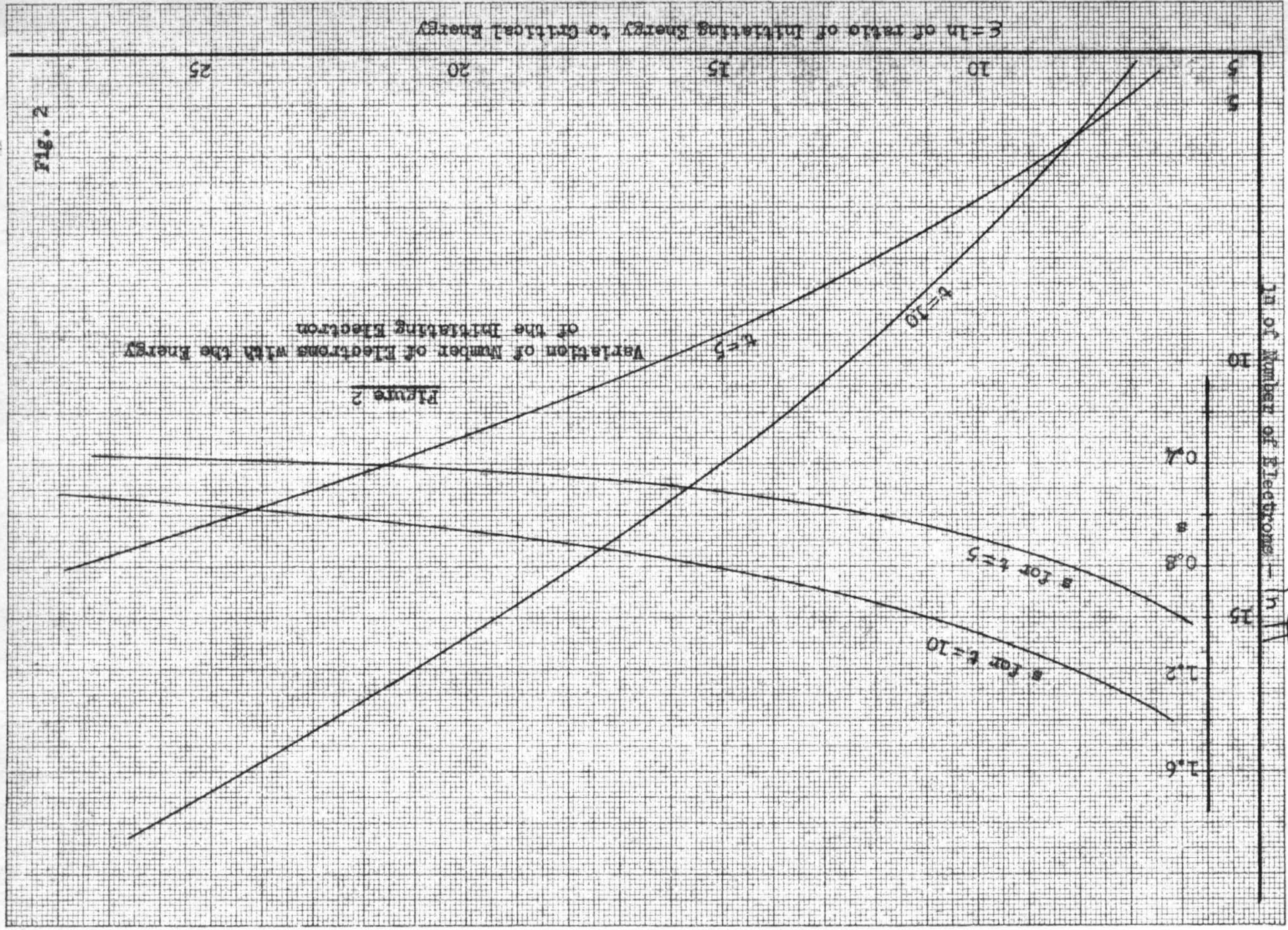


Fig. 2

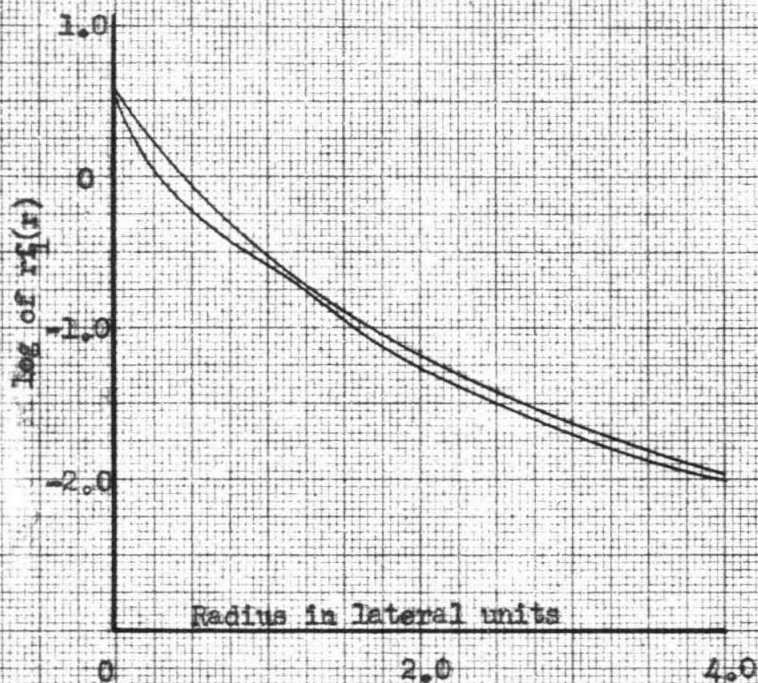
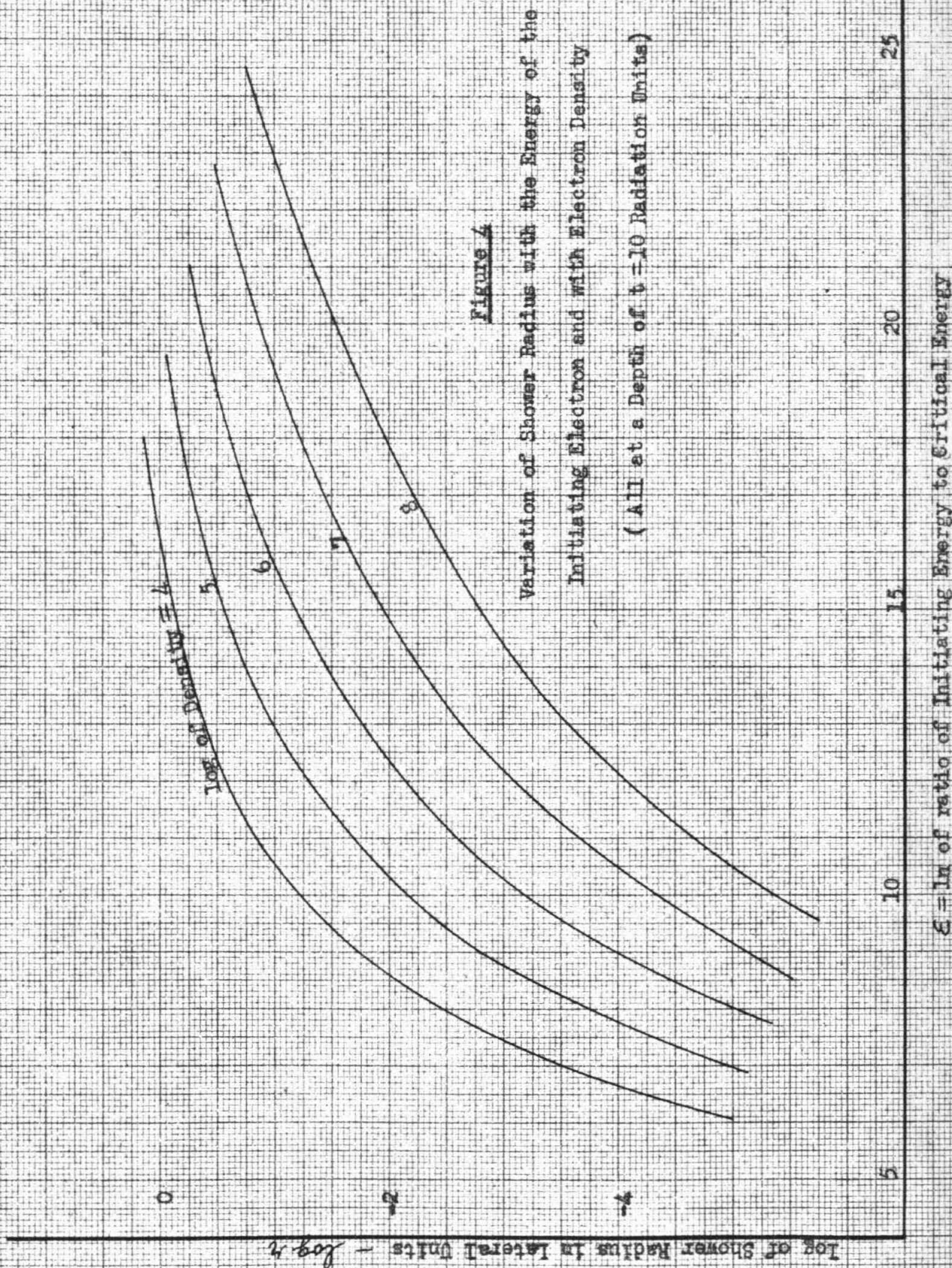
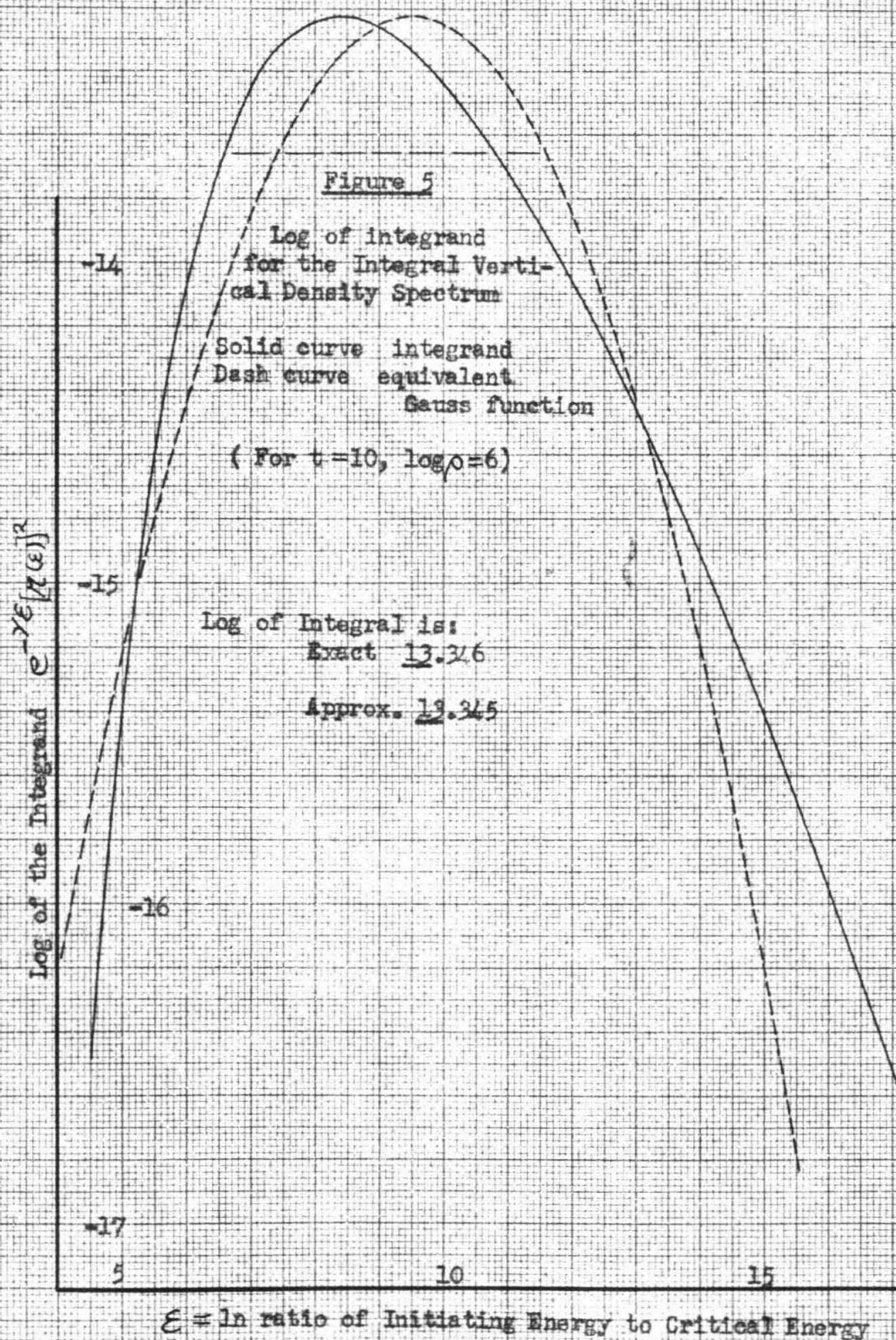


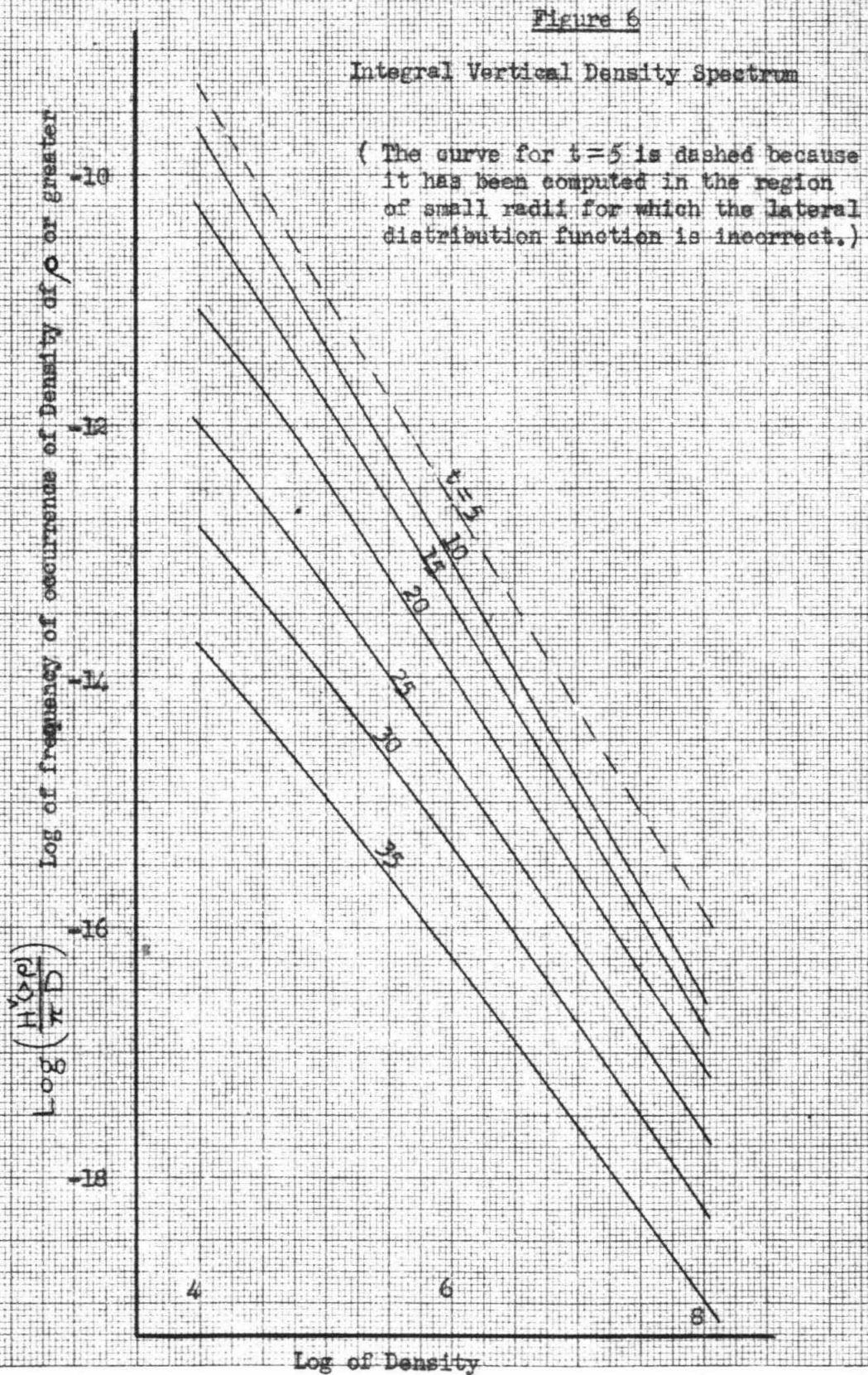
Figure 3

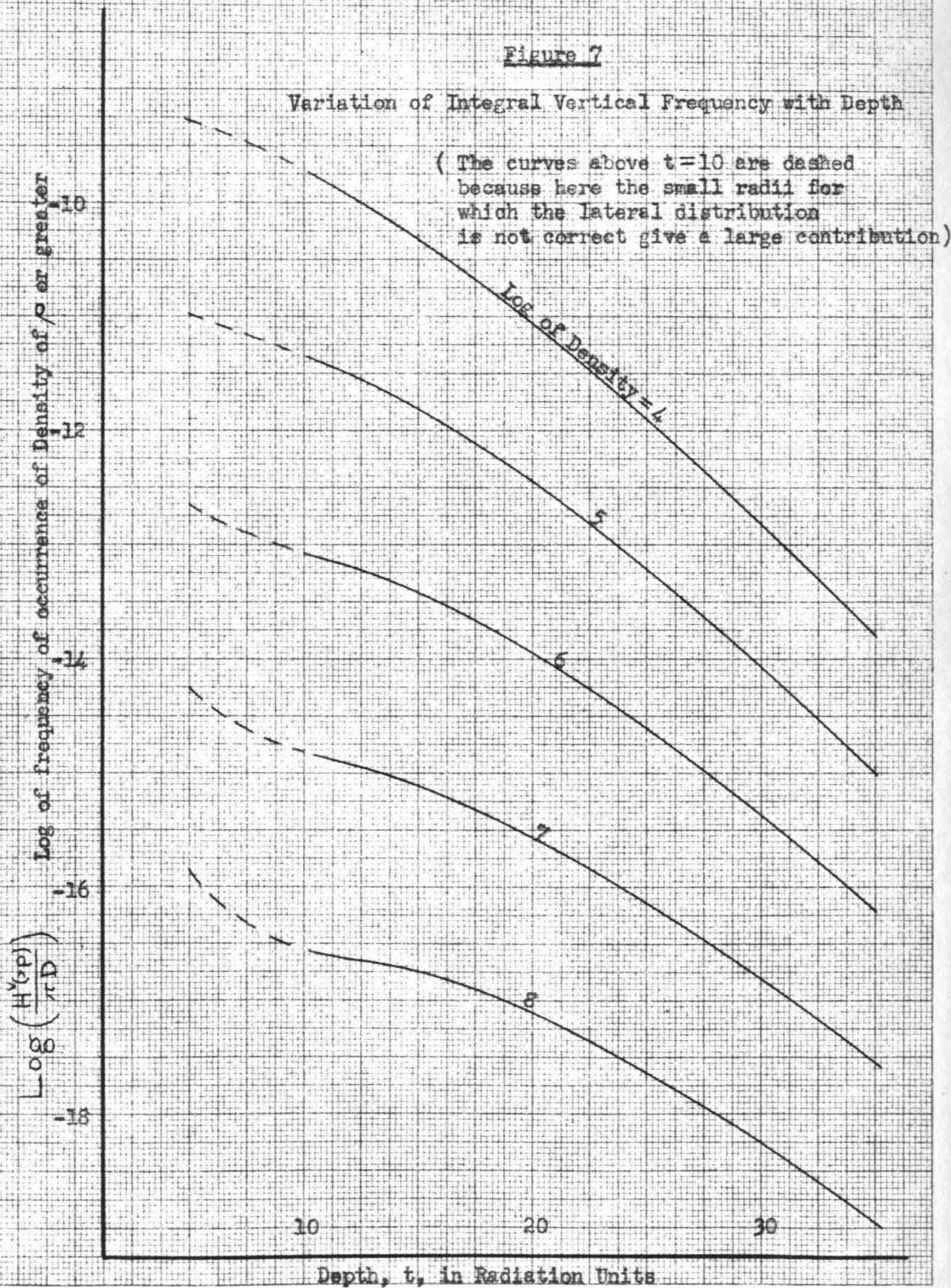
Radial Distribution Functions

The upper curve is the one adopted here; the lower curve is the one given by Moliere. The Normalization is slightly different to facilitate comparison.









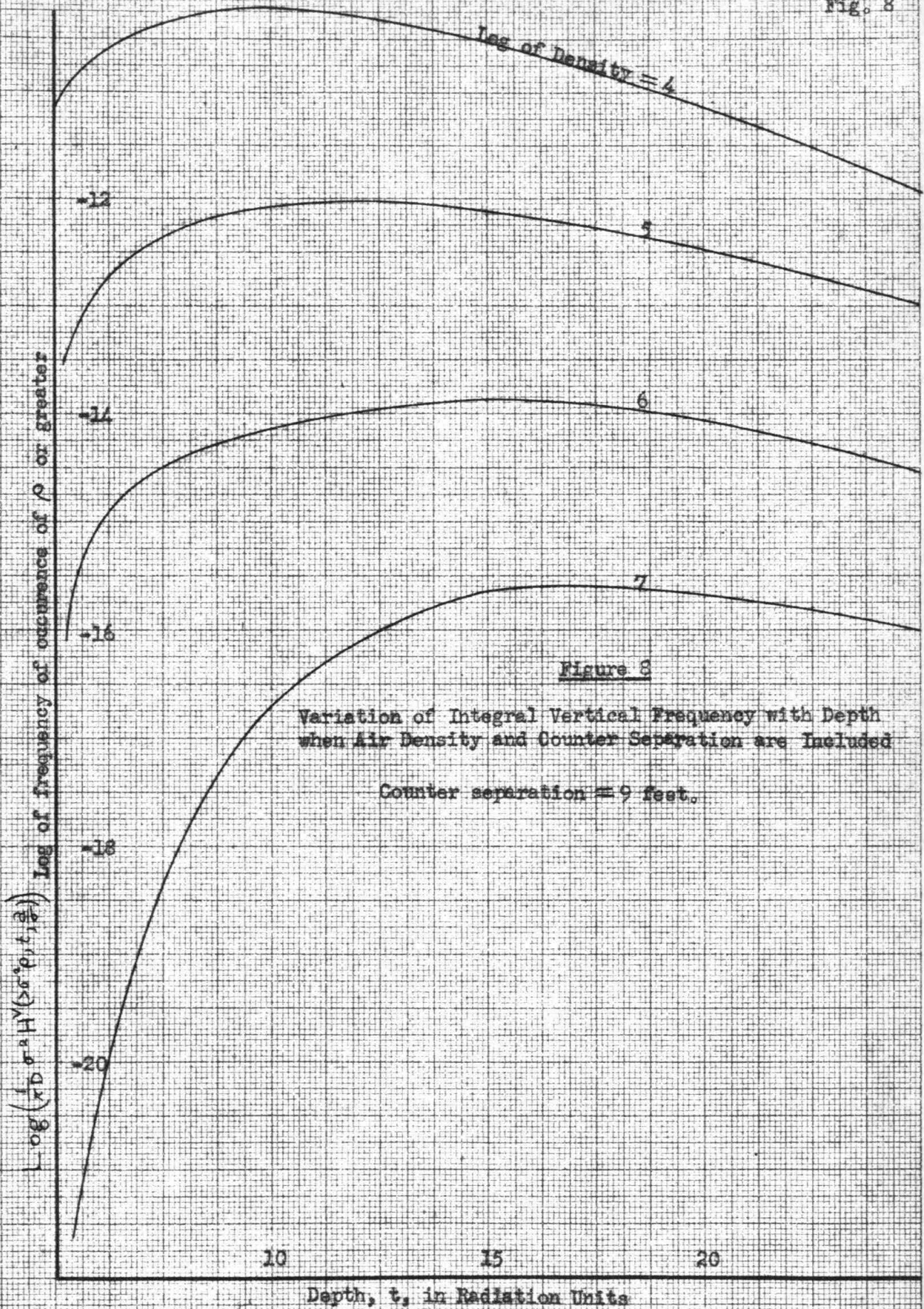


Figure 9

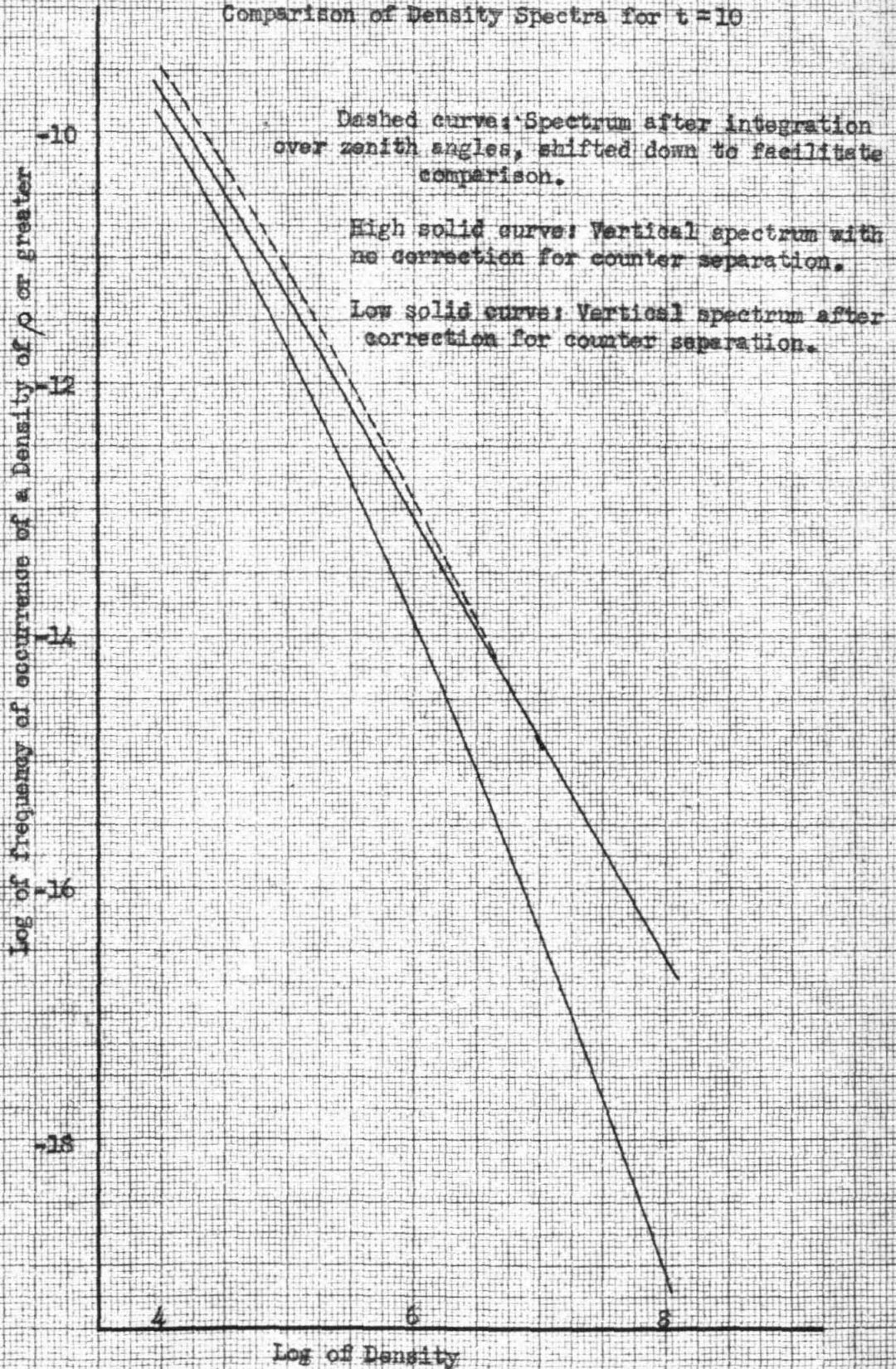
Comparison of Density Spectra for $t=10$ 

Figure 10

Fit of theoretical curve to observational data of Milberry

The curve is the normalized theoretical curve (Theory I 3),
and the experimental points are the data of Milberry.

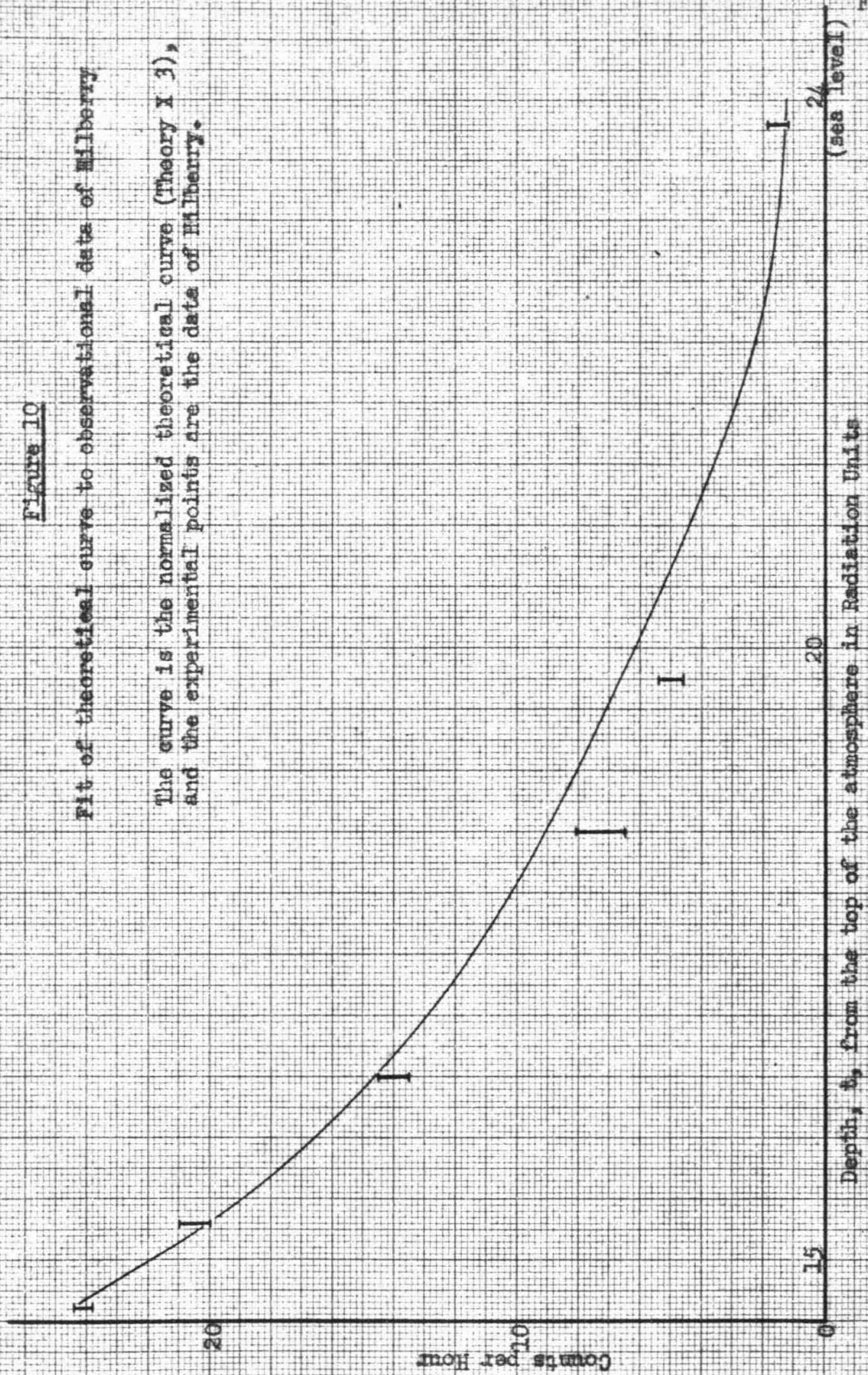


Figure 11

Comparison of Theory with the Observations of Kraybill

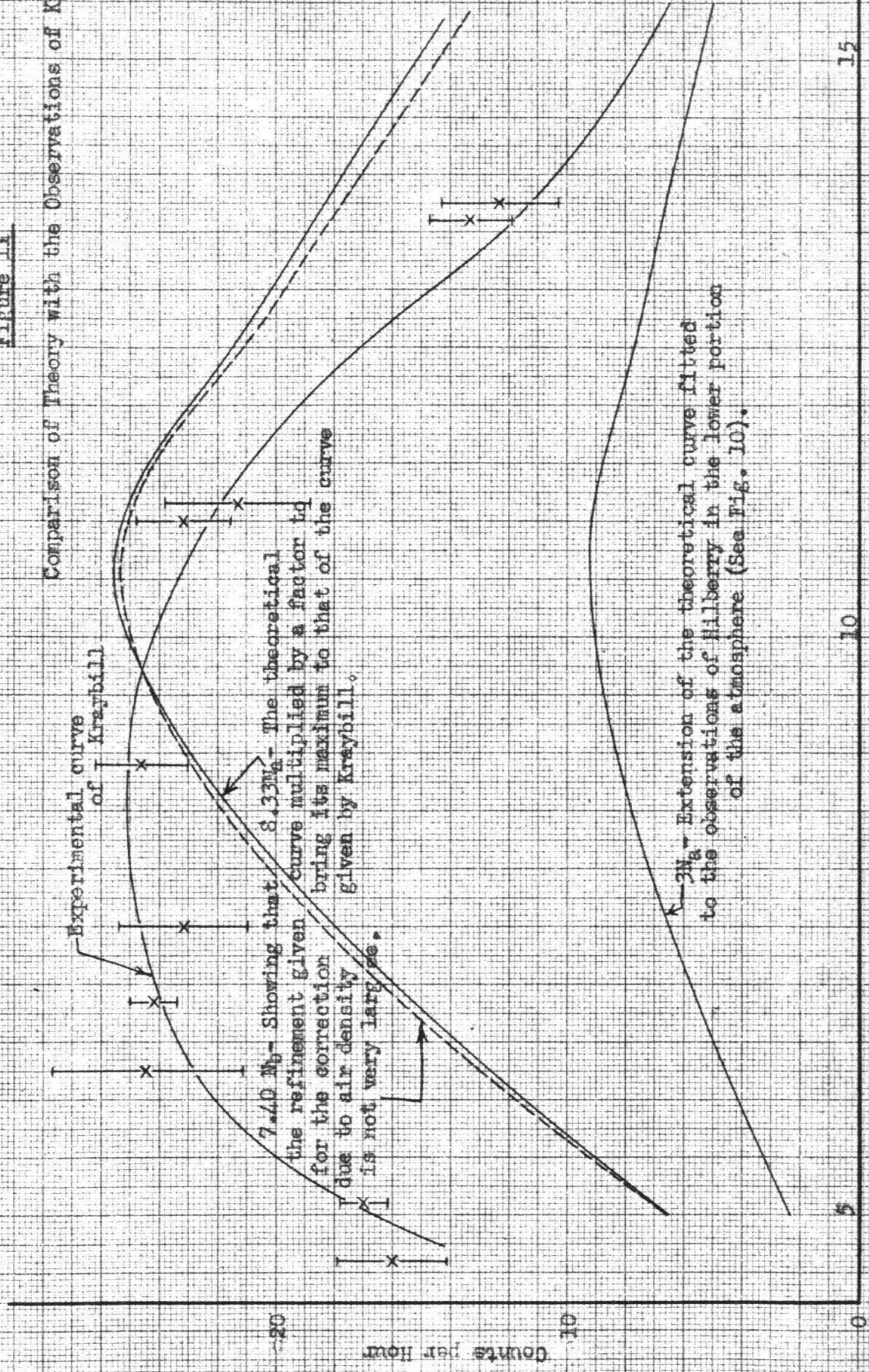


Fig. 11

10

Depth, t, from the top of the atmosphere in Radiation Units

5

15

Counts per Hour

7.40 Mg - Showing that the refinement given for the correction due to air density is not very large.

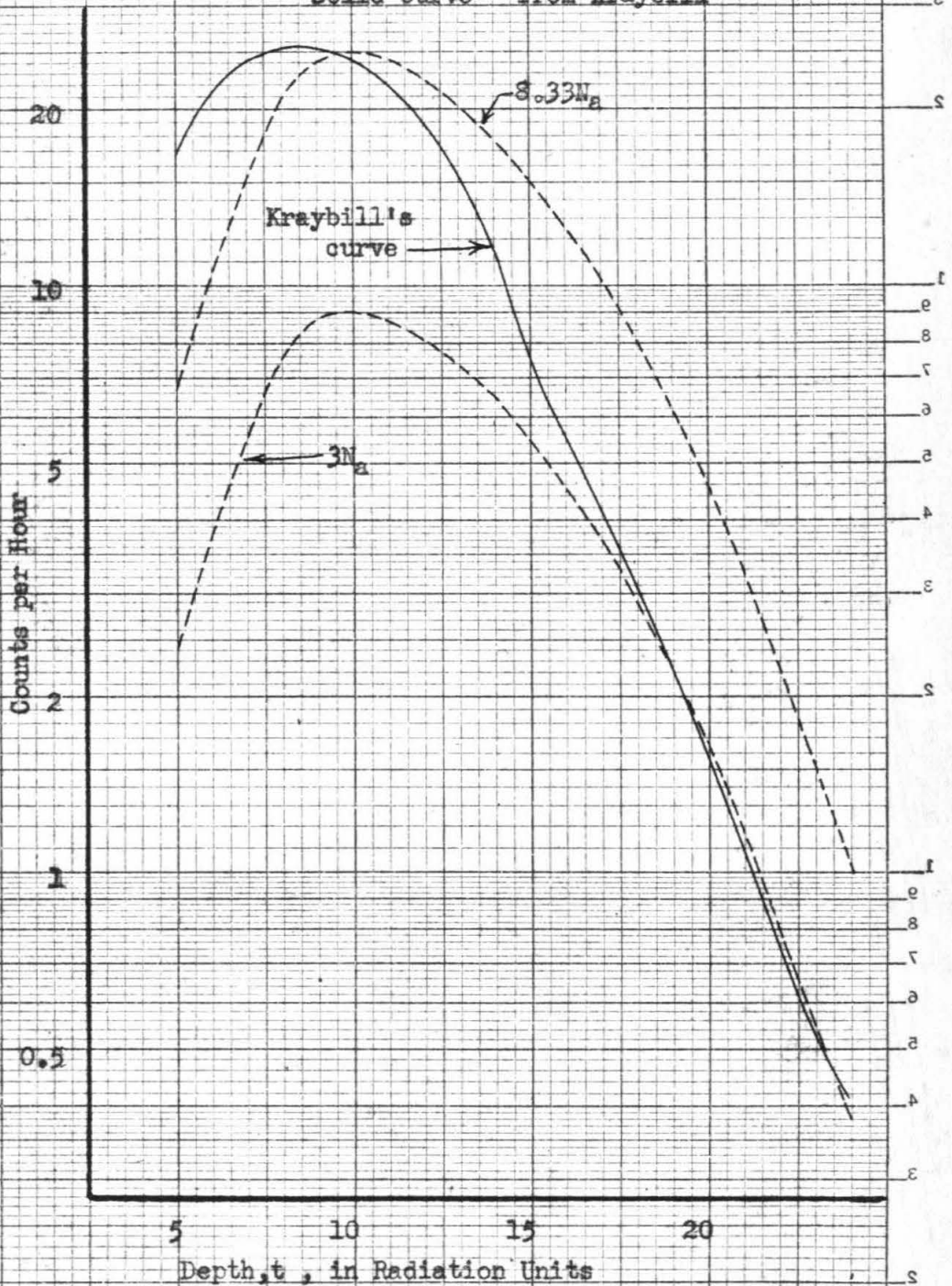
8.33 Mg - The theoretical curve multiplied by a factor 1.9 bring its maximum to that of the curve given by Kraybill.

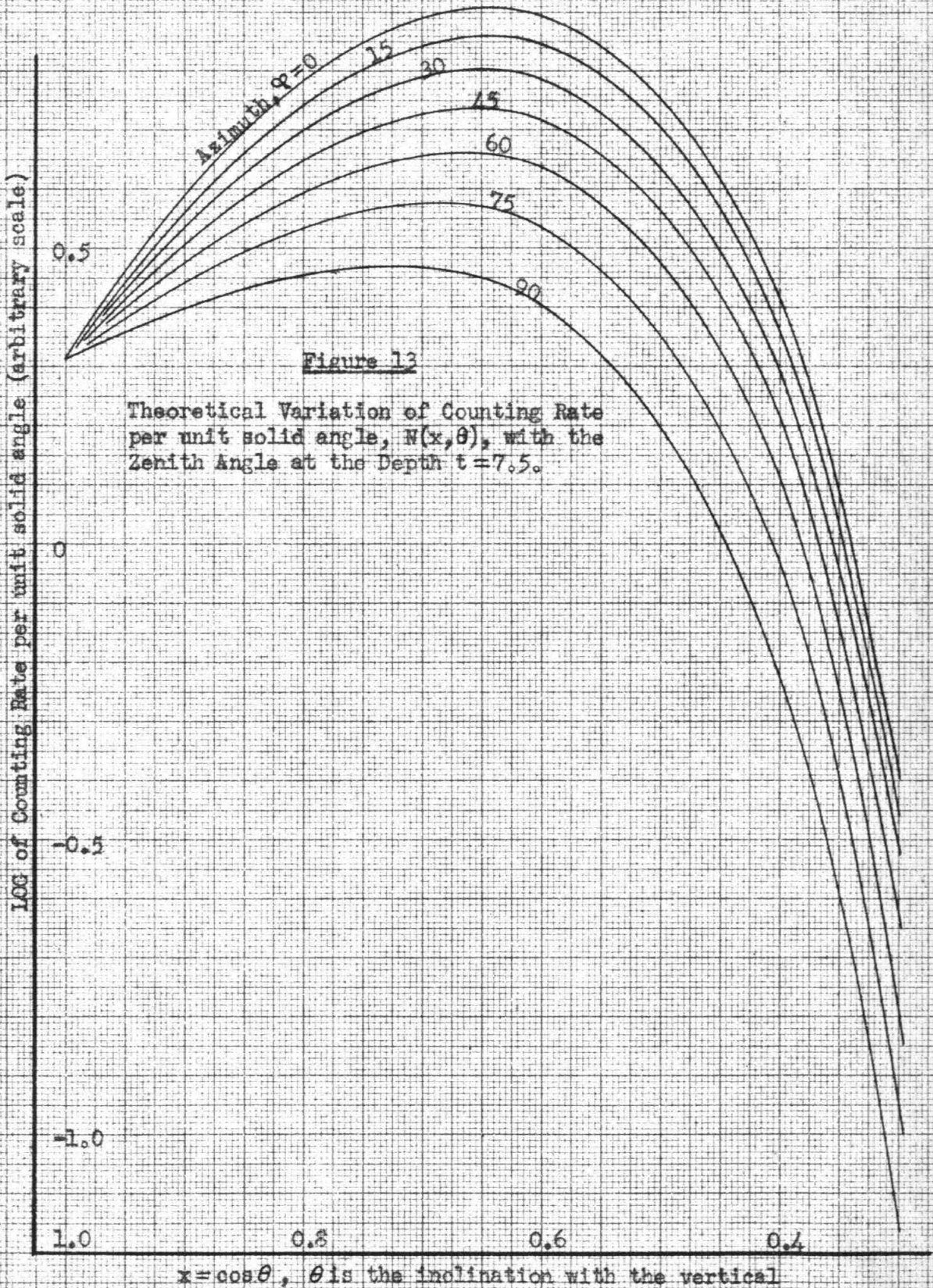
2Mg - Extension of the theoretical curve fitted to the observations of Hilberry in the lower portion of the atmosphere (See Fig. 10).

Figure 12

Comparison with the curve given by Kraybill
over the entire altitude range.

Dashed curves - Theoretical
Solid curve - from Kraybill





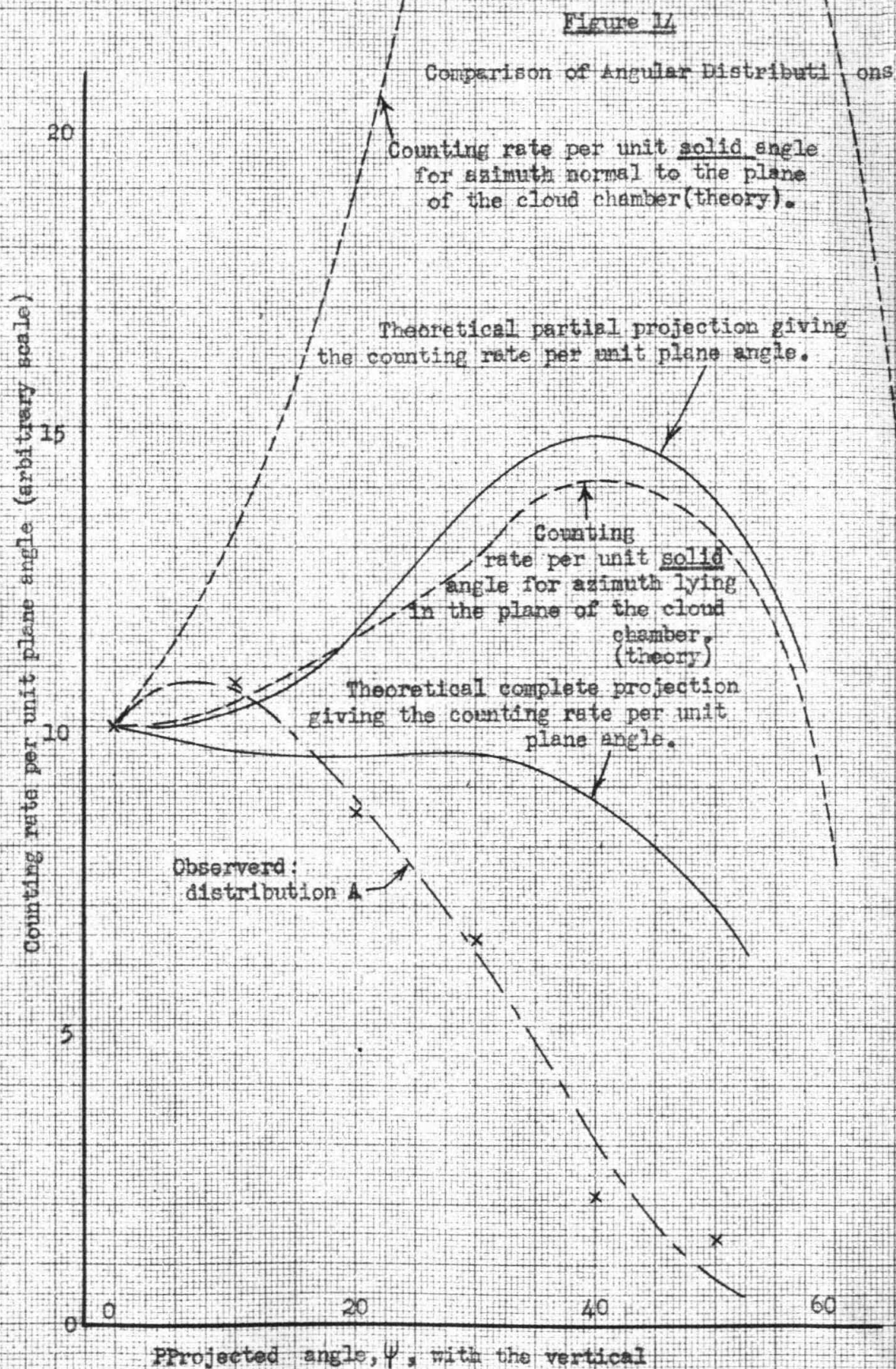
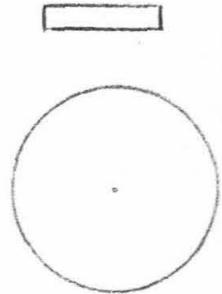
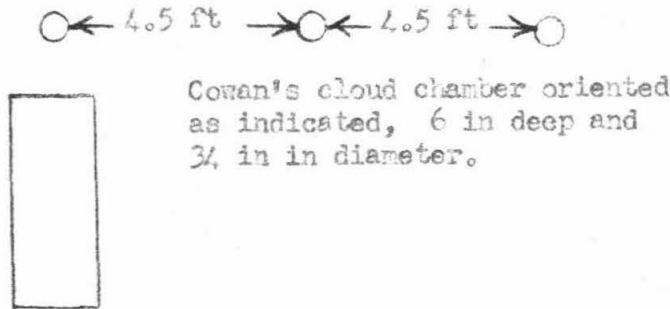


Fig. 15 Geometrical Arrangement

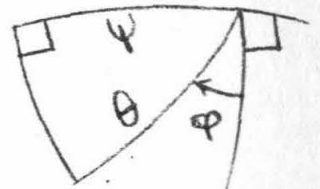
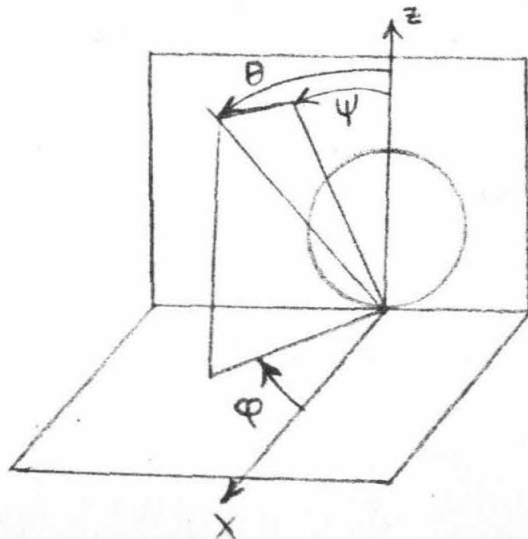
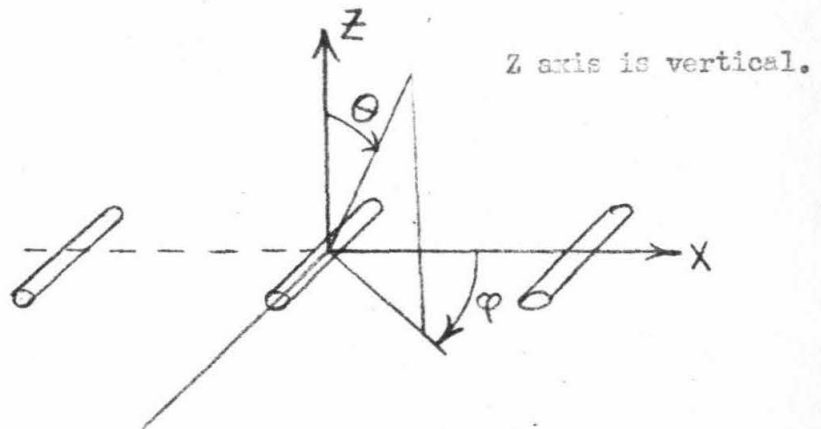
Kraybill's Counters

Sensitive area
13 sq in (84 sq cm)



Hilberry's Counters

Sensitive area 196 sq cm



$$\tan \psi = \sin \phi \tan \theta$$